Invited Speaker

1198 Data analysis workflows to measure material properties and structure using 4D-STEM
Colin Ophus[1], Stephanie Ribet[1], Georgios Varnavides[1,2], Steven Zeltmann[3], Karen Bustillo[1], Alexander Rakowski[1], Benjamin Savitzky[1], Min Chen[2], Yang Yang[2], Andrew Minor[1,2], Mary Scott[1,2]
[1]Lawrence Berkeley National Laboratory, Berkeley, USA, [2]University of California Berkeley, Berkeley, USA, [3]Cornell University, Ithaca, USA
1196 Exploiting dynamical diffraction theory in the crystal structure determination from 3D electron diffraction data
Dr. Lukas Palatinus

Oral Presentation

8 Role of phonon and plasmon inelastic scattering on Bragg diffracted beam intensities
Budhika Mendis[1]
[1]Dept of Physics, Durham University, , UK
158 Breaking barriers: Innovative methods for 4DSTEM diffraction data acquisition and processing in SEM
Nikita Denisov[1], Mr. Andrey Orekhov[1], Mr. Johan Verbeeck[1]
[1]EMAT, University of Antwerp, Antwerp, Belgium
742 Scanning precession electron diffraction tilt series for orientation analysis
Prof. Dr. Ir. Antonius (Ton) van Helvoort[1], Mr. Viljar J. Femoen[1], MSc Anders C. Mathisen[1], Ms Kaja E. Aune[1], Dr. Emil F. Christiansen[1], Dr. Inger-Emma Nylund[2], Dr. Tina Bergh[1,3], Dr. Ruben Bjørge[1,4]
[1]Department of Physics, Norwegian University of Science and Technology (NTNU), Trondheim, Norway, [2]Department of Materials Science and Engineering, Norwegian University of Science and Technology (NTNU), Trondheim, Norway, [3]Department of Chemical Engineering, Norwegian University of Science and Technology (NTNU), Trondheim, Norway, [4]Materials and Nanotechnology, SINTEF Industry, Trondheim, Norway , Trondheim, Norway
750 Solving the crystallographic phase problem by linearizing dynamical electron diffraction
Prof. Christoph Koch[1], Sam Fairman[1], Grigory Kornilov[1], Dr. Benedikt Haas[1], Dr. Niklas Delby[2]
[1]Humboldt-Universität zu Berlin, Dept. of Physics & Center for the Science of Materials Berlin, Berlin, Germany, [2]Bruker AXS (formerly Nion Co. R&D), Kirkland, USA
1107 Simultaneous nanoscale mapping of strain and electric field in semiconductor heterostructures using 4D-STEM
Yucheng Zou[1], Dr. Lei Jin[1], Peng-Han Lu[1], Prof. Dr Rafal Dunin-Borkowski[1]
[1]Research Center Jülich, Jülich, Germany
1119 Towards direct imaging of defects in carbon nanotubes with 4DSTEM
Dr. Antonin Louiset[1], Dr. Daniel FÖRSTER[2], Dr. Jean-Luc ROUVIERE[1], Dr. Vincent JOURDAIN[3], Dr. Christophe BICHARA[4], Dr. Hanako OKUNO[1]
[1]IRIG-MEM, CEA, Université Grenoble Alpes, Grenoble, France, [2]Laboratoire d'Etude des Microstructures, ONERA-CNRS, Université Paris-Saclay, Châtillon, France, [3]Laboratoire Charles Coulomb, CNRS, Université de Montpellier, Montpellier, France, [4]CINaM, CNRS, Université Aix-Marseille, Marseille, France
12 Single Crystal Analysis of Nanocrystals by Three-Dimensional Electron Diffraction
Dr. Zhehao Huang[1]
[1]Stockholm University, Stockholm, Sweden
97 Exploring the limits of 3D ED for accurate structure analysis at the nanometer scale
Ms Sara Passuti[1], Ms Erica Cordero Oyonarte[1], M Valérie Pralong[1], M Adrian David[1], M Emmanuel Guilmeau[1], M Lukas Palatinus[2], Mr. Philippe Boullay[1]

[1]Normandie Université, ENSICAEN, UNICAEN, CNRS, CRISMAT, Caen, France , [2]Czech Academy of Sciences, Department of Structure Analysis, Na Slovance 2, Prague, Czechia

298 Quantitative comparison between the diffuse scattering from three-dimensional electron diffraction and single-crystal X-ray diffraction

Romy Poppe[1], Dr. Nikolaj Roth[2], Prof. Reinhard B. Neder[3], Dr. Lukáš Palatinus[4], Prof. Bo B. Iversen[2], Prof. Joke Hadermann[1]

[1]University of Antwerp, Department of Physics , Groenenborgerlaan 171, B-2020 Antwerp, Belgium, [2]Aarhus University, Department of Chemistry , Langelandsgade 140, 8000 Aarhus, Denmark, [3]Friedrich-Alexander-Universität Erlangen-Nürnberg, Kirstallographie und Strukturphysik , Staudtstraße 3, 91058 Erlangen, Germany, [4]Czech Academy of Sciences, Department of Structure Analysis , Na Slovance 2, 182 21 Prague, Czech Republic

328 Quantification of Dynamic Scattering Effects in Molecular Crystals using Large Angle Rocking Beam Electron Diffraction

Robert Busch[1,2], Hsu-Chih Ni[1,2], Prof. Jian-Min Zuo[1,2]

[1]University of Illinois at Urbana Champaign, Urbana, United States, [2]Materials Research Laboratory, Urbana, United States

822 Liquid Phase 3D Electron Diffraction Combination Provides New Possibilities for Polymorphism Studies

Joakim Lajer[2], Edward T. Broadhurst[1], Murat N. Yesibolati[2], Emil C. S. Jensen[3], Xiaodong Zou[1], Kristian S. Mølhave[2], Hongyi Xu[1], Huiqiu Wang[1]

[1]Materials and Environmental Chemistry, Stockholm University, Stockholm, Sweden, [2]National Centre for Nano Fabrication and Characterization, Technical University of Denmark, Lyngby, Denmark, [3]Insight Chips Aps, Lyngby, Denmark

981 Structural Study of Polyphasic Mixtures Using 3d Electron Diffraction:A Case Study of Oxyresveratrol

Ms Vincentia Emerson Agbemeh[2]

[1]Electron Crystallography, Center for Materials Interfaces, Istituto Italiano di Tecnologia, Pontedera, Italy, [2]Department of Chemistry, Life Sciences and Environmental Sustainability, University of Parma, Parma, Italy

206 Determination of 3D strain fields from dynamical diffraction effects

Dr. Laura Niermann[1], Mr. Tore Niermann[1], Mr. Michael Lehmann[1]

[1]Technische Universität Berlin, Institut für Optik und Atomare Physik, Berlin, Germany

247 Unveiling Structural Heterogeneity and Imbalance of Gold Decahedral Nanoparticles using Four-dimensional Scanning Transmission Electron Microscopy

Oliver Lin[1], Dr. Zhiheng Lyu[1], Mr. Hsu-Chih Ni[1], Ms. Yetong Jia[2], Prof. Kejie Zhao[2], Prof. Jian-Min Zuo[1], Prof. Qian Chen[1]

[1]University of Illinois, Urbana-Champaign, Urbana, USA, [2]Purdue University , West Lafayette, USA

250 Atomic resolution observation of zeolitic framework and captured cations using low-dose OBF STEM technique

Dr. Kousuke Ooe[1,2], Dr. Takehito Seki[3,4], Mr. Koudai Tabata[3], Dr. Kaname Yoshida[2], Prof. Atsushi Nakahira[5], Mr. Yuji Kohno[6], Prof. Yuichi Ikuhara[2,3], Prof. Naoya Shibata[2,3]

[1]Monash University, Clayton, Australia, [2]Japan Fine Ceramics Center, Nagoya, Japan, [3]The University of Tokyo, Bunkyo, Japan, [4]JST PRESTO, Kawaguchi, Japan, [5]Osaka Metropolitan University, Sakai, Japan, [6]JEOL Ltd., Akishima, Japan

256 OpenECCI - A Streamlined Open-Source Workflow for Electron Channelling Contrast Imaging of Crystal Defects

Zhou Xu[1], Dr. Håkon W. Ånes[2,3], Dr. Sergey Gorelick[1,4], Dr. Xiya Fang[1], Dr. Peter Miller[1]

[1]Monash Centre for Electron Microscopy, Clayton, Australia, [2]Department of Materials Science and Engineering, Norwegian University of Science and Technology, Trondheim, Norway, [3]Xnovo Technology Aps, Køge, Denmark, [4]Ramaciotti Centre for Cryo-Electron Microscopy, Clayton , Australia

324 Towards in-situ 4D-STEM observation of texture evolution in nano-crystalline thin films

Dr. Mingjian Wu[1], Chang-Lin Hsieh[1], Daniel Stroppa[2], Philipp Pelz[1], Colin Ophus[3], Penghan Lu[4], Rafal Dunin-Borkowski[4], Christina Harreiss[1], Peter Denninger[1], Erdmann Spiecker[1]
[1]IMN & CENEM, FAU Erlangen-Nurnberg, Erlangen, Germany, [2]DECTRIS Ltd, Baden-Daettwil, Switzerland, [3]NCEM, Lawrence Berkeley National Laboratory, Berkeley, USA, [4]Ernst Ruska-Centre for Microscopy and Spectroscopy with Electrons, Juelich, Germany

361 QCBED Measurements of Vacancy Concentrations, Lattice Contraction, and Bonding Electron Densities Surrounding Aluminium Nanovoids

Associate Professor Philip Nakashima[1], Dr Yu-Tsun Shao[2,3], Dr Zezhong Zhang[4,5,6], Dr Andrew Smith[7], Dr Tianyu Liu[8], Professor Nikhil Medhekar[1], Professor Joanne Etheridge[7,9], Professor Laure Bourgeois[1,9], Professor Jian-Min Zuo[10,11]
[1]Department of Materials Science and Engineering, Monash University, Clayton, Australia, [2]Mork Family Department of Chemical Engineering & Materials Science, University of Southern California, Los Angeles, USA, [3]Core Center of Excellence in Nano Imaging, University of Southern California, Los Angeles, USA, [4]Electron Microscopy for Materials Research (EMAT), University of Antwerp, Antwerp, Belgium, [5]NANOlab Center of Excellence, University of Antwerp, Antwerp, Belgium, [6]Department of Materials, University of Oxford, Oxford, United Kingdom, [7]School of Physics and Astronomy, Monash University, Clayton, Australia, [8]Institute of Multidisciplinary Research for Advanced Materials, Tohoku University, Sendai, Japan, [9]Monash Centre for Electron Microscopy, Monash University, Clayton, Australia, [10]Department of Materials Science and Engineering, University of Illinois at Urbana-Champaign, Urbana, USA, [11]Materials Research Laboratory, University of Illinois at Urbana-Champaign, Urbana, USA

483 Structure retrieval by parameterised inverse multislice accounting for partial coherence and thermal effects

Prof. Dr. Knut Müller-Caspary[1], Dr. Benedikt Diederichs[1,2], Ziria Herdegen[1], Achim Strauch[1,3]
[1]LMU München, Munich, Germany, [2]HMGU München, Munich, Germany, [3]Forschungszentrum Jülich, Jülich, Germany

1117 Towards Single-Pattern Absolute High angular Resolution EBSD without using Simulated Patterns as Reference

Dr. Tijmen Vermeij[1,2], Lloyd Dodsworth[1], Dr. Aimo Winkelmann[3], Dr. René De Kloe[4], Dr. Johan Hoefnagels[1]
[1]Mechanical Engineering, Eindhoven University of Technology, Eindhoven, Netherlands, [2]Laboratory for Mechanics of Materials and Nanostructures, Swiss Federal Laboratories for Materials Science and Technology (EMPA), Thun, Switzerland, [3]AGH University of Science and Technology, Krakow, Poland, [4]EDAX, Tilburg, Netherlands

Poster Presentation

38 HeXI: The High-energy Electron Xtallography Instrument at Diamond Light Source

Pedro Nunes[1], Mark Lunnon[1], Bodvar Olafsson[1], Andrew Foster[1], Richard Littlewood[1], Graham Duller[1], Gwyndaf Evans[1,2], Alistair Siebert[1]
[1]Diamond Light Source, Harwell, United Kingdom, [2]The Rosalind Franklin Institute, Harwell, United Kingdom

55 Using Virtual Detectors as a Compression Tool for Electron Ptychography

Anton Gladyshev[1,2], Mr. Marcel Schloz[1,2], Mr. Johannes Müller[1,2], Dr. Benedikt Haas[1,2], Prof. PhD Christoph Koch[1,2]
[1]Humboldt-Universität zu Berlin , Berlin, Germany, [2]Center for the Science of Materials Berlin, Berlin, Germany

113 Determining alloy concentration by analyzing dynamic diffraction at strained semiconductor interfaces

Frederik Otto[1], Dr. Laura Niermann[1], Dr. Tore Niermann[1], Prof. Dr. Michael Lehmann[1]

[1]Technische Universität Berlin, Berlin, Germany

120 Depth Dependence of Electron Channeling Contrast Imaging in Gallium Nitride

Etienne Lavallee[1,2], Mr. Antoine Guitton[2], Mr. Peter Imrich[1], Ms. Claire Chisholm[1]
[1]KAI Kompetenzzentrum Automobil-und Industrieelektronik GmbH, 9524 Villach, Austria, [2]Université de Lorraine, CNRS, Arts et Métiers, LEM3, Metz, France

201 Three-dimensional classification of dislocations from single projections

Dr. Tore Niermann[1], Ms. Laura Niermann[1], Mr. Michael Lehmann[1]
[1]Technische Universität Berlin, Institut für Optik und Atomare Physik, Berlin, Germany

229 Gigabytes to Megabytes – Rapidly analyzing in-situ videos to track lattice spacing changes

Ben Miller[1], Cory Czarnik[1]
[1]Gatan, Inc., Pleasanton, USA

261 Texture analysis of radiation sensitive organic films: Comparative study by electron diffraction tomography and GIWAXS

Irene Kraus[1], Dr. Mingjian Wu[1], Dr. Stefanie Rechberger[1], Dr. Johannes Will[1], Dr. Santanu Maiti[2], Andreas Kuhlmann[3,4], Marten Huck[3,4], Marc Steinberger[5], Prof. Dr. Christoph Brabec[5], Prof. Dr. Hans-Georg Steinrück[3,4], Prof. Dr. Tobias Unruh[2], Prof. Dr. rer. nat. habil. Erdmann Spiecker[1]
[1]Institute of Micro- and Nanostructure Research (IMN) & Center for Nanoanalysis and Electron Microscopy (CENEM), FAU Erlangen-Nürnberg, Erlangen, Germany, [2]Institute for Crystallography and Structural Physics (ICSP), FAU Erlangen-Nürnberg, Erlangen, Germany, [3]Institute for a Sustainable Hydrogen Economy (INW), Forschungszentrum Jülich GmbH, Jülich, Germany, [4]Institute of Physical Chemistry, RWTH Aachen University, Aachen, Germany, [5]Institute Materials for Electronics and Energy Technology (i-MEET), FAU Erlangen-Nürnberg, Erlangen, Germany

275 Electron channeling pattern imaging – a novel approach for the determination of wafer offcut angles

Han Han[1], Mr. Libor Strakos[2], Mr. Clément Porret[1], Ms. Valérie Depauw[1], Mr. Tomas Vystavel[2], Mr. Olivier Richard[1], Ms. Eva Grieten[1], Mr. Thomas Hantschel[1]
[1]imec, Leuven, Belgium, [2]Thermo Fischer Scientific, Brno, Czech Republic

314 Measuring electric fields with 4D-STEM: Demonstration of pitfalls by the example of GaN and SiGe

Tim Grieb[1,2], Christoph Mahr[1,2], Florian F. Krause[1,2], Knut Müller-Caspary[3], Marco Schowalter[1,2], Martin Eickhoff[1,2], Andreas Rosenauer[1,2]
[1]Institute of Solid State Physics, University of Bremen, Bremen, Germany, [2]MAPEX Center for Materials and Processes, University of Bremen, Bremen, Germany, [3]Department of Chemistry and Centre for NanoScience, Ludwig-Maximilians-Universität München, Munich, Germany

322 Retrieving sub-angstrom resolution from low order dynamical diffraction intensities

Grigory Kornilov[1], Sam Fairman[1], Sherjeel Shabih[1], Dr. Benedikt Haas[1], Dr. Niklas Dellby[2], Adnan Hammud[3], Dr. Zbigniew Galazka[4], Prof. Christoph Koch[1]
[1]Department of Physics, Humboldt-Universität zu Berlin, Berlin, Germany, [2]Bruker AXS (formerly Nion Co. R&D), Kirkland, USA, [3]Fritz Haber Institute of the Max Planck Society, Berlin, Germany, [4]Leibniz-Institut für Kristallzüchtung, Berlin, Germany

330 Fully Integrated Pixelated 4D-STEM Detector for Scanning Electron Microscopes

Pavel Stejskal[1], Rastislav Motúz[2], Michal Horák[3], Tomáš Šikola[4]
[1]AdvaScope, Brno, Czech Republic, [2]TESCAN Group, Brno, Czech Republic, [3]Brno University of Technology, CEITEC, Brno, Czech Republic, [4]Brno University of Technology, Institute of Physical Engineering, Brno, Czech Republic

422 Determination of Magnetic Symmetries by Electron Diffraction

Oleksandr Zaiets[1,2], Carsten Timm[3], Jan Rusz[4], Subakti Subakti[1], Axel Lubk[1,2]
[1]Leibniz Institute for Solid State and Materials Research Dresden, Dresden, Germany, [2]Institute of Solid State and Materials Physics, TU Dresden, Dresden, Germany, [3]Institute of Theoretical Physics, TU Dresden, Dresden, Germany, [4]Department of Physics and Astronomy, Uppsala University, Uppsala, Sweden

432 4D-STEM/PNBD: Fast and easy powder electron diffraction in SEM
Miroslav Slouf[1], Ms. Pavlina Sikorova[2], Mr. Radim Skoupy[2], Mr. Martin Slouf[3], Mrs. Ewa Pavlova[1], Mr. David Rendl[4], Mr. Filip Sroubek[4], Mr. Vladislav Krzyzanek[2]
[1]Institute of Macromolecular Chemistry CAS, Praha, Czech Republic, [2]Institute of Scientific Instruments CAS, Brno, Czech Republic, [3]LiveSystems Ltd., Praha, Czech Republic, [4]Institute of Information Theory and Automation CAS, Praha, Czech Republic
438 Scanning electron diffraction reveals the nanoscale ordering of cellulose in a hierarchically structured hybrid material
Mathias Nero[1], Dr Hasan Ali[2], Professor Yuanyuan Li[3], Dr Tom Willhammar[1]
[1]Stockholm University, Stockholm, Sweden, [2]Uppsala University, Uppsala, Sweden, [3]Royal Institute of Technology, Stockholm, Sweden
455 Improving Transmission Kikuchi Diffraction workflows
Dr. Mark Coleman[1], Mr Kim Larsen[1]
[1]Oxford Instruments NanoAnalysis, High Wycombe, United Kingdom
460 Characterization of the crystal structure of In-Ga-Zn-O materials via Precession Electron Diffraction
Marta Antonella Agati[1], Pradyumna Kumar Parida[1], Olivier Richard[1], Athanassios S. Galanis[2], Harold Dekkers[1], Eva Grieten[1], Paola Favia[1]
[1]IMEC, Leuven, Belgium, [2]NanoMegas, Brussels, Belgium
525 Assessing the Accuracy of Strain Mapping using 4D-STEM
Petr Vacek[1], Paul Midgley[1]
[1]Department of Materials Science and Metallurgy, University of Cambridge, 27 Charles Babbage Road, Cambridge, United Kingdom
542 Study of Lithiation Dynamics in Cathode Materials by in situ TEM Electrochemical Liquid Technics.
Student Kevyn Gallegos-Moncayo[1], Justine Jean[1,2], PhD Nicolas Folastre[1], PhD Arash Jamali[1,2], PhD Arnaud Demortière[1,2,3]
[1]CNRS-LRCS, Amiens, France, [2]RS2E-French Research Network on Electrochemical Energy Storage, Amiens, France, [3]ALISTORE- European Research Institute, Amiens, France
568 eCHORD crystalline orientation maps: channeling contrast at interfaces
Dr. Hdr Cyril Langlois[1], Dr. Gabriel Denhez L'Hôte[1], M. Thierry Douillard[1], Dr. Matthieu Bugnet[1], Dr. Claire Maurice[2]
[1]INSA Lyon, MATEIS laboratory, Lyon, France, [2]Ecole des Mines Saint-Etienne, LGF laboratory, Saint Etienne, France
607 Multi-Dimensional Data Restoration from Subsampled EBSD Data
Zoe Broad[1], Jack Wells[2], Daniel Nicholls[3], Alex W. Robinson[3], Amirafshar Moshtaghpour[4], Robert Masters[5], Louise Hughes[5], Angus I. Kirkland[4], Nigel D. Browning[1,3]
[1]Department of Mechanical, Materials and Aerospace Engineering, University of Liverpool, Liverpool, UK, [2]Distributed Algorithms Centre for Doctoral Training, University of Liverpool, Liverpool, UK, [3]SenseAI Innovations Ltd, Liverpool, UK, [4]Rosalind Franklin Institute, Didcot, UK, [5]Oxford Instruments NanoAnalysis, High Wycombe, UK
653 Tilted multislice approach for quantitative STEM simulation
Xian Li[1], Changlin Zheng[1]
[1]State Key Laboratory of Surface Physics and Department of Physics, Fudan University, Shanghai, China
655 4DSTEM-in-SEM by placing a pixelated detector below the sample
Johannes Müller[1], Christoph T. Koch[1]
[1]Department of Physics & IRIS Adlershof, Humboldt-Universität zu Berlin, Berlin, Germany
698 Low dose and in situ 4D-STEM powered by real-time sparse-array analytics on an event-driven detector

Penghan Lu[1], Yucheng Zou[1], Tingting Yang[1], Janghyun Jo[1], Deli Kong[1], Dieter Weber[1], Alexander Clausen[1], Matthew Bryan[2], Dmitry Byelov[3], Giuseppe Spano[3], Thorbjörn Schönbeck[3], Rafal E. Dunin-Borkowski[1]
[1]Ernst Ruska-Centre for Microscopy and Spectroscopy with Electrons, Forschungszentrum Juelich, Juelich, Germany, [2]Université Grenoble-Alpes, CEA, Leti, , France, [3]Amsterdam Scientific Instruments, Amsterdam, The Netherlands

703 ePattern: an adaptive 4D-STEM Pattern Registration Algorithm to Optimize ACOM Pattern Matching

Dr. Arnaud Demortière[1,2], Dr. Nicolas Folastre,[1,2], Junhao Cao[1,2], Dr. Arash Jamali[1], Fayçal Adrar[1,2]
[1]Laboratoire de Réactivité et Chimie des Solides (LRCS) CNRS UMR7314, Amiens, France, [2]Réseau sur le Stockage Electrochimique de l'Energie (RS2E) CNRS FR3459. , Amiens, France

726 Evaluating spherical models of EBSD patterns for forward modelling indexing

Dr René De Kloe[1], William Lenthe[2], Stuart Wright[2], Matt Nowell[2]
[1]EDAX-Gatan, Tilburg, The Netherlands, [2]EDAX-Gatan, Pleasanton, USA

740 Revealing the vacancy ordering in Prussian blue analogues through serial electron diffraction

Mr Shihui Feng[1], Dr Hanna Boström[1], Dr Cheuk-Wai Tai[1]
[1]Department of Materials and Environmental Chemistry, Stockholm University, Stockholm, Sweden

757 EBSD analysis of twin boundaries of prismatic calcite in oyster shells

Dr Katarzyna Berent[1], Prof. Kinga Nalepka[2], Prof. Antonio Checa[3,4]
[1]AGH University of Krakow, Academic Centre for Materials and Nanotechnology, Krakow, Poland, [2]AGH University of Krakow, Department of Strength and Fatigue of Materials and Structures, Krakow, Poland, [3]Universidad de Granada, Departamento de Estratigrafía y Paleontología, Granada, Spain, [4]CSIC-Universidad de Granada, Instituto Andaluz de Ciencias de la Tierra, Armilla, Spain

789 3D Electron Diffraction Study on the Local Structure of a doped Metal-organic Framework TCNQ@ZIF-4

Dr. Jianbo Song[1], Dr. Zhehao Huang[1]
[1]Department of Materials and Environmental Chemistry, Stockholm University, Stockholm, Sweden

816 Simultaneous Indexing of Spot and Kikuchi Patterns in Scanning Electron Microscopy (SEM)

PhD Student Yuxuan Zhang[1], Senior Researcher Alice Bastos da Silva Fanta[1], Professor Jakob Schiøtz[2]
[1]DTU Nanolab, Technical University of Denmark, Lyngby, Denmark, [2]DTU Physics, Technical University of Denmark, Lyngby, Denmark

845 Impact of improved tracking method on structure determination of perovskites from 3D ED data

Dr. Magdalena Cichocka[1]
[1]Technische Universität Darmstadt, Darmstadt, Germany

855 Achieving High-Resolution Electron Nano-crystallography using HVEM and PED

Master Sang-gil Lee[1], Doctor Seung Jo Yoo[1], Doctor Jin-Gyu Kim[1], Doctor Hyung Joong Yun[1]
[1]Korea Basic Science Institute, Daejeon, South Korea

931 Direct observation of charge modulation in nanoprecipitates by 4D STEM

Dr. Juhyun Oh[1], Prof. Young-Woon Kim[1], Prof. Cheol-Woong Yang[2], Prof. Cheol-Hee Ahn[1], Prof Miyoung Kim[1]
[1]Department of Materials Science and Engineering, Seoul National University, Seoul, Korea, [2]Department of Materials Science and Engineering, Sungkyunkwan University, Suwon, Korea

972 Characterization of Precipitates in Petroleum Steels by Using Precession Electron Diffraction Technique

Umut Savaci[1], Servet Turan[1]
[1]Department of Materials Science and Engineering, Eskisehir Technical University, Eskisehir, Türkiye

995 Detection of quasicrystalline symmetries in electron diffraction data

Oskar Ryggetangen[1], Dr. Ruben Bjørge[2], Dr. Sigurd Wenner[2], Prof. Randi Holmestad[1]
[1]Department of Physics, Norwegian University of Science and Technology, Trondheim, Norway, [2]Department of Materials and Nanotechnology, SINTEF Industry, Trondheim, Norway

997 Ultrafast Microbeam Electron Diffraction at 15-keV

Johannes Otto[1,2,3], Leon Brauns[1,2], Rudolf Haindl[1,2], Jan Gerrit Horstmann[1,2], Armin Feist[1,2], Murat Sivis[1,2], Claus Ropers[1,2,3]
[1]Department of Ultrafast Dynamics, Max Planck Institute for Multidisciplinary Sciences, Göttingen, Germany, [2]4th Physical Institute, University of Göttingen, Göttingen, Germany, [3]Max Planck School of Photonics , ,
1026 Differentiation of phases in phase change memory materials using 4D STEM
Xue Bai[1], Dr. Janghyun Jo[1], Prof. Dr. Rafal E. Dunin-Borkowski[1]
[1]Ernst Ruska-Centre for Microscopy and Spectroscopy with Electrons, Forschungszentrum Jülich, Jülich, Germany
1032 Anomalous effects of strain in selected area diffraction patterns due to boron doping in silicon
Miss Kaviyadharshini Dhamotharan[1], Dr Buddhika Mendis[1]
[1]Durham University , Durham, United Kingdom
1045 Electron Diffraction on Biological Samples
Ing. Vendula Hrabalová[1], dr. Jaromír Bačovský[1], Ing. Radka Martínková[1], Helmut Gnaegi[2]
[1]Delong Instruments, Brno, Czech Republic, [2]Diatome Ltd., Port, Switzerland
1149 Impact of In Situ and Ex Situ Annealing on Al-Cu Heterogeneous Nanostructures: A Comparative Study
Lucia Bajtosova[1], Elena Chochoľaková[1], Barbora Kihoulou[1], Jan Hanuš[1], Miroslav Cieslar[1]
[1]Faculty of Mathematics and Physics, Charles University, Ke Karlovu 3,12116, Prague, Czech Republic
1248 TEM strain measurement methods on SiGe/Si films for accuracy tests

Late Poster Presentation

Dr. Roberto Balboni[1], Prof. Matteo Ferroni[1,2], Dr. Fabiola Liscio[1], Dr. Anacleto Proietti[3], Dr. Chiara Mancini[3]
[1]CNR-IMM, Bologna, Italy, [2]University of Brescia, Brescia, Italy, [3]University of La Sapienza, Roma, Italy
1261 Combining 3D-ED and Z-contrast imaging: crystallographic structure solution of Ca2MnO3Cl
Dr Stéphanie Kodjikian[1], Dr Christophe Lepoittevin[1], Dr Fabio Denis Romero[1]
[1]Univ. Grenoble Alpes, CNRS, Grenoble INP, Institut Néel, 38000 Grenoble, France
1277 Evaluating the Efficacy of Laboratory-Based X-ray Diffraction Tomography for Crystallographic Analysis in Pure Iron
Postdoc Fellow pardis Mohammadpour[1,2], PhD student Mehdi Mosayebi[1,2,3], Research scientist Daniel Paquet[3], Research scientist Pierre-Antony Deschênes[3], Research scientist Laurent Tôn-Thât[3], Facilities Manager Brian Langelier[1], Proffesor Nabil Bassim[1,2]
[1]Canadian Center for Electron Microscopy, Hamilton, Canada, [2]Materials Science and Engineering Department, McMaster University, Hamilton, Canada, [3]Hydro-Québec, Institut de recherche d'Hydro-Québec, Varennes, Canada

1198

Data analysis workflows to measure material properties and structure using 4D-STEM

Colin Ophus[1], Stephanie Ribet[1], Georgios Varnavides[1,2], Steven Zeltmann[3], Karen Bustillo[1], Alexander Rakowski[1], Benjamin Savitzky[1], Min Chen[2], Yang Yang[2], Andrew Minor[1,2], Mary Scott[1,2]
[1]Lawrence Berkeley National Laboratory, Berkeley, USA, [2]University of California Berkeley, Berkeley, USA, [3]Cornell University, Ithaca, USA

IM-06 (1), Lecture Theater 1, august 29, 2024, 14:00 - 16:00

Background including aims
Scanning transmission electron microscopy (STEM) has become an essential tool for materials science research, where it has been applied to atomic-scale imaging, diffraction, spectroscopy, and 3D tomography of many materials. High speed direct electron detectors have now become ubiquitous, allowing researchers to record full 2D diffraction patterns for each electron probe position in a 2D grid, producing very large 4D-STEM datasets [1]. Extracting material properties and structures from 4D-STEM datasets requires efficient and robust software methods. In this talk, I will highlight various 4D-STEM analysis workflows using our open source py4DSTEM toolkit [2].

Methods
The py4DSTEM toolkit is an open-source python library hosted on GitHub, along with many tutorials and example datasets. It contains various analysis modules including those aimed at calibration, classification, diffraction pattern simulation and matching, Bragg diffraction analysis, amorphous diffraction analysis, phase contrast imaging, and others. To analyze nanobeam diffraction patterns generated by crystalline samples, we use template matching for disk detection, correlation for orientation mapping, and lattice fitting to measure strain [2,3]. Phase contrast imaging modes are implemented using iterative gradient descent with regularization [4].

Results
We have performed high resolution 4D-STEM strain mapping on metallurgical samples and energy materials, both ex situ and in situ. We have also demonstrated improved precision and accuracy for nanobeam strain measurements by using patterned apertures [5]. We have also used 4D-STEM to characterize the morphology of highly beam-sensitive soft matter samples, including block copolymers with both crystalline and amorphous constituent phases. We have also used dictionary lookup methods to determine the crystalline phases of complex samples, and machine learning methods for blind estimation of crystal systems, space groups and lattice constants. Finally, we have also used STEM phase contrast imaging methods to measure the atomic structure of materials in 2D and 3D. I will show how each of these results were generated using the py4DSTEM code. I will also demonstrate how modern machine learning methods can be used to analyze the most challenging 4D-STEM experiments: those where multiple scattering and dynamical effects from thick samples produce highly nonlinear diffraction contrast.

Conclusion
While 4D-STEM is a powerful tool to characterize the material structure and properties, modern high speed electron detectors produce a truly prodigious amount of data. These experiments therefore require highly robust and efficient software analysis tools to analyze the results. We have implemented many algorithmic methods in the open source py4DSTEM code, and we welcome additional contributions from the microscopy community.

Keywords

Scanning Transmission Electron Microscopy, 4D-STEM, Electron Diffraction

Graphic

(top) Geometry of a 4D-STEM experiment where many diffraction patterns are recorded from a sample. (bottom) Examples of analysis methods implemented in py4DSTEM. Adapted from [2].

References

1. C Ophus, Microscopy and Microanalysis 25, 563 (2019).
2. B Savitzky et al., Microscopy and Microanalysis 27, 712 (2021).
3. C Ophus et al., Microscopy and Microanalysis 28, 390 (2022).
4. G Varnavides*, SM Ribet*, et al., arXiv:2206.08958.
5. SE Zeltmann et al., Ultramicroscopy 209, 112890 (2020).

1196

Exploiting dynamical diffraction theory in the crystal structure determination from 3D electron diffraction data

Dr. Lukas Palatinus

IM-06 (2), Lecture Theater 1, august 30, 2024, 10:30 - 12:30

8

Role of phonon and plasmon inelastic scattering on Bragg diffracted beam intensities

Budhika Mendis[1]
[1]Dept of Physics, Durham University, , UK

IM-06 (1), Lecture Theater 1, august 29, 2024, 14:00 - 16:00

The strong interaction of an electron beam with matter has enabled 3D electron diffraction of specimens that are otherwise too small for X-ray analysis. For improved crystal structure refinement it is known that the Bragg diffracted beam intensities must be calculated dynamically, rather than kinematically. Inelastic scattering, especially low energy phonon and plasmon excitations with relatively large cross sections, are also unavoidable. Bloch wave models for high energy electron diffraction can however deal with only phonon losses phenomenologically, i.e. thermal diffuse scattering (TDS) is modelled by introducing an imaginary term to the crystal potential, which has the undesirable effect of depleting the electron beam intensity as it propagates through the specimen. Furthermore, there is as yet no method for including plasmons in Bloch wave calculations.

Here Monte Carlo methods are combined with Bloch waves to calculate the inelastic scattering due to phonons and plasmons. The Monte Carlo approach treats the incident electron as a particle, and relies on computer generated random numbers to estimate parameters such as the scattering path length and scattering angles. Since it assumes particle-like behaviour, it is only valid for highly delocalised scattering events such as phonon and plasmon excitations. In such cases the periodic nature of the incident electron in the crystal (i.e. Bloch wave) will be averaged out and therefore has no effect on the scattering. The diffuse scattering is simulated by rigidly shifting the Bragg diffraction spots over reciprocal space; the direction of shift and magnitude of diffuse intensity being determined by the inelastic scattering vector and cross section respectively. Simulated phonon and plasmon diffuse scattering distributions show striking similarities with experiment. For example, the TDS exhibit Kikuchi lines and bands (see figure), while the plasmon diffuse scattering shows ‘halos’ around the Bragg beams. Furthermore, unlike the phenomenological Bloch wave model there is no loss in electron beam intensity due to inelastic scattering.

The new Bloch wave model as well as experiment are used to determine the role of inelastic scattering on Bragg beam intensities. Energy filtered diffraction patterns were acquired from a 1990 Å thick, [110]-Si specimen at single and double plasmon energy losses, as well as at ‘zero’ loss (due to the limited energy resolution energy filtering cannot remove phonon losses). The unscattered beam intensity was found to decrease with increasing energy loss, although the Bragg diffracted beam intensities remained constant within the measurement error. It should be noted that the total intensity for each diffraction pattern was normalised and that no background subtraction was performed, i.e. the diffuse scattering around each Bragg reflection was included in the intensity for that beam. The same trends were also reproduced with the inelastic Bloch wave calculations. For crystal structure refinement the unscattered beam is often ignored and only the relative intensities of the diffracted beams are utilised. Both theory and experiment indicate that the relative intensities are unchanged provided that the diffuse background is not subtracted and correctly assigned to the relevant Bragg reflection. This highlights the importance of the diffuse background in energy unfiltered 3D electron diffraction. To ensure crystal structure refinement is robust to inelastic scattering the diffuse background must be included in the intensity measurements.

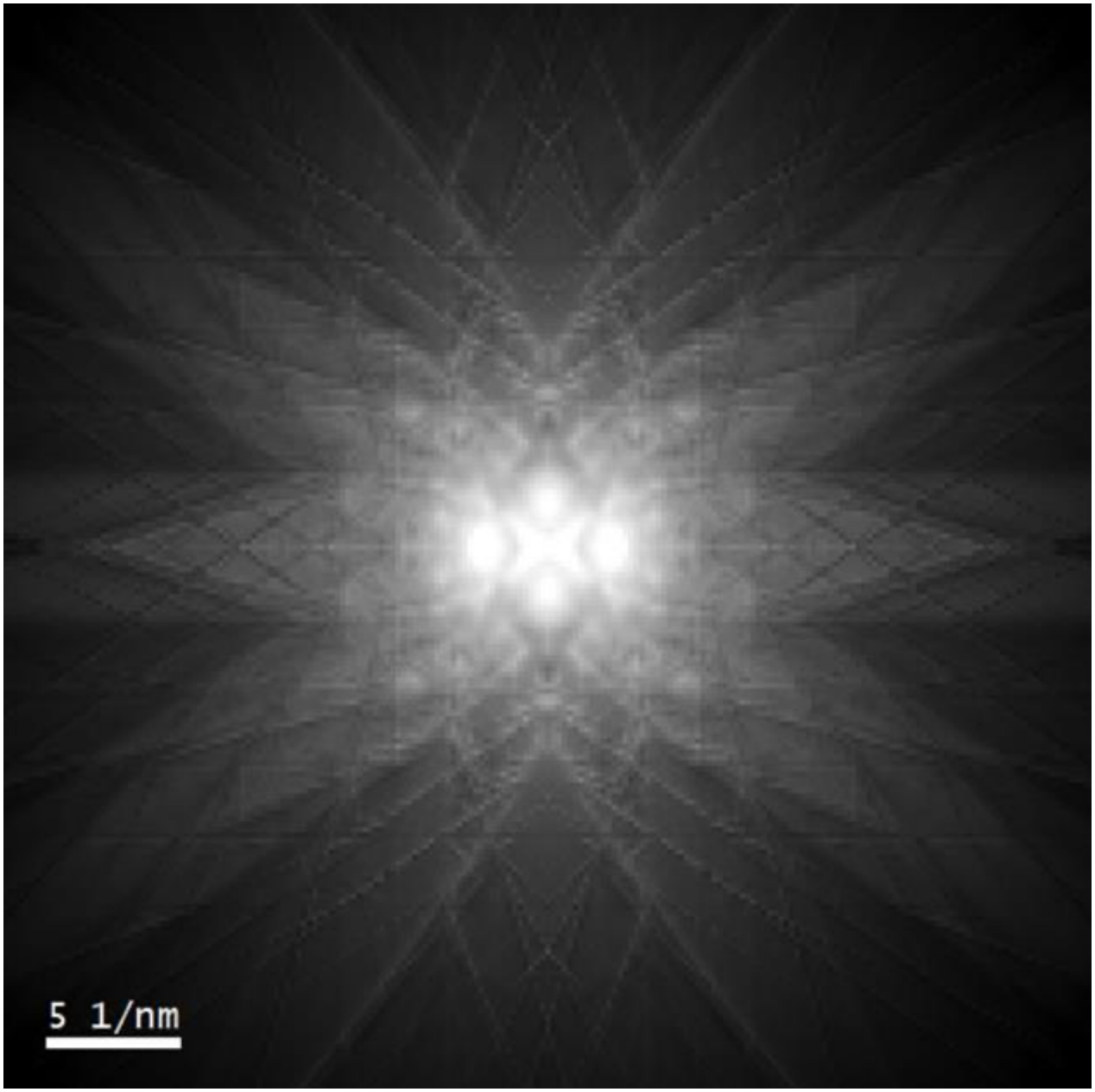

Keywords:

Bloch waves, phonons, plasmons

158

Breaking barriers: Innovative methods for 4DSTEM diffraction data acquisition and processing in SEM

Nikita Denisov[1], Mr. Andrey Orekhov[1], Mr. Johan Verbeeck[1]
[1]EMAT, University of Antwerp, Antwerp, Belgium

IM-06 (1), Lecture Theater 1, august 29, 2024, 14:00 - 16:00

Background incl. aims
Electron diffraction is a reliable tool to obtain information about the crystalline structure of nanoscale materials. With the recent emergence of more sensitive detector technology (Direct electron detectors e.g., Timepix and Medipix) the requirement for the dose applied to the sample in experiment drastically decreases.
Diffraction requires a far simpler setup as compared to conventional transmission electron microscopy as the diffraction pattern can be obtained without any lenses. This lends itself ideally to an implementation in a conventional SEM tool having several advantages such as providing more space for sample stimuli and manipulation, lower cost, and much smaller footprint. Typically, the acceleration voltage in SEM is lower compared to TEM. However, in the past years the tendency for particles' size decrease can be observed and SEM could become an attractive alternative to TEM for such materials.

Rather than taking a single diffraction pattern, the combination of a SEM tool and a fast direct electron detector allow for the efficient acquisition of 4DSTEM diffraction data, having a diffraction pattern for each probe position in a STEM scan.

There are however a few challenges:
- A lower acceleration voltage compared to TEM leads to a decrease of maximum sample thickness that can be used.
- The field of view in a SEM is much larger than in TEM. On the one hand, this is advantageous to gather statistical information on a much higher number of particles. On the other hand, a large part of this field of view is often empty resulting in long recording times with large portions of the data being empty.
- Distinguishing diffraction reflexes from the background can become challenging at the reduced acceleration voltage. This reduces the intensity of the reflections and results in poor averaged diffraction patterns which are dominated by the background signal.

To negotiate these issues new methods for data acquisition and processing should be developed. In the current work we aim to push the limit of transmission electron diffraction in SEM, mitigate beam damage and sample contamination, to make SEM a versatile tool for a high-resolution electron diffraction structure investigation.

Methods
Experiments made on a Tescan Mira FEG SEM. Diffraction data collected via an Advacam AdvaPix. Sample manipulated by custom stage of 3 Xeryon linear piezo motors in XYZ configuration mounted on rotation stage for tomography. Data processing is done in Hyperspy, controls are made with Python, image denoising is achieved with a convolutional neural network, Edge detection is realized with OpenCV.

Results
To reduce the acquisition time and avoid empty areas in the 4DSTEM dataset we use a fast overview scan from which we detect all particles positions and shapes with computer vision. In a second step

we determine a scan pattern to visit only those areas which likely to give diffraction patterns. We call this approach ROI 4DSTEM: each detected particle is marked with a bounding box. We then use the assumption that particles or agglomerated particle sets tend to be much thinner on their outer boundaries as compared to their centers. These boundaries are therefore the ideal positions to get good quality diffraction data from if the assumption holds that the core of the particles is the same crystal structure as its perimeter area. We call this method Edge Detected 4DSTEM. By utilizing image denoising via a modern convolutional neural network and edge detection algorithms we were able to create with high precision a mask of scan positions that is later used to position the incident beam only at those areas that most likely will lead to good quality diffraction patterns.
This approach allows us to perform 4DSTEM in SEM in a much more effective manner. Indeed, for a standard 4DSTEM raster scan of 1024x1024 scan positions we would get 1,048,576 diffraction patterns, or approximately 182 GB of data to store and 18 minutes to collect all this data at 1 ms exposure time. In our ED4DSTEM method, we only collect 23,000 positions, resulting in 4 GB of data and 23 seconds of total recording time for the same 1ms exposure time. This is almost 50 times faster/more efficient as compared to conventional raster scanning resulting in a significant reduction of beam damage and contamination on top of the benefit of pre-filtered diffraction data of much higher average quality.
By processing each individual diffraction pattern and storing only the peak positions and their intensities we can obtain a massive data reduction that considerably simplifies the following data analysis steps. This reduced dataset can then be used for any kind of diffraction analysis. In our case we are collecting “virtual” ring patterns as a radially integrated histogram of the scattering angle of all observed peaks, weighted by their intensity. This method has the advantage of suppressing the background in the diffraction pattern that originated from substrate/noise/amorphous content in the sample that otherwise would dramatically deteriorate the quality of a position averaged diffraction pattern. An added benefit is the sub-pixel position accuracy that can compensate for beam convergence and pixel size effect.

Conclusion

In this work we present methods that allow for more effective 4DSTEM diffraction data acquisition on dispersed crystalline nanoparticles at low acceleration voltages as well as methods for more reliable data processing. Our method, compared to conventional 4DSTEM raster scan, drastically decreases the total 4DSTEM acquisition time, beam damage and contamination while providing a dramatic data reduction in the process that could significantly simplify follow the data analysis. These approaches are also amenable to TEM and could be especially useful in case of beam-sensitive objects.

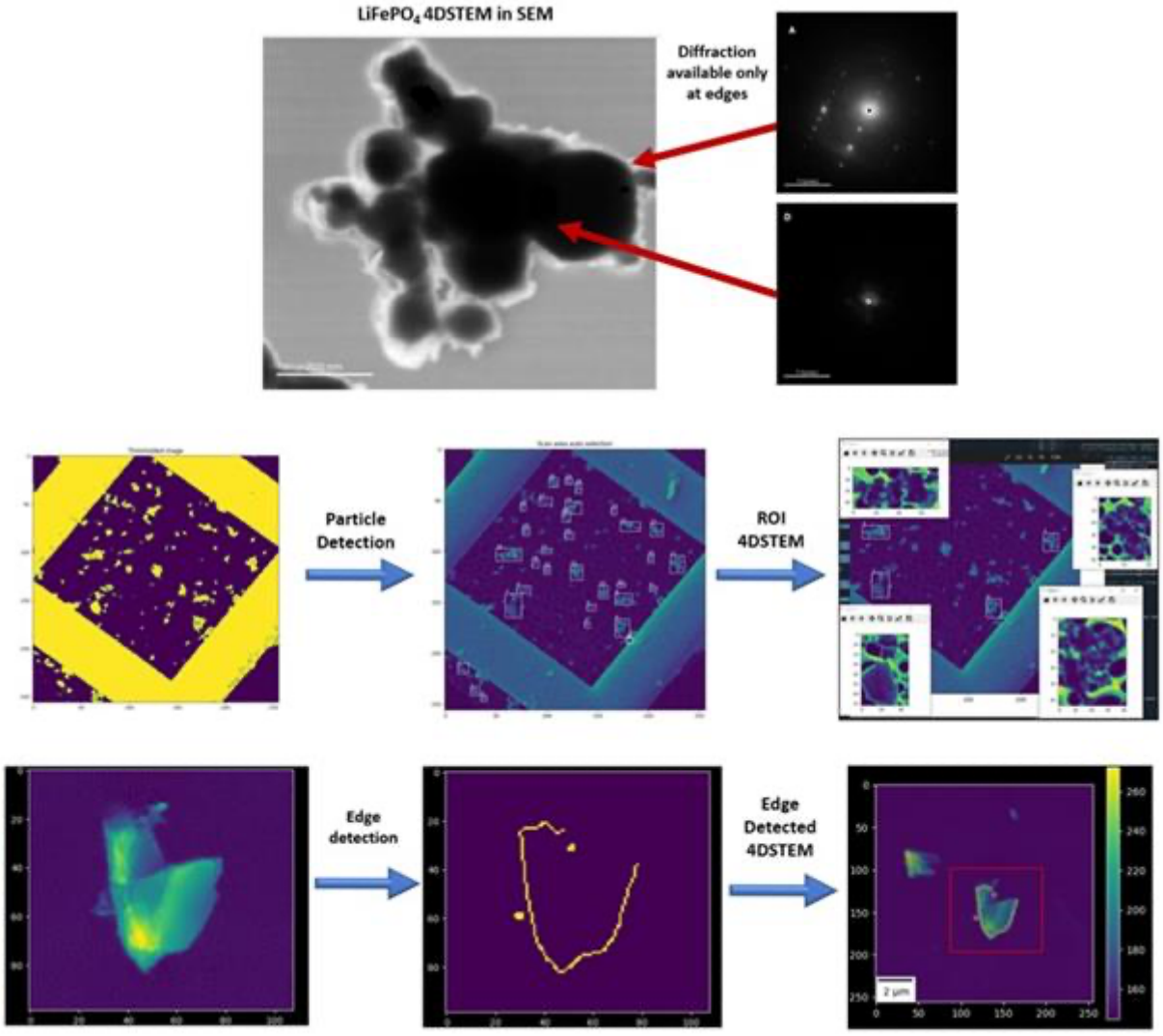

Keywords:

4DSTEM, SEM, TEM, EdgeDetection, ImageRecognition

Reference:

[1] A. Orekhov et al. https://doi.org/10.48550/arXiv.2011.01875
[2] I. Lobato et al. https://doi.org/10.1038/s41524-023-01188-0
[3] G. Bradski - The OpenCV Library. Dr. Dobb's Journal of Software Tools, 2000
[4] Hyperspy package. https://doi.org/10.5281/zenodo.592838
[5] The authors acknowledge the financial support of the Research Foundation Flanders (FWO) project SBO S000121N

742

Scanning precession electron diffraction tilt series for orientation analysis

Prof. Dr. Ir. Antonius (Ton) van Helvoort[1], Mr. Viljar J. Femoen[1], MSc Anders C. Mathisen[1], Ms Kaja E. Aune[1], Dr. Emil F. Christiansen[1], Dr. Inger-Emma Nylund[2], Dr. Tina Bergh[1,3], Dr. Ruben Bjørge[1,4]
[1]Department of Physics, Norwegian University of Science and Technology (NTNU), Trondheim, Norway, [2]Department of Materials Science and Engineering, Norwegian University of Science and Technology (NTNU), Trondheim, Norway, [3]Department of Chemical Engineering, Norwegian University of Science and Technology (NTNU), Trondheim, Norway, [4]Materials and Nanotechnology, SINTEF Industry, Trondheim, Norway , Trondheim, Norway

IM-06 (1), Lecture Theater 1, august 29, 2024, 14:00 - 16:00

Identifying the orientation of crystalline phases at the nanometer scale is relevant for understanding materials properties. Here we will demonstrate that collecting and processing scanning precession electron diffraction (SPED) datasets collected at a few different specimen tilts can improve the accuracy of template-based orientation mapping [1,2]. In addition, the tilt series allows complete determination of the relation between the specimen crystallographic setting and the goniometer axes. This insight, combined with the orientation map, can be used in a convenient semi-automatic approach to predict the tilts required to reach a target specimen orientation for further structure analysis.

SPED of different polycrystalline systems (Si, Ag, and oxides) were recorded in a JEOL JEM2100F with a NanoMegas DigiStar precession system and a Quantum Detectors MerlinEM direct electron detector. Scans were taken over areas up to 15 x 15 µm containing 10's of grains using a nominal precession angle of 1˚. Tilts series using one or two axes contained 3-5 tilts in the range 0 - 20˚ from the initial flat specimen position. For data analysis and visualization, we used primarily the open-source python library pyxem [3].

The indexed frames, taken at different tilts, were compared, after manually aligning the frames, using the set tilt as expected misorientation. Together with considering as well the best 5 to 25 normalized cross correlations between the experimental patterns and the simulated pattern bank, orientation-dependent misindexations can be identified and the orientation estimate refined. Compared to the standard approach of collecting SPED using only a single specimen tilt and the best correlation scores for each pattern, the tilt series approach reduces indexation variations within grains. This gives a more uniform representation of the grains in the final orientation maps.

The accuracy of the refined orientation analysis can be determined with a known orientation relation, here for example Σ3 twins in face-centered cubic and diamond crystal systems. The misorientation deviation between the measured and expected misorientation between twin domains is used as the metric [4]. The found accuracy is below the used precession angle.

The refined orientation mapping based on a small tilt series has a further practical use. From a single axis tilt series, the position of the two perpendicular tilt axes can be determined. As the tilt series is small and over a limited angular range, sufficient probe positions must be used to accurately determine the tilt axis position. Misaligned between frames and areas with overlap, such as grain boundary areas, were excluded through thresholding. A second tilt axis series or grains correctly indexed in different frames can be used to verify the found axes positions. Using the determined orientation of a grain together with the deduced axes positions, the tilts to reach a target zone for a grain can be predicted. Based on tests on different TEMs and holders, the target zone was within 2˚. In the tests the specimen was placed at approximately the same rotation relative to the holder axes. However, should the specimen be differently placed compared to where the orientation was mapped out, an additional transformation matrix can be included in the navigation tool to recalculate the target tilts for the given specimen placing. This correction is based on a manual estimation of

misorientation from the tilts to the actual target zone, diffraction (using the Laue circle), or imaging (assuming in-plane rotation).
To conclude, template matching based on multiple SPED scans at a few varying specimen tilts improves the accuracy and the final orientation visualization. In addition, the approach is used to make a practical navigator tool that widens to use of template matching results for subsequent lattice imaging and further crystallographic analysis. With the advancements in automatic scan controls, faster detectors and optimized transparent open-source routines, the benefits gained will more than compensate for the drawbacks of acquiring and processing multiple scans.

Keywords:

Texture, diffraction, open-source, template-matching, ACOM

Reference:

[1] E.F, Rauch et al., Z. für Kristall. 225 (2010), p. 103. doi:10.1524/zkri.2010.1205
[2] N. Cautaerts et al., Ultramicr. 237 (2022), p. 113517. doi:10.1016/j.ultramic.2022.113517
[3] D. Johnstone et al., Zenodo (2024), 10551678. https://zenodo.org/records/10551678
[4] Q. Shi et al., Meas. Sci. Technol. 35 (2024), 045030. doi:10.1088/1361-6501/ad204d
[5] The Research Council of Norway is acknowledge for support to the Norwegian Center for Transmission Electron Microscopy, NORTEM (197405).

750

Solving the crystallographic phase problem by linearizing dynamical electron diffraction

Prof. Christoph Koch[1], Sam Fairman[1], Grigory Kornilov[1], Dr. Benedikt Haas[1], Dr. Niklas Delby[2]
[1]Humboldt-Universität zu Berlin, Dept. of Physics & Center for the Science of Materials Berlin, Berlin, Germany, [2]Bruker AXS (formerly Nion Co. R&D), Kirkland, USA

IM-06 (1), Lecture Theater 1, august 29, 2024, 14:00 - 16:00

Background and aims

In contrast to kinematical diffraction intensities, which are insensitive to the phases of structure factors, dynamical diffraction intensities, as observed in most electron diffraction patterns, encode sums of phases of structure factor triplets and higher order multiplets, i.e. sets of structure factors for which the sum of the corresponding reciprocal lattice vectors vanishes. The scattering matrix S(kt)n,m = [exp(iTA(kt)]n,m, which is given by the matrix exponential of the product of the wavelength-scaled specimen thickness T and the structure factor matrix A(kt), the diagonal of which depends on the incident beam tilt kt, can be expanded to a sum of monomials in the structure factors, as shown in eqn. (1) [1] with the C-coefficients given by expression (2) and examples by expressions (4). Having diffraction data for multiple angles of incidence for a tilt range of several tens of mrad along kx and ky [2] allows the T- and kt-dependent C-coefficients (eqns. (3) & (4)) to be different enough, so that the individual monomials can be determined. For thicker specimen, the expansion order q would be very high, so a stacking of layers with a limited expansion order is proposed.

Methods

Large-angle rocking-beam electron diffraction (LARBED) [2] is a technique which can be used to acquire 2D rocking curve information from nearly arbitrarily small areas of the specimen for beam tilt angles of up to +/- 100 mrad in both tilt dimensions, and more, if the specimen is tilted as well. The diffracted intensities for every beam tilt are then extracted from these 4D datasets and the corresponding coefficients computed according to expression (2) [3]. In order to limit the number of terms in the linear set of equations, only coefficients of significant amplitude should then be kept. An alternative approach which also works for thicker specimen, is to consider the crystalline sample to consist of many identical layers that are stacked on top of each other, use a very limited expansion order (q = 1 is sufficient – in that case we call the approximation first-order expansion stacked Bloch wave (FOESBW) see eqn. (4)), but consider the structure factors in each layer to be independent from one another. This makes the complex scattering amplitude then a linear function in the structure factors, and a solution may then be found by solving this system of equations under the constraint that the structure factors in all of the layers are as close to each other as possible.

Results

Figure (a) shows a simulated LARBED pattern of GaN (110) (thickness 10 nm, acc. voltage 200 kV, max. g-vector 20 1/nm, as indicated by the white dash-dotted circle) on a logarithmic scale. The green dashed circle indicates the tilt range of the illumination during the LARBED simulation. Fig. (b) shows the central part of the diffraction pattern on a linear scale. The geometry of the representation of the LARBED dataset is illustrated by highlighting that the scale of the LARBED discs is 10 times larger than that of the distance between discs (descan = 0.9 [2]). Fig. (c) shows the structure of GaN in the (110) zone axis (1 x 2 unit cells are being displayed). Fig. (d) shows the original crystal potential simulated using independent atom scattering factors. Fig. (e) shows the crystal potential resulting from all 194 structure factors that have been reconstructed using the FOESBW approach. Fig. (f) shows a bandwidth-limited potential resulting from a set of structure factors that

was refined from the FOESBW-reconstruction using a simplex optimization of the full scattering matrix. The potential has been bandwidth limited to the resolution of the diffraction data (20 1/nm). All three potential maps are displayed using the same color map and -range. While these simulated results have also been presented in [3], we will also demonstrate the application to experimental data of various structures acquired using the Nion HERMES equipped with a Dectris ELA detector [4].

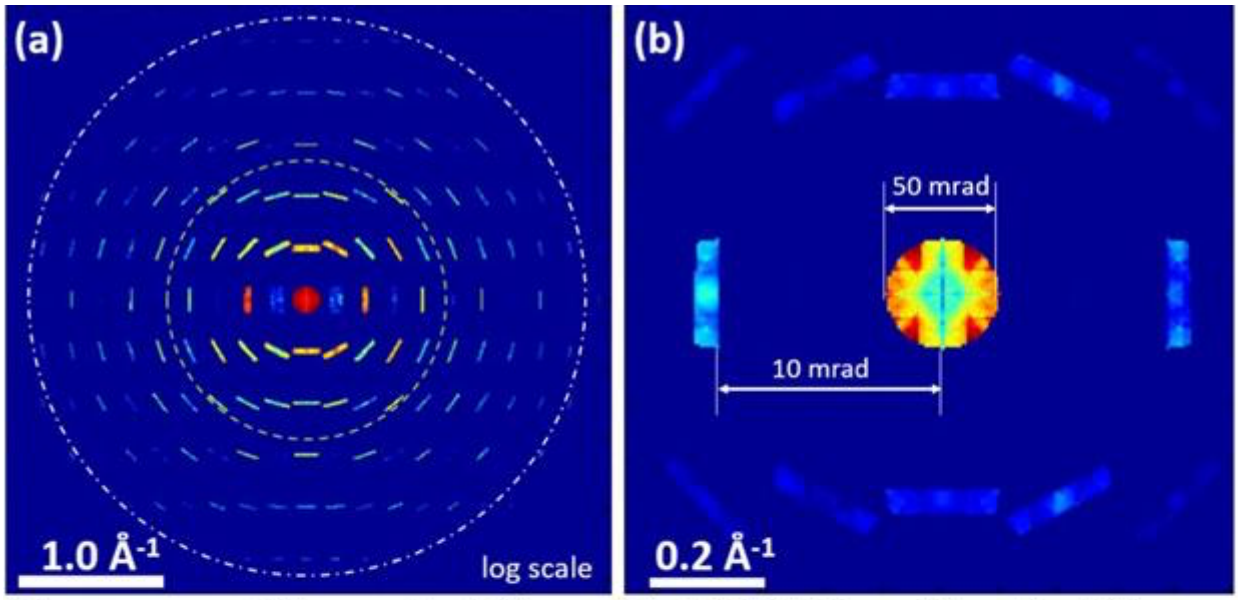

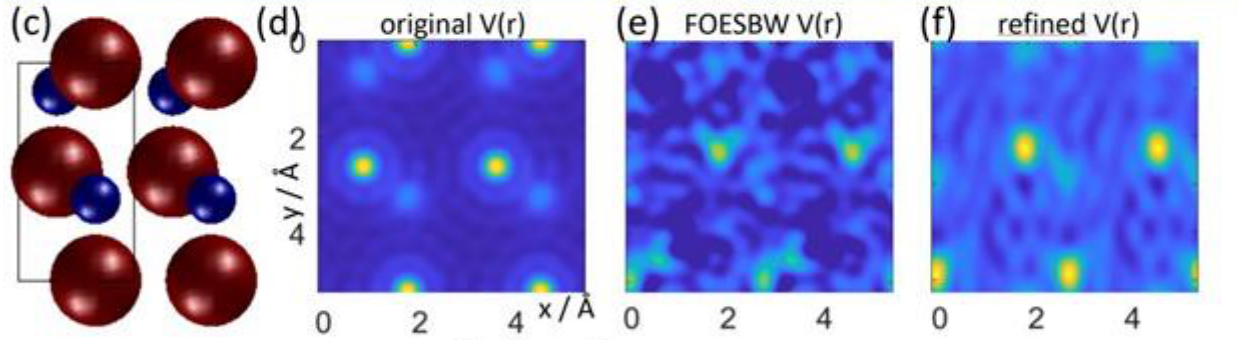

$$(1)\quad |S(T,\vec{k}_t)_{n,m}|^2 = |e^{Tb_n(\vec{k}_t)}\delta_{n,m} + \sum_{q=1}^{\infty}\sum_{l_1=0}^{N}\sum_{l_2=0}^{N}\cdots\sum_{l_{q-1}=0}^{N}\underbrace{U_{\vec{g}_n-\vec{g}_{l_1}}U_{\vec{g}_{l_1}-\vec{g}_{l_2}}\cdots U_{\vec{g}_{l_{q-1}}-\vec{g}_m}}_{q} C^q_{n,l_1,\ldots,l_{q-1},m}(T,\vec{k}_t)|^2$$

$$(2)\quad c^{q_1,q_2}_{n,l_1,\ldots,l_{q_1-1},h_1,\ldots,h_{q_2-1}}(T,\vec{k}_t) = C^{q_1}_{n,l_1,\ldots,l_{q_1-1},m}(T,\vec{k}_t)\cdot C^{q_2}_{n,h_1,\ldots,h_{q_2-1},m}(T,\vec{k}_t)^*$$

$$(3)\quad C^q_{n,l_1,\ldots l_{q-1},m} = \sum_{k=0}^{u}\sum_{j=0}^{d_k}\frac{T^j}{j!}D^{(j,k,q)}_{n,l_1,\ldots l_{q-1},m}\left[e^{Tb'_{l_k}} - \sum_{s=0}^{q-j-1}\frac{(Tb'_{l_k})^s}{s!}\right]$$

$$(4)\quad C^0_{n,m} = \delta_{n,m}\quad C^1_{n,m} = \frac{e^{Tb_n}-1}{b_n}\quad b_n = -(|\vec{g}_n|^2+2\vec{g}_n\cdot\vec{k})/\gamma\quad \gamma = 1+|e|v/m_0c^2$$

Keywords:

electron diffraction, crystallographic phase problem

Reference:

[1] C. Koch and J. Spence, “A useful disentanglement of the exponential of the sum of two non-commuting matrices one of which is diagonal”, J. Phys. A: Meth. Gen. 36 (2003) 803
[2] C.T. Koch, “Aberration-Compensated Large-Angle Rocking-Beam Electron Diffraction”, Ultramicroscopy 111 (2011) 828
[3] C.T. Koch, “Solving the crystallographic phase problem using dynamical scattering in electron diffraction”, Ultramicroscopy 247 (2023) 113701

[4] B. Plotkin-Swing, et al., „Hybrid pixel direct detector for electron energy loss spectroscopy“, Ultramicroscopy 217 (2020) 113067

1107

Simultaneous nanoscale mapping of strain and electric field in semiconductor heterostructures using 4D-STEM

Yucheng Zou[1], Dr. Lei Jin[1], Peng-Han Lu[1], Prof. Dr Rafal Dunin-Borkowski[1]
[1]Research Center Jülich, Jülich, Germany

IM-06 (1), Lecture Theater 1, august 29, 2024, 14:00 - 16:00

Background incl. aims
High-performance semiconductor devices are the basis of modern electronic equipment and have a very important impact on the processing, transmission and storage of information and energy fields. In many of those devices, the built-in electric field, depending on the distribution of dopants, plays a vital role in their performance and operating characteristics. On the other hand, introducing strain in the semiconductor structures, either during epitaxial growth or by external stresses, has been often used to optimize the functional properties of the semiconductor materials. Therefore, how to measure the electric field and strain at the nanoscale accurately and ideally simultaneously is crucial to the development and improvement of miniaturized semiconductor devices. Transmission electron microscopy (TEM) would be able to offer such a spatial resolution, but it is usually required to adopt different imaging modes to measure the strain and electric field. This would make it particularly difficult when measuring them during in situ straining experiments as the measured strain and electric field may not correspond to the same state over serial measurements.
The emergence of four-dimensional scanning transmission electron microscopy (4D-STEM) has enabled an alternative solution to measuring electromagnetic field and strain at the nanoscale. 4D-STEM, employing a pixelated electron detector for recording 2D images of convergent beam electron diffractions over a 2D grid of beam positions, offers a wide range of applications. Its resolutions in high-precision strain measurement and electromagnetic field determination can be up to the sub-nanometer scale. The technique allows nanoscale field mapping by measuring the center-of-mass (CoM) shift of the bright-field (BF) disk which is linearly proportional to the field, and the integration of CoM (iCoM) leads to the projected phase shift comparable to other techniques such as electron holography. For strain mapping, the variation of the reciprocal distance between a pair of diffraction disks is typically quantified to measure the strain.
Methods
Precession-assisted 4D-STEM dataset including both dark field disks and bright field disks were acquired. Precession was used to overcome the effect of dynamic diffraction. The long range electric field will cause a physical shift of the whole disk rather than the intensity redistribution inside the disks. In view of this, an edge detection method was used to determine the position of the diffraction disks, in contrast to the traditional CoM method. In theory, the shift of the bright disk is only caused by the electric field (EdgeBF), while the shift of the dark disks contain the effects from both electromagnetic fields (EdgeD¬¬¬¬_field) and the strain (EdgeD_strain). Since the EdgeD_strain in a pair of diffraction disks are equal in magnitude and opposite in direction, we can add the vectors of a pair of diffraction disks together and divide by two to obtain the pure contribution from the electrical field.

Results
Applying this method with semiconductor, the electric field and strain result are obtained simultaneously in a same 4dstem data. In principle, one pair of dark field spots are enough if they are the zone axis we want and uniform and bright enough, but if we can get 3 pairs of diffraction spots edge results respectively and average them up is also credible. In second figure, there is a demo experiment result with this method, the EdgeBF, from bright disk, is compared with the average

EdgeD¬¬¬¬_field, especially the profile and the difference in (d), the dark field is same direction of (b) and (c) in vertical, the (e),(f) and (g) is the strain along x and y direction.

Conclusion

In this contribution, we describe the procedure for decouple the influences attributed to strain and electromagnetic fields from the observed edge detection of a pair of diffraction patterns within a same 4D STEM dataset, as shown in the Figure. This procedure is applied with semiconductor samples to ensure the perfect correspondence between electric field and strain data acquired under identical conditions. After comparing with electric field from bright disk, the EdgeD_strain result is credible to some extent.

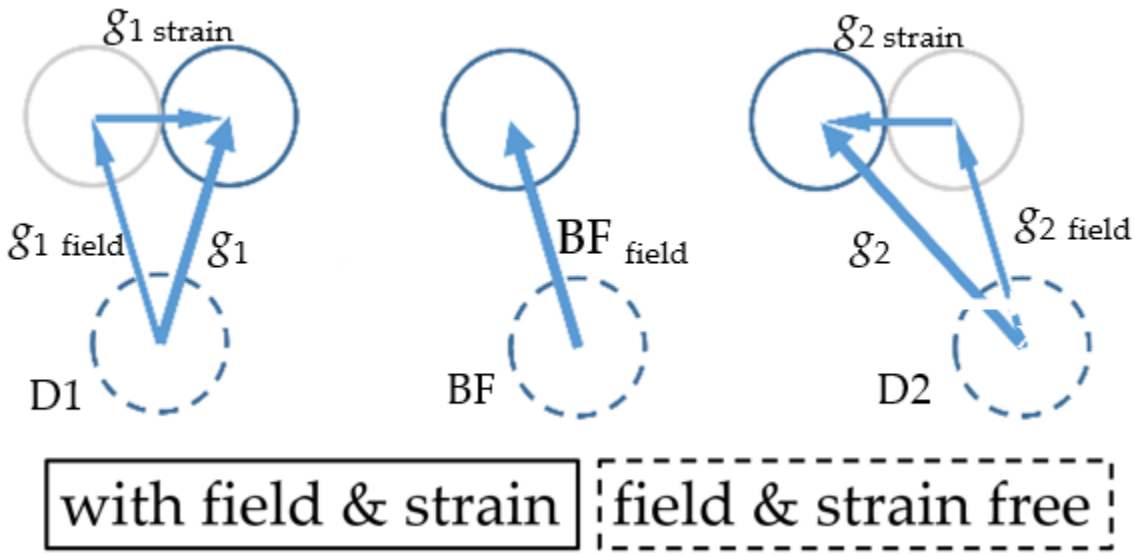

Keywords:

4DSTEM, Electric field, Strain, Semiconductors

Reference:

da Silva, Bruno César, et al. Nano Letters 22.23 (2022): 9544-9550.
Wortman, J, et al. Journal of applied physics 35.7 (1964): 2122-2131.
Armigliato, A., et al. Applied Physics Letters 93.16 (2008).
Béché, A., et al. Applied Physics Letters 95.12 (2009).

1119

Towards direct imaging of defects in carbon nanotubes with 4DSTEM

Dr. Antonin Louiset[1], Dr. Daniel FÖRSTER[2], Dr. Jean-Luc ROUVIERE[1], Dr. Vincent JOURDAIN[3], Dr. Christophe BICHARA[4], Dr. Hanako OKUNO[1]
[1]IRIG-MEM, CEA, Université Grenoble Alpes, Grenoble, France, [2]Laboratoire d'Etude des Microstructures, ONERA-CNRS, Université Paris-Saclay, Châtillon, France, [3]Laboratoire Charles Coulomb, CNRS, Université de Montpellier, Montpellier, France, [4]CINaM, CNRS, Université Aix-Marseille, Marseille, France

IM-06 (1), Lecture Theater 1, august 29, 2024, 14:00 - 16:00

4-dimensional scanning transmission electron microscopy (4DSTEM) based imaging techniques, in particular multislice electron ptychography, demonstrated unprecedented lateral spatial resolution while also providing depth-resolved imaging of the sample [1]. It is therefore, one of the most promising technique for 3D imaging of TEM samples at the atomic scale. Carbon nanotubes (CNT) are an ideal test subject for multislice ptychographic reconstructions using electron beams. While CNT atomic scale imaging can be achieved by high-resolution HR(S)TEM imaging, resolving their complex atomic structure is still a challenge, mainly because of the overlapping signal coming from both side of the tubes [2]. It becomes even more difficult when one wants to solve the structure of atomic defects inside CNTs. Here, we investigate the efficiency of 4DSTEM experiments combined with multiple iterative phase retrieval methods to resolved topological defects in CNTs. In particular, our goal is to resolve separately both sides of nanotubes using multislice ptychographic reconstructions of a single projection.

We used defective carbon nanotube structures, obtained by molecular dynamic calculations in a previous work [2], to simulate 4DSTEM datasets. Diffraction pattern simulations were computed using the open source abTEM package [3]. These simulated datasets serve two purposes: optimizing experimental conditions for high resolution imaging of nanotubes and evaluating the efficiency of phase retrieval algorithms. We performed phase images reconstruction using the open source py4DSTEM package [4], which features several iterative phase retrieval algorithms. We focused our work on the following methods: differential phase contrast, parallax, single and multislice ptychography [5]. 4DSTEM experiments were conducted on a double corrected TEM operating at 80kV and equipped with a Schottky field emission gun (X-FEG) and a direct electron detector. Experimental parameters were set as close to the optimum previously determined by simulations and phase images were reconstructed using the previously presented methods

In order to preserve tubes from contamination and irradiation damage, 4DSTEM experiments must be carried out in less than ideal conditions; i.e. low beam current (<20pA), short dwell time per pixel (<2ms), large real space step size (>1.5Å) and defocused STEM probe (tens of nm). In these conditions, the efficiency of the iterative ptychographic reconstructions strongly depends on the first guess given for the incident probe wave function. To optimize the determination of the initial probe parameters, i.e. defocus and residual aberrations, from experimental datasets, we computed differential phase contrast and parallax reconstructions [5], prior to the ptychographic reconstructions. We also acquired a vacuum probe reference in a separated dataset to constrain the incident wave function intensity. This method allowed the reconstructions to converge and strongly improved the resolution of CNTs images compared to high-resolution STEM images. However, phase images did not achieve the ultimate spatial resolution. Using simulated 4DSTEM datasets, we found out that both lateral and depth (in the case of multislice ptychography) resolutions were strongly degraded when dealing with partial temporal coherence, i.e. energy spread, of electron beams. The energy resolution of the microscope used in this study is limited to a FWHM of 1.5 eV. We showed

that with a greater energy resolution, which is available on microscopes equipped with a cold FEG gun for example, it is possible to improve lateral resolution and even perform CNT depth sectioning using multislice electron ptychography to capture a direct image of topological defects.

4DSTEM based high-resolution imaging techniques, are very promising to obtain direct imaging of topological defects in carbon nanotubes. By conducting two parallel studies, one based on simulation and one based on real 4DSTEM experiments, we were able to improve the resolution of CNT STEM images by performing iterative phase retrieval reconstructions. We demonstrated that 3D imaging of carbon nanotubes is even possible using multislice electron ptychography when the electron beam's energy spread is reduced. We argue that this limitation can be overcome by state-of-the-art-microscopes and improved reconstruction algorithms.

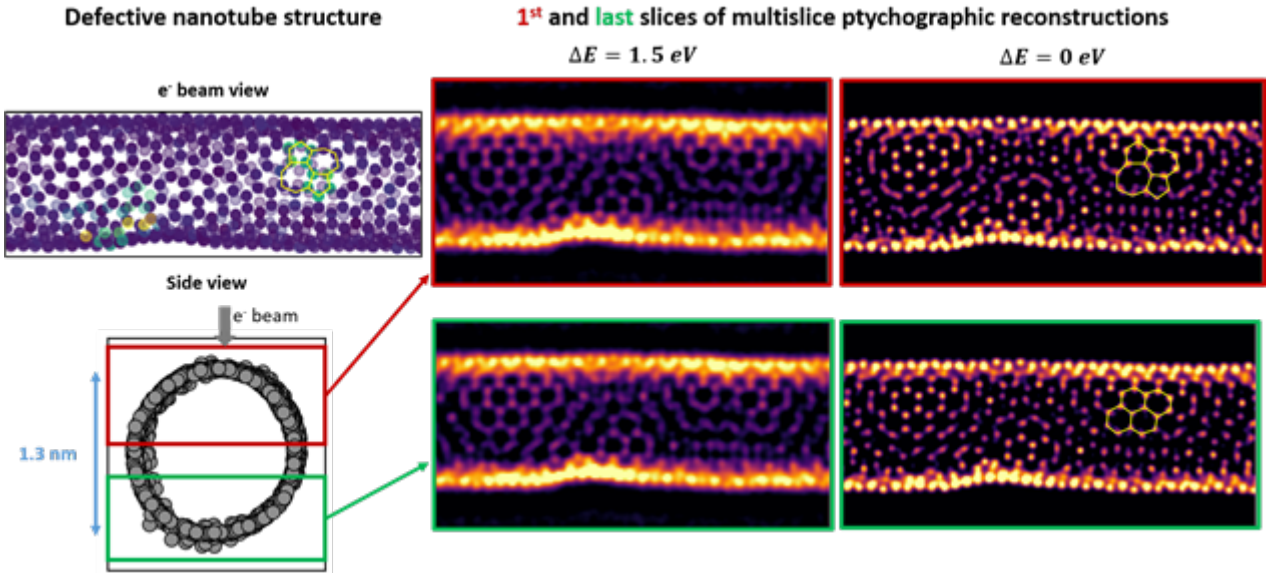

Keywords:

4DSTEM, electron ptychography, carbon nanotubes

Reference:

[1] Chen, Zhen, et al. "Electron ptychography achieves atomic-resolution limits set by lattice vibrations." Science 372.6544 (2021): 826-831.
[2] Förster, Georg Daniel, et al. "A deep learning approach for determining the chiral indices of carbon nanotubes from high-resolution transmission electron microscopy images." Carbon 169 (2020): 465-474.
[3] Madsen, Jacob, and Toma Susi. "The abTEM code: transmission electron microscopy from first principles." Open Research Europe 1 (2021).
[4] Savitzky, Benjamin H., et al. "py4DSTEM: A software package for four-dimensional scanning transmission electron microscopy data analysis." Microscopy and Microanalysis 27.4 (2021): 712-743.
[5] Varnavides, Georgios, et al. "Iterative Phase Retrieval Algorithms for Scanning Transmission Electron Microscopy." arXiv preprint arXiv:2309.05250 (2023).

12

Single Crystal Analysis of Nanocrystals by Three-Dimensional Electron Diffraction

Dr. Zhehao Huang[1]
[1]Stockholm University, Stockholm, Sweden

IM-06 (2), Lecture Theater 1, august 30, 2024, 10:30 - 12:30

X-ray diffraction is the predominant method used for structural determination of crystalline materials. However, challenges remain on structural analysis of nanocrystalline materials which are too small to be studied by single crystal X-ray diffraction. Three-dimensional electron diffraction (3DED) has been developed to tackle the challenges. By taking advantages of the strong interaction between electrons and matter, 3DED allows single crystal structural analysis even when the crystal sizes are down to the range of nanometers[1].
In this talk, I will give an overview of the development of low-dose 3DED method for analyzing fragile materials, where we overcome the challenges of electron beam damage to the compounds such as metal-organic frameworks (MOFs) and covalent-organic frameworks (COFs). I will talk about the high-throughput advantage of 3DED on discovery of new MOF materials among phase mixtures[2], and discovery of unknown layer stacking behavior in a 2D COF[3]. By using 3DED, I will further talk about how to probe molecular motions in MOF nanocrystals[4] and study host-guest interactions[5]. Last but not least, I will present our recent development on further reducing electron dose for studying fragile unknown compounds. We believe that using 3DED as a powerful analytical tool for discovering new compounds, and revealing their unique properties at an atomic level would help to accelerate research in physical and life science.
References:
[1] Yang, T.; Willhammar, T.; Xu, H.; Zou, X.; Huang, Z. Nat. Protoc. 2022, 17 (10), 2389–2413.
[2] Ge, M.; Wang, Y.; Carraro, F.; Liang, W.; Roostaeinia, M.; Siahrostami, S.; Proserpio, D. M.; Doonan, C.; Falcaro, P.; Zheng, H.; Zou, X.; Huang, Z. Angew. Chem. Int. Ed. 2021, 60 (20), 11391–11397.
[3] Kang, C.; Yang, K.; Zhang, Z.; Usadi, A. K.; Calabro, D. C.; Baugh, L. S.; Wang, Y.; Jiang, J.; Zou, X.; Huang, Z.; Zhao, D. Nat. Commun. 2022, 13 (1), 1370.
[4] Samperisi, L.; Jaworski, A.; Kaur, G.; Lillerud, K. P.; Zou, X.; Huang, Z. J. Am. Chem. Soc. 2021, 143 (43), 17947–17952.
[5] Ge, M.; Yang, T.; Xu, H.; Zou, X.; Huang, Z. J. Am. Chem. Soc. 2022, 144 (33), 15165–15174.

Keywords:

electron diffraction; electron crystallography

97

Exploring the limits of 3D ED for accurate structure analysis at the nanometer scale

Ms Sara Passuti[1], Ms Erica Cordero Oyonarte[1], M Valérie Pralong[1], M Adrian David[1], M Emmanuel Guilmeau[1], M Lukas Palatinus[2], Mr. Philippe Boullay[1]
[1]Normandie Université, ENSICAEN, UNICAEN, CNRS, CRISMAT, Caen, France , [2]Czech Academy of Sciences, Department of Structure Analysis, Na Slovance 2, Prague, Czechia

IM-06 (2), Lecture Theater 1, august 30, 2024, 10:30 - 12:30

Background incl. aims
The most common method for robust and reliable structure determination of materials is single crystal X-ray diffraction (SCXRD). However, it is not suitable for nanoparticles (NP) and nanodomains due to their size and geometry. When it comes to structural characterization on the scale of a few nanometers, electron microscopy offers an incomparable range of tools. In this contribution, we focus on accurate nanoscale crystallography using electron diffraction and, more specifically, precession-assisted 3D electron diffraction (3D ED), serial ED and scanning precession-assisted electron diffraction tomography (SPET). The aim is to test the limits of these parallel-beam electron diffraction methods for the accurate structure analysis of isolated NP and nanodomains measuring a few tens of nanometers or less.

Methods
For 3D ED on NPs and nanodomains, the first instrumental requirement appears to be the ability to form parallel beams well below 100 nm in size. If you want to collect single-crystal 3D ED data from a 10 nm domain embedded in a matrix, you must work with an electron nanobeam of this size or smaller. When the diffraction volume is greatly reduced, much lower diffracted intensities are expected. In this case, hybrid pixel detectors is a real asset for studying the size limit of NPs or domains for 3D ED experiments. For this work, our experimental setup is based on a JEOL F200 electron microscope equipped with a ASI Cheetah M3 hybrid-pixel detector. Beam precession movement, combined or not with beam scanning, is achieved via a Nanomegas DigiStar unit.

Results
The question of the lower limit of crystal size compatible with accurate structure analysis by 3D ED is briefly addressed with tests carried out on isolated Indium Tin oxide (ITO) and TiO2 nanoparticles around 10 nm in size. Our study provides experimental evidence that the effect of multiple scattering is still present but significantly reduced for tiny crystals. In such cases, it is possible to obtain fairly accurate structure refinements using kinematical approximation only.
Regarding nanodomains, we explore the limitations associated with their size and the extent to which we can track structural changes at a nanoscale. For this, we shall consider an approach that uses an appropriately sized parallel beam to collect ED patterns at different region of interest (ROI). One way to perform such an analysis is to combine a scanning procedure with precession-assisted 3D ED. The area of interest is selected, and the electron beam is scanned across it with the desired step size while collecting the precession-assisted diffraction patterns. Afterwards, the sample is tilted and the scanning procedure is performed again, and so on, obtaining this way a tomography of a 2D space. Eggeman et al. [1] actually exploited a similar approach for analysing the volume and orientation of domains in crystalline Ni-based superalloys, and used the acronym SPET for Scanning Precession-assisted Electron Tomography data acquisition. We extend the use of SPET for the structure solution and accurate structure refinement of nanodomains. This implies that after the acquisition, we are able to distinguish, and sort accordingly, the diffraction patterns generated by different ROI in the sample. By doing so, several nanodomains of the specimen can be probed

without the need of tracking them while tilting, and therefore to perform structure solution and accurate structure refinements of multiple ROI with a single acquisition.
We first demonstrate the usefulness of SPET for accurate structural characterizations of subtle structural changes in a 35 nm thick PrVO3 thin film [2] using a line scan in a direction perpendicular to the film/substrate interface (see Graphic). Second, we take a step forward employing it for the analysis of nanodomains embedded in ceramics [3] using an area scan and show how it is possible to extract 3D ED data corresponding to single domains/ROI from the SPET data stack.

Conclusion
Regarding the possibility to reveal unknown nano-structure, we propose a shift in the paradigm of 3D ED data collection, from a "point" acquisition, focused on a single ROI, to a multidimensional data acquisition method using scanning precession-assisted 3D ED. With this approach it is possible to obtain accurate crystallographic information from multiple ROI at a scale less than 10 nm.

These results were obtained as part of the European project NanED (Electron Nanocrystallography – H2020-MSCA-ITN GA956099).

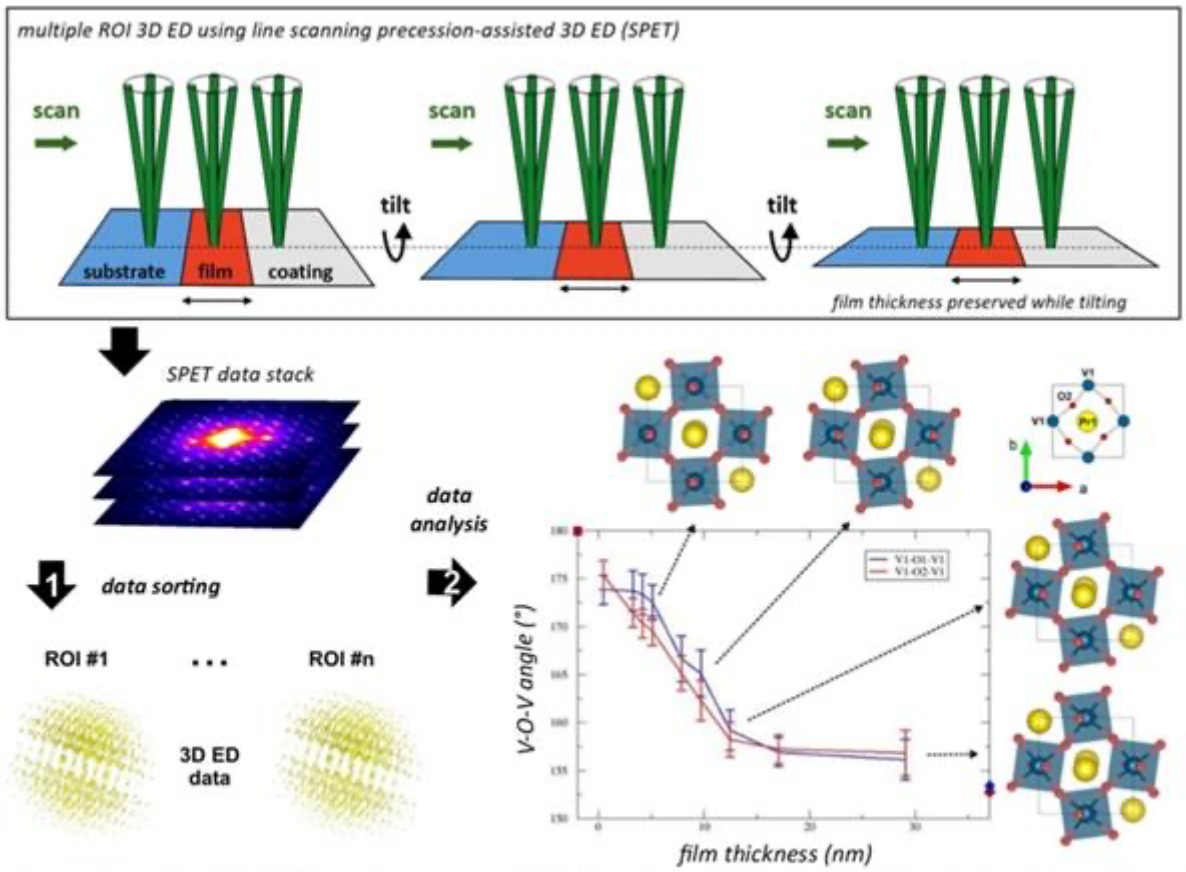

On top, schematic of SPET for a line scan on thin films. To every position of the electron beam (in green) corresponds the acquisition of a precession ED pattern. Below, the SPET data stack shall be processed in order to extract the contribution from different ROI and obtain the crystal structure for each ROI.

Keywords:

3D ED; serialED; Precession; nano-crystallography

Reference:

[1] Eggeman, A. S., Krakow, R. and Midgley, P. A. Nature communications 6 (2015) 7267.
[2] Passuti, S., Varignon, J., David, A. and Boullay, P. Symmetry 15 (2023) 1459.
[3] Pavan Kumar, V., Passuti, S., ... and Guilmeau, E. Angewandte Chemie 134 (2022) e202210600.

298

Quantitative comparison between the diffuse scattering from three-dimensional electron diffraction and single-crystal X-ray diffraction

Romy Poppe[1], Dr. Nikolaj Roth[2], Prof. Reinhard B. Neder[3], Dr. Lukáš Palatinus[4], Prof. Bo B. Iversen[2], Prof. Joke Hadermann[1]
[1]University of Antwerp, Department of Physics , Groenenborgerlaan 171, B-2020 Antwerp, Belgium, [2]Aarhus University, Department of Chemistry , Langelandsgade 140, 8000 Aarhus, Denmark, [3]Friedrich-Alexander-Universität Erlangen-Nürnberg, Kirstallographie und Strukturphysik , Staudtstraße 3, 91058 Erlangen, Germany, [4]Czech Academy of Sciences, Department of Structure Analysis , Na Slovance 2, 182 21 Prague, Czech Republic

IM-06 (2), Lecture Theater 1, august 30, 2024, 10:30 - 12:30

Background incl. aims
In contrast to perfectly periodic crystals, materials with short-range order produce diffraction patterns that contain both Bragg reflections and diffuse scattering. In this talk, we will show a quantitative comparison between three-dimensional electron diffraction (3D ED) and synchrotron single-crystal X-ray diffraction, both for the Bragg reflections and the diffuse scattering. The thermoelectric material Nb0.83CoSb was chosen as a reference material.
Methods
3D ED allows the study of nanometre-sized crystals, which are too small to be studied with single-crystal X-ray diffraction. The average structure (occupancies and atomic positions) was refined from the Bragg reflections, whereas the local structure (the vacancy distribution) was refined from the diffuse scattering. A model of the short-range order in Nb0.83CoSb was created by assuming that nearest and next-nearest neighbour vacancies avoid each other. The correlations between the first and next-nearest neighbour vacancies were refined using both a Monte Carlo refinement in DISCUS [1] and a three-dimensional difference pair distribution function (3D-ΔPDF) refinement in Yell [2].
Results
We found that diffuse scattering data used for quantitative analysis are best acquired in selected area electron diffraction (SAED) mode using an energy filter. Both the average and the local structure could successfully be refined from both the 3D ED and synchrotron single-crystal X-ray diffraction data acquired on Nb0.83CoSb. Fig. 1 shows that a good agreement was achieved between the simulated and the experimental intensity distribution of the diffuse scattering. The higher R-value for 3D ED compared to single-crystal X-ray diffraction is likely due to residual multiple scattering. The model of the short-range order in Nb0.83CoSb can easily be applied to determine the short-range order parameters in other materials with similar diffuse scattering, such as the lithium-ion battery cathode material LiNi0.5Sn0.3Co0.2O2.
Conclusion
The diffuse scattering in 3D ED data can be obtained with a quality comparable to that from single-crystal X-ray diffraction. Short-range order parameters could successfully be refined from the diffuse scattering in 3D ED data. As 3D ED requires much smaller crystal sizes than single-crystal X-ray diffraction, this allows to refine short-range order parameters in many technologically relevant materials for which no crystals large enough for single-crystal X-ray diffraction are available.

This research was funded by the Research Foundation Flanders (FWO) (grant No. G035619N).

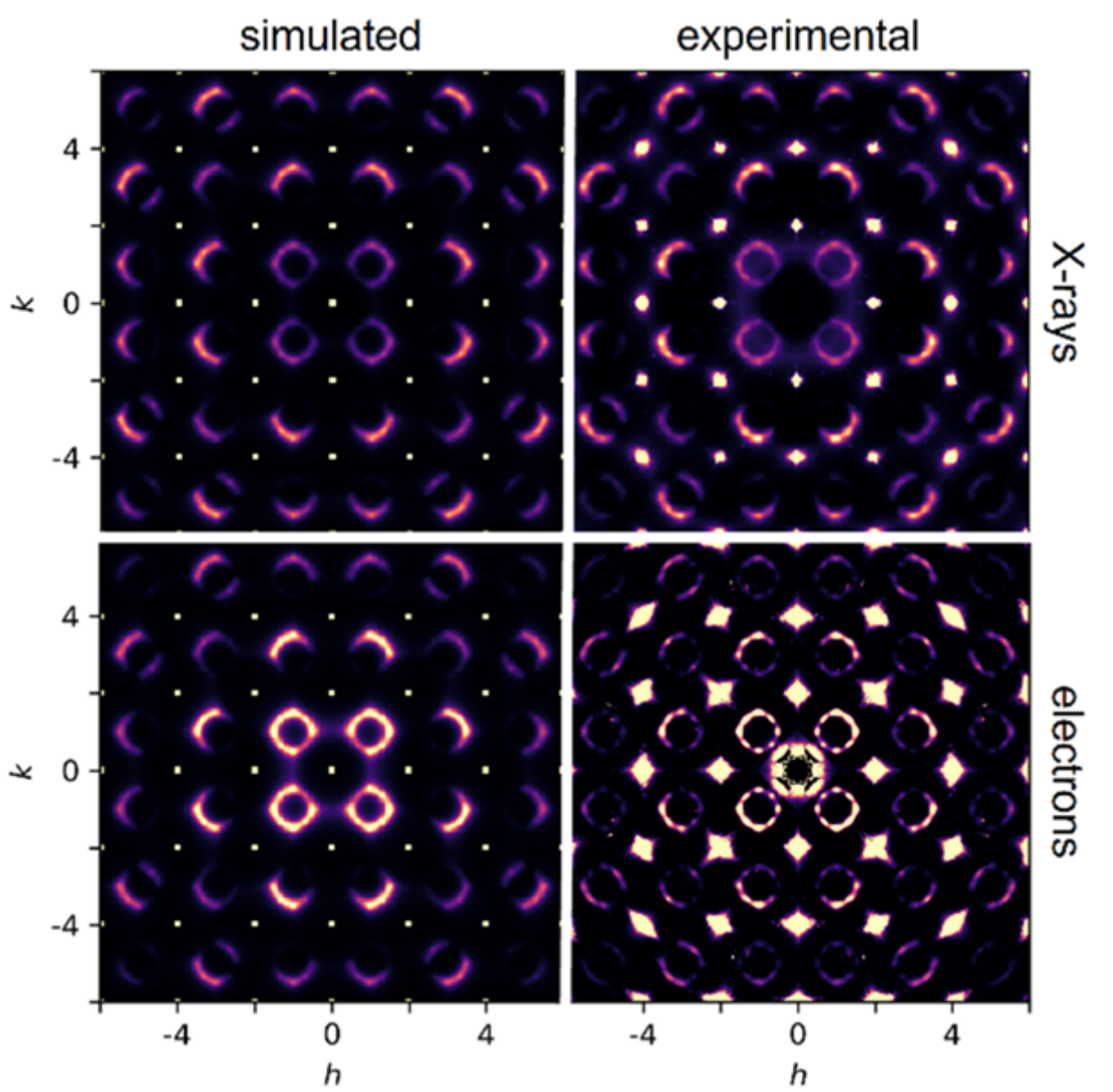

Keywords:

3D ED, diffuse scattering, thermoelectrics

Reference:

[1] Proffen, Th. & Neder, R. B. (1997). J. Appl. Cryst. 30, 171–175.
[2] Simonov, A., Weber, T. & Steurer, W. (2014). J. Appl. Cryst. 47, 1146–1152.

328

Quantification of Dynamic Scattering Effects in Molecular Crystals using Large Angle Rocking Beam Electron Diffraction

Robert Busch[1,2], Hsu-Chih Ni[1,2], Prof. Jian-Min Zuo[1,2]
[1]University of Illinois at Urbana Champaign, Urbana, United States, [2]Materials Research Laboratory, Urbana, United States

IM-06 (2), Lecture Theater 1, august 30, 2024, 10:30 - 12:30

Background
Electron crystallography provides a pathway to solve structure of small crystals (< 1um) in size, and thus overcomes difficult synthesis constraints involved in growing large crystals. Generally, electron diffraction data is collected in the form of integrated intensity using continuous rotation or by precession. The measured intensities in 3D are utilized for structure solution. Using this approach, structure solution of difficult crystals, such as small crystals of zeolites, metal-organic frameworks, molecular crystals, and proteins , can be solved by electron diffraction.
However, electron structure solutions are regularly reported with higher R-values than x-ray or neutron diffraction. While similar structures are found despite the high R-values, the differences in the measure intensity and theory calculated intensity limit information that can be extracted by electron diffraction. Previous work demonstrated that including multiple-scattering effects significantly reduce the R-values . Thus, it is critical to be able to quantify the dynamical diffraction effects in molecular crystals.
Aims
Here, we introduce the large-angle rocking beam electron diffraction (LARBED) technique implemented with hardware synchronization for the quantifying dynamical scattering in large unit cell and dose sensitive crystals, such as zeolites. We report LARBED measurement from zeolite-Y crystal. The resulting patterns show the effects of dynamical interactions when scattering through an imperfect crystal. Our aim is to provide an example of the type of interactions which are limiting the statistical accuracy of methods like microED. Furthermore, we suggest that LARBED can be utilized as a complementary method, where solving the LARBED pattern will provide enhanced statistical accuracy.
Methods
The LARBED technique was implemented on an FEI Themis-Z microscope operating in precession mode with a TEM nanobeam diffraction probe. Here we establish a dark field pivot point aligned to the bottom of the sample with the range of the LARBED pattern set as the precession angle, here, 60mrad. This setup allows for a scan generator to drive the scan coils to tilt the beam rather than rastering the beam in real-space as in standard 4D-STEM techniques. The signal then incrementally tilts the beam with a step size corresponding to the precession angle divided by the integer size of supplied signal grid. The signal was provided using the synchronized scan generator of an electron direct detector. This allows for high-throughput data collection, where 128x128 scans are taken in 17seconds providing high resolution rocking beam curves while maintaining a lower dose. Additionally, dose was minimized using the monochromator slit to 2pA and ~ 0.2mrad convergence angle as a 4.5nm FWHM probe. The Zeolite-Y sample was prepared as a dried powder on an ultrathin lacey carbon grid.
Results
Figure 1 shows the LARBED pattern of a 60 mrad [100] obtained from a Zeolite-Y crystal. The collected datasets are a 4-dimensional stack of diffraction patterns of shape. Here, data are individual point-like diffraction patterns as a 2D array, with one pattern taken at each point on a 2D array grid of tilts. Figure 1a is the average electron diffraction pattern over all tilts, where the intensities are quasi-kinematic due to the averaging of the intensities. Figure 1b shows the expected structure of

the Zeolite at the [100] orientation. Figure 1c is the recovered LARBED Patterns for individual selected disks from the incident beam to the (0,2,6) family of reflections. The bright lines perpendicular to the g-vector direction are generally where the Bragg excitation is satisfied. Note the exact zone axis displays the most complex interactions with highly varying intensity in nearly all beams. This is indicative of multiple scattering effects between many beams as they are all in or near excited conditions. This represents, to our knowledge, the first example of this type of pattern on a large unit-cell, dose-sensitive crystal.

The details within the disk excitation lines also show the effects of small crystalline differences. For a perfect Ia-3d cubic crystal we expect each family of reflections to maintain expected mirror and rotational symmetries(4mm1R). In this case, there are several excitation lines with variations in the families of reflections. These deviations will also be present when performing microED and will subsequently affect the intensity integration. These types of deviations are not accounted for by multiple scattering alone.

Conclusions

Our results show unexpected intensity variation relevant to electron diffraction intensity integration. The splitting of excitation lines is the result of dynamic effects from small defects, orientation, or thickness differences in the sampled region of the crystal. These effects are apparent in LARBED patterns and can potentially be utilized to supplement microED data in the future. Careful selection of the intensities from LARBED patterns have the potential to aid statistical analysis of solved crystal structures.

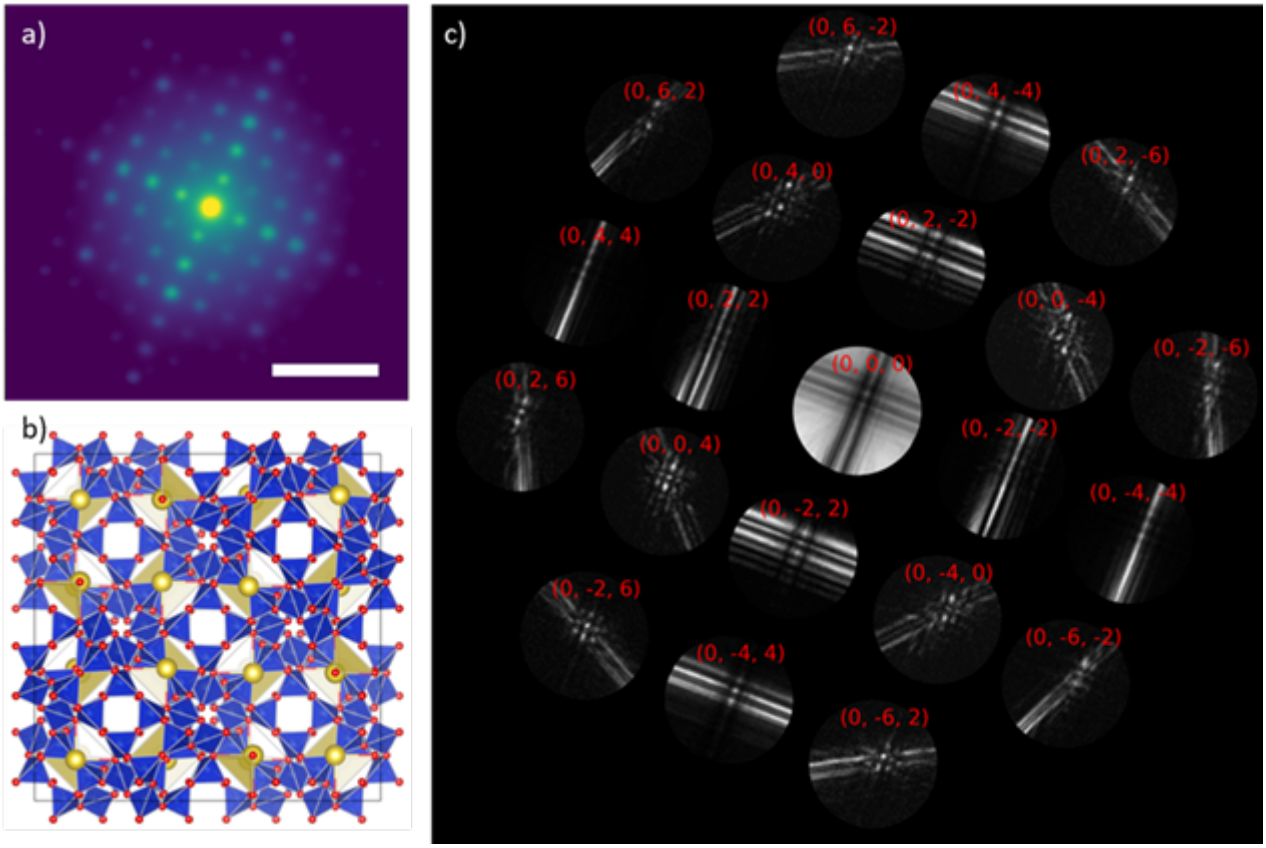

Keywords:

Electron Diffraction, Crystallography, Dynamic Scattering

Reference:

Gemmi et. al. ACS Cent. Sci. 2019, 5, 8, 1315–1329
Klar et. al. Nature Chemistry volume 15, pages848–855 (2023)
Eades Ultramicroscopy Volume 5, Issues 1–3, 1980, Pages 71-74,

Koch Ultramicroscopy. Volume 111, Issue 7, June 2011, Pages 828-840
Beanland et. al. Acta Crystallogr A. 2013 Jul 1; 69(Pt 4): 427–434.
This work is supported by the U.S. Department of Energy, Office of Science, Office of Basic Energy Sciences, under Award Number DE-SC0024064

822

Liquid Phase 3D Electron Diffraction Combination Provides New Possibilities for Polymorphism Studies

Joakim Lajer[2], Edward T. Broadhurst[1], Murat N. Yesibolati[2], Emil C. S. Jensen[3], Xiaodong Zou[1], Kristian S. Mølhave[2], Hongyi Xu[1], Huiqiu Wang[1]
[1]Materials and Environmental Chemistry, Stockholm University, Stockholm, Sweden, [2]National Centre for Nano Fabrication and Characterization, Technical University of Denmark, Lyngby, Denmark, [3]Insight Chips Aps, Lyngby, Denmark

IM-06 (2), Lecture Theater 1, august 30, 2024, 10:30 - 12:30

Background incl. aims
Liquid Phase Transmission Electron Microscopy (LPTEM) is a powerful method for investigating in-situ fluidic reactions and materials under liquid conditions. Traditionally, this involves enclosing liquids within silicon nitride membranes, thus eliminating the need for cryogenic or dry samples. However, it comes with a downfall of low spectroscopical signal due to large liquid and membrane thickness. To address this limitation, we introduce a novel nanochannel system capable of nanofluidic regulation for LPTEM. With a SiNx membrane thickness of 25 nm and a sub-200 nm liquid height, this system offers high resolution and enables excellent spectroscopic data [1,2]. This opens the possibility of developing completely new techniques with LPTEM, contributing to its rapid expansion in various atomic-scale characterization methods.
By combining the nanochannel system with existing methodologies for atomic characterization, we can observe samples in-situ during liquid transformations. This eliminates the need to remove samples from their liquid environment, allowing for direct observation of transient intermediate phases during processes like crystallization or polymorphic form changes.
To ensure accurate crystal determination inside the nanochannel, we utilize 3D Electron Diffraction (3D ED). This method enables the spatial structure determination of nano-scaled crystals.
In this work, we aim to combine 3D ED with nanochannel chips from Insight Chips, seen in Figure b to study the crystallization of glycine from liquid and characterize any observed transformations. Glycine is commonly used as a model system for polymorphism as it exhibits different polymorphic states depending on its liquid medium. Previous research has demonstrated the utility of 3D ED in tracking the crystallization of glycine from aqueous solution [3].

Methods
In this study, we utilize a TEM holder from Figure a, which has four tubes connected to four O-ring sealed in/outlets on a chip. The chips in/outlets are sealed during fabrication with a nitride membrane, ensuring the nanochannels are clean and hydrophilic upon puncturing before use. After puncturing the membrane, a 50% saturated glycine solution in deionized water was drop-casted on the inlet and the solution entered the channels through capillary forces. Pure ethanol was subjected to the other side of the chip with the same drop-casting method. Crystals of glycine were observed under an optical microscope, in Figure b, as they have a different refractive index than water and give rise to different colors due to multilayer reflection. Thereafter, the presence of crystals was observed in a TEM, displayed in Figure c.
The 3D ED data from the crystals was collected on a Thermo Fisher Themis TEM with an acceleration voltage of 300 keV. 3D ED data was obtained using a selected area aperture on individual crystals in the channels, with crystal lengths ranging from 1.5 to 4.0 µm. All 3D ED data were collected at room temperature while rotating the chip continuously between –20° and +25° in α tilt, illustrated in Figure d. The exposure time (0.2 s) and rotation speed (0.85 s^–1) were chosen so that individual diffraction frames were integrated over 0.17° of reciprocal space. The estimated dose rate was 2 e Å^–2 s^–1,

with each collection taking on average 240 s, the total estimated dose per 3D ED data collection was 480 e Å^−2.
REDp was used to determine the unit cell and space group from 3D ED data. Data reduction and integration were performed with XDS. Structures were solved via dual space methods using SHELXT and refined with SHELXL in the Shelxle interface.

Results
The phase change precipitated chip was investigated using LPTEM. A total of 18 crystals were identified and analyzed by 3D ED, and out of these, 8 were identified as α-glycine and 4 were identified as β-glycine. The remaining 6 datasets did not provide conclusive results due to limited completeness or the crystal being polycrystalline. Due to low data completeness (24.2%), ab-initio structure determination was not possible. However, 3D ED data could still be used to refine the positions and isotropic atomic displacement of all non-H atoms. The presence of SiNx windows and concentrated glycine solution surrounding the crystal led to slightly increased background noise and diffuse scattering in TEM analysis. 3D ED data collected on crystals immersed in liquid were sufficient for structure determination. The results of crystallization in nanochannels and in-situ 3D ED experiments provided us with the opportunity to capture the early stages of the glycine crystallization process.
Although the overall crystallographic information was worse than the data collected on conventional TEM grids [3], the structure model could still be accurately determined.

Conclusion
The work carried out here demonstrates that the combination of LPTEM and 3D ED was successful in studying the structure of glycine crystals in liquid. 3D ED data from crystals of α-glycine and β-glycine polymorphs, both in and out of liquid were eligible for structure analyses. Both α- and β-glycine polymorphs were identified via imaging and crystallographic data. Liquid phase 3D ED is an advanced and challenging technique, but the findings and experimental capability established here raise the prospect of future works on studying structural responsiveness to external stimuli, like temperature or even chemical processes in solution using a combination of LPTEM and 3D ED.

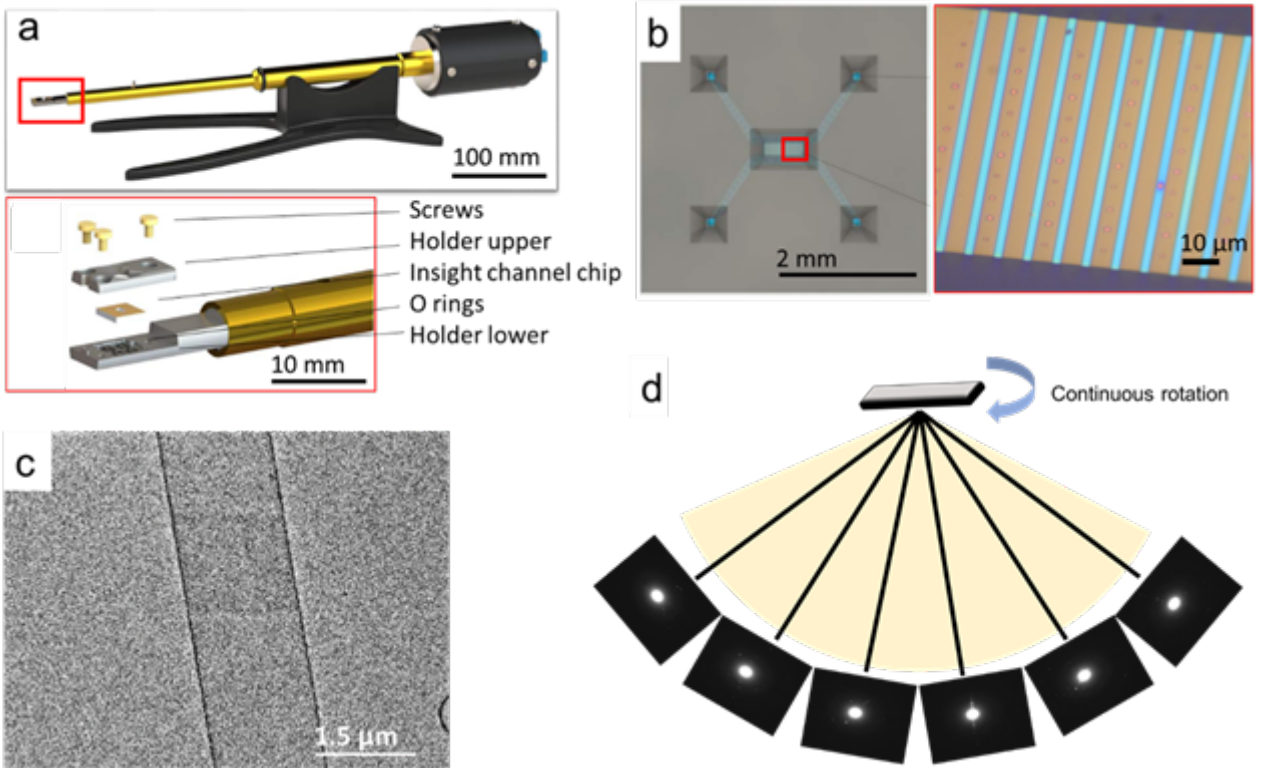

Keywords:

3DED, LPTEM, Nanochannel, Crystallography, Polymorphism

Reference:

[1]: Yesibolati, M. N., Laganá, S., Kadkhodazadeh, S., Mikkelsen, E. K., Sun, H., Kasama, T., Hansen, O., Zaluzec, N. J., & Mølhave, K. (2020). Electron inelastic mean free path in water. Nanoscale, 12(40), 20649-20657. The Royal Society of Chemistry. DOI: 10.1039/D0NR04352D.
[2]: Yesibolati, M. N., Laganá, S., Sun, H., Beleggia, M., Kathmann, S. M., Kasama, T., & Mølhave, K. (2020). Mean Inner Potential of Liquid Water. Phys. Rev. Lett., 124(6), 065502. American Physical Society. DOI: 10.1103/PhysRevLett.124.065502.
[3]: Broadhurst, E. T., Xu, H., Clabbers, M. T. B., Lightowler, M., Nudelman, F., Zou, X. & Parsons, S. (2020). Polymorph evolution during crystal growth studied by 3D electron diffraction. IUCrJ, 7, 5-9.

981

Structural Study of Polyphasic Mixtures Using 3d Electron Diffraction:A Case Study of Oxyresveratrol

Ms Vincentia Emerson Agbemeh[2]
[1]Electron Crystallography, Center for Materials Interfaces, Istituto Italiano di Tecnologia, Pontedera, Italy, [2]Department of Chemistry, Life Sciences and Environmental Sustainability, University of Parma, Parma, Italy

IM-06 (2), Lecture Theater 1, august 30, 2024, 10:30 - 12:30

Background
Oxyresveratrol is a naturally occurring compound found in Artocarpus Lakoocha which is known for its antioxidant and anti-inflammatory properties. We try to understand more about this compound by studying its crystal structure in the pure anhydrous form. This a crucial information for understanding how the crystal structure can be modified to address one of the problems with this natural product; its low solubility and bioactivity. The only known crystal structure of oxyresveratrol was reported by Deng et al. in a dihydrate form however the anhydrate form has not been reported. So far, there has been no success in growing single crystals of the anhydrate form large enough for structure determination using Single Crystal XRay Diffraction (SCXRD). An initial attempt to solve the anhydrate crystal structure using Powder XRay Diffraction (PXRD) was unsuccessful due to overlapping peaks and the presence of more than one phase. The PXRD pattern of the reported hydrated phase also did not fit all the peaks of the PXRD pattern of our sample. 3D electron diffraction (3DED) is a technique for structure solution of single crystals below 1µm and ideal for identifying phase mixtures. We apply 3DED for crystal structure determination and to better investigate all the possible phases that were present in the sample.

Method
3D ED data collection was performed in the Zeiss Libra 120kV Transmission Electron Microscope (TEM) at both room temperature and at -180˚C. Sample for the cooling experiment were put in water and plunged frozen in liquid ethane by applying a technique commonly used in cryo Electron Microscopy (cryoEM) to prevent sample dehydration. This method is used to identify possible hydrates in our sample whose crystal structure collapses in the high vacuum condition present in the TEM. Experimental PXRD was performed using a STOE Stadi P equipped with Cu-Kα1 radiation.
Results
In the room temperature experiment, we identified a new anhydrate oxyresveratrol crystal structure which has not been reported. It crystallizes non-centrosymmetric space group Pc and refined using dynamical refinement. Additionally, in the cryo experiment, a new polymorph of the dihydrate form of oxyresveratrol with the same space group as the anhydrous phase was found different from the reported hydrated phase which was P-1. The simulated PXRD pattern of the two new structures were compared with the experimental PXRD. We observed the presence of both phases of the new structures and a minor phase of the form 1 hydrated phase and fully fitted the patterns using Rietveld refinement.
Conclusion
The successful structural determination of these two new polymorphs demonstrates the possibility of directly determining structures from polyphasic mixtures by combining the power of both 3D ED and PXRD. This will improve efficiency and broaden the scope of phase identification which plays a crucial role in pharmaceutical development and within the field of crystal engineering.

The authors acknowledge the support from the European Union's Horizon 2020 research and innovation programme under the Marie Skłodowska-Curie grant agreement No 956099 (NanED – Electron Nanocrystallography – H2020-MSCA-ITN).

Keywords:

3delectron diffraction polymorphism crystal structure

Reference:

Reference

Likhitwitayawuid K. (2021). Oxyresveratrol: Sources, Productions, Biological Activities, Pharmacokinetics, and Delivery Systems. Molecules (Basel, Switzerland), 26(14), 4212. https://doi.org/10.3390/molecules26144212.

Deng, H., He, X., Xu, Y. & Hu, X. (2012). Oxyresveratrol from Mulberry as a dihydrate Acta Cryst. E68, o1318-o1319. https://doi.org/10.1107/S1600536812014018

Gemmi, M., Mugnaioli, E., Gorelik, T. E., Kolb, U., Palatinus, L., Boullay, P., Hovmöller, S., & Abrahams, J. P. (2019). 3D Electron Diffraction: The Nanocrystallography Revolution. ACS central science, 5(8), 1315–1329. https://doi.org/10.1021/acscentsci.9b00394

206

Determination of 3D strain fields from dynamical diffraction effects

Dr. Laura Niermann[1], Mr. Tore Niermann[1], Mr. Michael Lehmann[1]
[1]Technische Universität Berlin, Institut für Optik und Atomare Physik, Berlin, Germany

IM-06 (3), Lecture Theater 1, august 30, 2024, 14:00 - 16:00

Background incl. Aims
Strain fields have a large influence on many material properties. Examples range from electronic properties like the band gap or charge carrier mobilities in semiconductors to structural properties like nucleation energies of extended defects. Several techniques for a nanometer-resolved measurement of strain fields within the S/TEM are available, like nanobeam electron diffraction, geometric phase analysis, or dark field electron holography (DFEH). However, these methods typically only reveal strain field variations in directions perpendicular to the electron beam and assume a constant strain field in the beam direction. Within these methods, dynamical diffraction effects are often seen as a nuisance since they often complicate the interpretation of the data. However, strain fields are seldom purely two-dimensional and often also exhibit inhomogeneities along the electron beam. Here we show that dynamical diffraction effects can be leveraged in several ways to obtain information about the 3D strain field.
Methods
We use the scanning convergent beam electron diffraction (SCBED) with non-overlapping disks to capture the dynamical diffraction data, where for each scan point a CBED pattern is obtained. The scan coordinates add spatial context to the individual CBED patterns, which enables their comparison with numerical strain field models.
We demonstrate the validity of this approach by investigating the dynamical diffraction effects originating from an epitaxially grown layered structure, where the layer exhibits a 45° angle with respect to the specimen surface. The inclined layer creates a well-known inhomogeneity of the strain field in the beam direction. Due to the 45° inclination of the layer, the depth of the inhomogeneity is constantly changing with the lateral position of the beam. The specimen is investigated under systematic row conditions with reflections in the direction perpendicular to the layer. The SCBED data then can be fully represented by a reduced two-dimensional (q, x)-dataset, where both the spatial dimension x and the diffraction dimension q are oriented in the direction perpendicular to the layer.
Additionally, we performed DFEH measurements of the specimen. As DFEH requires parallel illumination, a beam tilt series is acquired to achieve similar (q, x)-datasets. In contrast to the SCBED data, the DFEH datasets also contain the phase of the diffracted beam [1].
Results
The experimentally obtained (q, x)-data are compared with simulated (q, x)-data, which are calculated from a strain model using numerical multi-beam propagation of the Darwin-Howie-Whelan equations. A very good agreement between the experimental and simulated plots is found. The results show that the inclusion of surface relaxation effects into the strain model becomes mandatory for matching the simulation to the data, which further demonstrates the high sensitivity of the dynamical diffraction data to the 3D strain field.
A striking feature of these (q, x)-data is a mirror symmetry with respect to the specimen's midplane, which is also expected theoretically [2]. This mirror symmetry forbids discrimination between the case where the strain inhomogeneity is located at a certain distance behind the entrance surface of the specimen from the case where the inhomogeneity is located at the same distance before the exit surface. However, this midplane symmetry occurs only in the intensities of the diffracted beams, not in the diffracted beam's phases. The phases recorded in the DFEH tilt series do not exhibit this

ambiguity and allow even the differentiation between these cases and thus the unique determination of the depth of the inhomogeneity.

Conclusion

Within dynamical diffraction effects information about the 3D strain field is encoded. Using techniques like SCBED or DFEH tilt series allows to record dynamical diffraction data obtained from small variations of the incident beam tilt together with spatial information. This data can be quantitatively compared with numerical strain field models. The determination of the 3D strain field enables several new applications: for instance, the depth and Burgers vectors of dislocations can be obtained from a single 4D-STEM measurement [3]. Another example is the determination of the thickness and concentration of layers in semiconductor heterostructures by detailed measurements of the strain relaxation at the specimen surfaces.

Keywords:

4D-STEM, DFEH, Strain, Dynamical diffraction

Reference:

[1] L. Meißner, T. Niermann, D. Berger, M. Lehmann; Ultramicroscopy 207 (2019), 112844
[2] T. Koprucki, A. Maltsi, A. Mielke; Proc. R. Soc. A 478 (2022), 20220317
[3] T. Niermann, L. Niermann, M. Lehmann; Nature Communications 15 (2024), 1356

247

Unveiling Structural Heterogeneity and Imbalance of Gold Decahedral Nanoparticles using Four-dimensional Scanning Transmission Electron Microscopy

Oliver Lin[1], Dr. Zhiheng Lyu[1], Mr. Hsu-Chih Ni[1], Ms. Yetong Jia[2], Prof. Kejie Zhao[2], Prof. Jian-Min Zuo[1], Prof. Qian Chen[1]
[1]University of Illinois, Urbana-Champaign, Urbana, USA, [2]Purdue University , West Lafayette, USA
IM-06 (3), Lecture Theater 1, august 30, 2024, 14:00 - 16:00

Background incl. aims
Multi-twinned structures have been observed in technologically important crystal systems, for example diamond cubic and face-centered cubic (FCC) lattices, that include materials such as diamond, silicon, a wide range of noble metals, and their nanoscale counterparts. Beyond atomic building blocks, the special arrangements also occur in the self-assembly of nanoparticles (NP) and µm-sized colloidal particles and occupy parts of their phase diagrams. Spanning a wide range of length scales, the universality of the structures arises when the systems attempt to achieve multi-twinned structures by overcoming geometric misfits during minimizing surface energies with entirely {111} or close-packing facets. While it is fundamental to understand how strain is sustained upon twinned structures and symmetry breaking, the knowledge will be paramount in practical aspects such as guiding and controlling the thin film growth, anisotropic NP growth, and self-assembly of NPs. Au decahedral (Dh) NP, as the most prevalent multi-twinned model system, fits five tetrahedral motifs into a circle by sharing an axis resulting in a geometric misfit angle of 7.35°, or a disclination with power of -7.35°. Postulating how Au FCC lattice adopts the misfit, theoretical models have been developed to address the underlying lattice symmetry and inhomogeneous strain distribution separately. Yet, experimental reports regarding the former have been limited due to the relatively large X-ray beam sizes that do not fit the sizes of NPs. On the other hand, though the latter has been widely adapted in the thermodynamics of small (<10 nm) multi-twinned nanoparticles, previous literature has shown that, at edge length of 17 nm, the theory's is invalidated by shear strain that is observed in a defect-free Au Dh NP by high-resolution transmission electron microscopy (HR-TEM) imaging. Though the advancement of aberration-corrected scanning transmission electron microscopy (AC-STEM) imaging and ab initio calculation techniques brings new opportunities, along with challenges in complicated image analysis and limitation in particle size (usually below 10 nm), the gap between nanoscale and mesoscale has never been extended to gain insight from atomic system with straightforward interaction potentials.
Methods
In this work, we performed strain mapping using four-dimensional STEM (4D-STEM) on Au Dh NPs with edge lengths between 18 and 50 nm at single particle level. In 4D-STEM, a nm-sized electron probe (at a convergent angle of 0.6 mrad) offers nm spatial resolution and decouples the complex diffraction patterns (DP) of the entire five-fold twinned structure into single-crystalline patterns corresponding to each tetrahedral grain. As such, NP's lattice plane directions can be easily identified and aligned with strain components. Diffraction disks were tracked by circular Hough transformation for sub-pixel accuracy. DPs are acquired on an Electron Microscope Pixel Array Detector (EMPAD) to reduce step size and acquisition time. Further integration of AC-STEM is utilized to confirm the absence of large-scale defects, such as additional twin boundaries and disclination, in the NPs and to focus on the geometric effects, excluding other known pathways of strain relaxation.
Results
The resulted strain mappings across various particle sizes exhibit values and distributions agree with previous Dh models: ~ 2% of tensile strain along {220} direction concentrated at particle edges. From reciprocal space, we also observed ~ ±0.5% of shear strain on two sides of twin boundaries. Other

results, such as strain along {002} direction, also match with finite element analysis (FEA) simulation based on the closing of geometric misfit. Additionally, since the crystallography of local lattice is being tacked across a particle, it is possible to map out local symmetries of Dh NP at nm spatial resolution for the first time. We have uncovered the particles we analyzed are mostly in body-centered tetragonal symmetry, yet as particle size increases, lattices near twin boundaries shift towards FCC symmetry. Furthermore, with the help of the small step size only made possible with EMPAD, our mappings show structural heterogeneity among tetrahedral grains and among particles we surveyed. The detailed features lead us to study how imperfect Dh geometry, such as particle edges, tip truncations, etc., contributes to variations in strain values and distributions. With FEA simulation, we associate the heterogeneity with the shifting of disclination away from the center of a particle because of statistical fluctuation of energetics during the fast growth of multi-twinned particles.

Conclusion

Using 4D-STEM strain mapping with an advanced pixelated detector at high frame rate, we have unveiled new information of Au Dh NP at particle sizes that were experimentally inaccessible before. The diffraction-based technique provides richness in the crystallographic information of nanostructure at high spatial resolution as well as approaches to in-depth data analysis beyond atomic imaging. The results help experimentally bridge a variety of previous theoretical concepts, including lattice symmetry, disclination shifting, and heterogeneity associated with particle growth energetics. The understanding of imbalanced geometry has future implication of precise control over anisotropic NP shapes and additional over-growth or etching. Fundamentally, the extension of length scale shows novel insights into mechanisms that nature choses to accommodate the geometric misfit by simple atomic potentials. We believe it will inspire assemblies at different length scales that leverage complex interactions.

Keywords:

4D-STEM, multi-twinned nanostructure, strain mapping

250

Atomic resolution observation of zeolitic framework and captured cations using low-dose OBF STEM technique

Dr. Kousuke Ooe[1,2], Dr. Takehito Seki[3,4], Mr. Koudai Tabata[3], Dr. Kaname Yoshida[2], Prof. Atsushi Nakahira[5], Mr. Yuji Kohno[6], Prof. Yuichi Ikuhara[2,3], Prof. Naoya Shibata[2,3]
[1]Monash University, Clayton, Australia, [2]Japan Fine Ceramics Center, Nagoya, Japan, [3]The University of Tokyo, Bunkyo, Japan, [4]JST PRESTO, Kawaguchi, Japan, [5]Osaka Metropolitan University, Sakai, Japan, [6]JEOL Ltd., Akishima, Japan

IM-06 (3), Lecture Theater 1, august 30, 2024, 14:00 - 16:00

Zeolite is a common porous material with a unique framework structure and periodically aligned nanosized pores. Zeolites have a wide range of industrial applications such as gas separation, catalysis, and ion exchange. In these applications, the material properties emerge from the interaction between the host zeolitic framework and guest materials, such as molecules or ions. However, zeolites are very weak to electron irradiation, and it is difficult to analyze this interaction at the atomic scale using electron microscopy.
Recently, we developed an optimum bright-field scanning transmission electron microscopy (OBF STEM) technique for low-dose observations [1]. OBF STEM uses a segmented-type STEM detector and can achieve a dose efficiency that is two orders of magnitude higher than that of annular bright field (ABF) STEM, a conventional phase-contrast-based STEM technique. Furthermore, the OBF STEM images can be acquired in real-time in sync with the probe scanning, which makes low-dose data collection much easier. It was shown that low-dose OBF STEM can visualize the atomic structure of zeolitic frameworks for both T (=Si or Al) and O sites, even in lattice defects such as twin interfaces. Furthermore, the Na-captured LTA-type sample, which is one of the most beam-sensitive zeolites, was observed using OBF STEM, which visualizes extra-framework Na sites with a lower occupancy of approximately 1/4 [2].
We then applied the low-dose OBF technique to the Cs-exchanged LTA-type zeolites. Cs exchange is a very important application for the removal of hazardous chemicals, and understanding how Cs species are captured inside this material is of great importance. The atomic structures of the Na- and Cs-captured LTA samples were investigated using high resolution TEM (HRTEM) in the literature [3]. However, because of the higher Al content inside the LTA framework (Si/Al=1), which decreases the electron illumination resistance, the attainable spatial resolution remains limited. In this study, we observed Cs-LTA zeolites using the OBF STEM technique with high spatial resolution (~1 Å) under low-dose conditions, with the aim of revealing the interactions between host zeolitic frameworks and captured guest cations.
We prepared Cs-exchanged LTA-type zeolite samples using the ion-exchange procedure of a commercially available Na-captured LTA zeolite sample with a CsCl aqueous solution. The Cs-LTA sample was gently crushed using an agate mortar and then dispersed onto a TEM grid with a carbon support film. We then observed the Cs-LTA sample using the OBF STEM technique with aberration-corrected STEM equipped with a segmented detector. To suppress the irradiation damage, the probe current was set to 0.16 pA, which is more than two orders of magnitude lower than the usual STEM observation conditions.
Figure 1(a) shows the OBF STEM image of the Na-LTA zeolite sample. The LTA-type has a cubic shape framework, and eight-membered rings (8MRs) can be observed along the [100] zone-axis. In Na-LTA-type zeolites, the Na cations captured inside the 8MRs split into four sites, with an occupancy of approximately 1/4 [4]. In addition to the clear visualization of the T and O atomic sites inside the LTA framework, the OBF image shows a slight contrast around the center of 8MR, corresponding to the captured Na cations [2]. We then observed the Cs-captured sample from the [100] zone-axis using OBF STEM, as shown in Figure 1(b). The OBF image contrast at the center of the 8MRs changed into a

distinct sharp one compared with the Na-LTA case, indicating that the captured Cs cations were rigidly confined into the LTA framework instead of splitting into multiple sites with low occupancy. This observation agrees well with the literature using HRTEM and density functional theory (DFT) calculations [3], showing the capabilities of OBF STEM to directly observe captured cation sites inside zeolites at the atomic scale.

We applied a low-dose OBF STEM technique to the Cs-exchanged LTA-type zeolite samples. The atomic structure was clearly visualized for not only the LTA framework structures but also the captured Cs sites, identifying the different behavior of the captured cations in comparison to the Na-LTA case. This result shows that the OBF STEM technique is promising for the atomic-scale analysis of zeolites, including extra-framework cations.

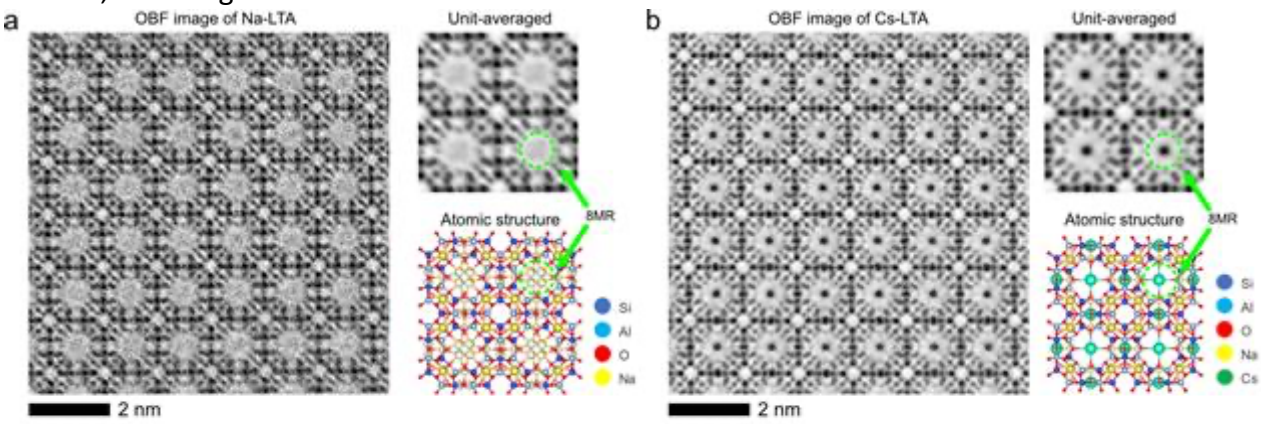

Figure 1. OBF STEM images of (a) Na- and (b) Cs-LTA zeolites. The experimentally acquired raw images, their unit-averaged OBF images, and corresponding atomic structure models are shown, respectively.

Keywords:

OBF-STEM, low-dose, zeolite, counter-cation

Reference:

[1] K. Ooe et al., Ultramicroscopy 220 (2021) 113133.
[2] K. Ooe et al., Science Advances 9 (2023) eadf6865.
[3] K. Yoshida et al., Microporous and Mesoporous Materials 259 (2018) 195-202.
[4] J.J. Pluth and J.V. Smith, Journal of American Chemical Society 102 (1980) 4704-4708.

256

OpenECCI - A Streamlined Open-Source Workflow for Electron Channelling Contrast Imaging of Crystal Defects

Zhou Xu[1], Dr. Håkon W. Ånes[2,3], Dr. Sergey Gorelick[1,4], Dr. Xiya Fang[1], Dr. Peter Miller[1]
[1]Monash Centre for Electron Microscopy, Clayton, Australia, [2]Department of Materials Science and Engineering, Norwegian University of Science and Technology, Trondheim, Norway, [3]Xnovo Technology Aps, Køge, Denmark, [4]Ramaciotti Centre for Cryo-Electron Microscopy, Clayton , Australia
IM-06 (3), Lecture Theater 1, august 30, 2024, 14:00 - 16:00

Background
Quantitative analysis of crystal defects, such as dislocations, stacking faults, etc., has traditionally been exclusive to transmission electron microscopes (TEM) for decades [1]. This technique involves stereo-tilting of a crystal to the “two-beam” diffraction orientations with the assistance of transmission Kikuchi pattern projected on a phosphor screen or a camera. Recent years, Electron Channelling Contrast Imaging (ECCI) techniques, including accurate ECCI [2], controlled ECCI [3] and rotational ECCI [4], have gained increasing interest for quantitative defect analysis in bulk specimens. Unlike TEM, ECCI in SEM offers easier, less intrusive sample preparation, and fewer sample-prep induced artifacts. Additionally, ECCI enables examination of larger polished surfaces, yielding more statistically representative results. Nevertheless, several challenges hinder its widespread adoption:

- High spatial resolution accurate ECCI requires modified SEM column alignment for orientation control [2].
- Controlled ECCI requires proprietary software and additional hardware for precise orientation control [3, 5].
- There is a lack of reliable method for measuring and controlling the electron beam convergence angle inside SEM.
- Absence of a quantitative method for assessing sample stage tilt/rotation accuracy and repeatability for ECCI.
- For controlled ECCI, coordinating the identification of a feature between EBSD map and SEM image, and applying stereo-tilt without losing the feature of interest could be challenging.

Hence, our current work aims to address these issues by leveraging the open-source software community to develop a more accurate and user-friendly ECCI workflow.

Methods
In this study, we present a refined controlled ECCI workflow using electron channelling patterns with moderate spatial resolution for automated orientation calibration. Utilizing open-source packages such as EMsoft, Orix, and Kikuchipy, we developed an interactive Python package to streamline the ECCI workflow. This package accurately predicts the required sample stage tilt and rotation to achieve "two-beam" orientations based on Kikuchi pattern simulations. Additionally, SEM stage tilt/rotation accuracy and repeatability have been quantitatively assessed by comparing experimental electron channelling patterns with simulations. Furthermore, an automated routine for measuring the electron beam convergence angle has been tested based on OpenCV package. Lastly, we have developed a routine for correlating EBSD maps with SEM images (or specimen stage position) to facilitate stereo-tilt without losing the region of interest.

Results
Fig. 1 illustrates a brief summary of the workflow. Fig.1A shows a blended image of a EBSD map overlaid on the corresponding BSE backscattered electron image. The EBSD map is homographically transformed to correct the scan distortion induced by 70 deg stage tilt, so that all the feature positions on EBSD map and BSE image are well aligned. The interactive plot allows users to click on

any point within the map to obtain SEM stage position and corresponding Euler angles from EBSD. The RKP reflected Kikuchi pattern from the point can also be simulated from the Euler angles, i.e. Fig. 1B, 1C. Fig. 1B is an overview Kikuchi pattern with relatively large angular range showing neighbouring poles and bands as a guiding map for stereo-tilt. Fig. 1C provides a zoomed-in region (blue box in Fig. 1B) for finding suitable "two-beam" orientations. By clicking on points within the pattern, users receive recommended stage rotation and tilt for orienting the point to the electron beam incident direction. Once a suitable orientation is achieved, ECC images can be acquired. For example, Fig. 1D and 1E depict ECC images acquired at 20kV, showing dislocations and stacking faults, respectively. Fig. 1D shows an array of dislocations piled up at a grain boundary. Most of the dislocations have dissociated into partial dislocations with Burgers vectors of ±1⁄2[10¯1]. Fig. 1E shows a few stacking faults on (1¯1 ¯1) close to a (11¯1) twin boundary. By analysing the beat pattern (oscillating intensity) across the stacking fault. The Effective extinction distance can be estimated ξ_g^eff = 13.7 nm. The total visibility depth of ECCI contrast at 20kV is approximately 80nm.

Conclusion

The OpenECCI package and the developed workflow offer a reliable and convenient method for ECCI experiments. Notable achievements include:

- With the stage accuracy and repeatability assessment routine, it has been demonstrated that many native SEM stages are accurate enough for ECCI without high precision substages.
- Providing reliable guidance on setting ECC imaging conditions through the measurement of electron beam convergence angle
- Streamlining the workflow for ECCI acquisition and data post-analysis through an interactive software interface that correlates EBSD maps, SEM images, and Kikuchi pattern simulations.
- OpenECCI is freely accessible to all researchers. Facilitated by its reliance on open-source packages, it could democratize the access to ECCI technique.

Acknowledgements

The authors would like to acknowledge Dr. Yuxiang Wu for sharing his samples for this technique development, and Dr. Jinqiao Liu, Prof. Xiaozhou Liao for the assistance in instrument testings. The authors acknowledge the use of the instruments at the Monash Centre for Electron Microscopy, a Node of Microscopy Australia. This research used equipment funded by Australian Research Council grant ARC Funding (LE200100132).

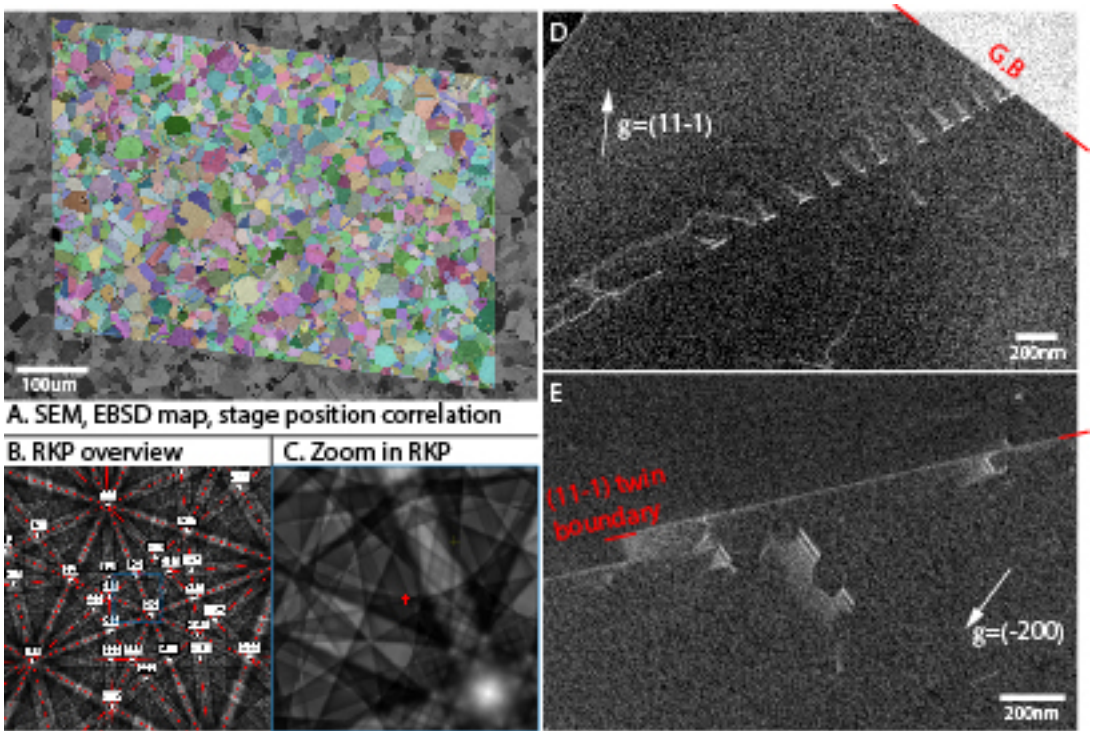

Keywords:

EBSD, ECCI, diffraction, defect-analysis, open-source

Reference:

1. Williams, D.B., et al., The transmission electron microscope. 1996: Springer.
2. Mansour, H., et al., Scripta Materialia, 2014. 84-85: p. 11-14.
3. Zaefferer, S. and N.-N. Elhami, Acta Materialia, 2014. 75: p. 20-50.
4. L'Hôte, G., et al., Scripta Materialia, 2019. 162: p. 103-107.
5. Harte, A., et al., Acta Materialia, 2020. 194: p. 257-275.

324

Towards in-situ 4D-STEM observation of texture evolution in nano-crystalline thin films

Dr. Mingjian Wu[1], Chang-Lin Hsieh[1], Daniel Stroppa[2], Philipp Pelz[1], Colin Ophus[3], Penghan Lu[4], Rafal Dunin-Borkowski[4], Christina Harreiss[1], Peter Denninger[1], Erdmann Spiecker[1]
[1]IMN & CENEM, FAU Erlangen-Nurnberg, Erlangen, Germany, [2]DECTRIS Ltd, Baden-Daettwil, Switzerland, [3]NCEM, Lawrence Berkeley National Laboratory, Berkeley, USA, [4]Ernst Ruska-Centre for Microscopy and Spectroscopy with Electrons, Juelich, Germany

IM-06 (3), Lecture Theater 1, august 30, 2024, 14:00 - 16:00

Background incl. aims
Texture describes the preferred orientation of grains in crystalline materials, which dictates their anisotropic, for example, (opto-)electronic, thermal transport, and mechanical properties. The texture is evaluated conventionally by probing the reciprocal space using X-ray and/or electron diffraction methods, where spatial information, e.g., the orientation relationship of particular grains, is hardly accessible. Probing the local diffraction pattern with a focused electron beam, i.e., nano-beam diffraction (NBD) 4D-STEM, provides local structure information. Recent detector technology opened new possibilities to perform such experiments at ever-higher temporal resolution.
In this contribution, we discuss the optimized conditions towards in-situ 4D-STEM observations of texture evolution in thin films by a combination of state-of-the-art fast direct electron detector (DED), dose-efficient experimental approach, and novel algorithms of data analysis.
Materials and methods
Two material systems, (I) a beam robust poly-crystalline gold thin film and (II) an extremely radiation-sensitive bulk hetero-junction (BHJ) blend used as active layers in organic solar cells serve as model samples in this study.
For poly-crystalline gold, we deposited 15 nm gold with PVD on the SiNx windows of MEMS heating chips (DENSsolutions Wildfire) and annealed the film in the TEM at 150^{o}C for 180 s while observing coarsening of the nano-crystalline structure. 4D-STEM experiments were carried out using a Thermo Fisher Scientific Spectra 200 TEM operated at 200 kV in a regular nano-beam diffraction setup and data was acquired using a DECTRIS ARINA detector. The orientation maps are then analyzed using the ACOM [1] routine within the py4DSTEM package and custom codes to streamline the output orientation matrix to the Orix package [2] for further evaluation of the texture evolution.
The BHJ thin film of nominal thickness of 80 nm comprises small molecule donor DRCN5T blended in fullerene acceptor PC71BM as reported earlier [3,4]. The major challenge is the dose budget (< 5 e-/Å2 at room temperature) that limits the applicable probe current for structural elucidation.
Results and discussions
For gold nano-crystal thin film (Fig. 1a), despite being radiation robust, it remains very challenging to observe evolution at high spatial and temporal resolution with sufficient angular resolution and sampling in diffraction space for orientation determination. This is due to the high dimensions of data required and the limited dose rate at the single pixel level of DED detection. To overcome this limit, we realized that an appropriate convergence angle and camera length are the key factors (using a standard NBD setup) that control the reciprocal space coverage and sampling. It is important to balance DED saturation in the primary beam and sufficient SNR of weak Bragg disks for accurate disk detection and subsequent crystal orientation matching. With a larger convergence angle, a higher probe current at a given high speed of detector readout, thus a higher dose, can be applied. While a small convergence angle seems arguably to favor angular resolution for Bragg disks detection, it lowers the applicable probe current due to detector saturation, resulting in weaker Bragg disks fading in the diffuse scattering background. After optimizing conditions on our experimental platform, we

found that time resolution of 5 – 10s and sub-3 nm sampling resolution (probe size <1 nm) for a statistically relevant field of view is realizable.
We further discuss strategies to improve the dose-effectiveness in terms of Bragg peak detection and eventually, in-situ 4D-STEM experiments supported by experimental results. These include (I) elastic energy filtering, (II) amplitude grating using patterned probe-defining aperture [1], and (III) applying precession-assisted 4D-STEM [5].
Finally, we were able to visualize the grain orientation from optimized, standard NBD 4D-STEM datasets and track the evolution of texture evolution of a defined ROI from the early stage on. We observed the growth of <111> oriented grains at the cost of neighboring high-index oriented grains (Fig. 1a). The 4D-STEM datasets allow grain orientation relationships to be analyzed qualitatively as well as quantitatively, shedding light on the complex interplay between various factors including types of grain boundaries, defects, and even local strain.
In the case of extremely dose-budget limited scenarios like the molecular nano-crystallites in the BHJ, the ultimate Bragg peak detectability is limited by the Poisson noise of the scattered electrons that strike on detector pixels. Therefore, the focused electron diffraction pattern is advantageous.
Inspired by earlier work of ultra-high angular resolution ω-q mapping [P. Midgley, Ultramicroscopy 76(1999) 91], we established a dose-efficient approach, 4D-scanning confocal electron diffraction (4D-SCED), to study the texture structure, i.e., face-on and edge-on domains, of nano-crystallites of the donor in the BHJ (Fig. 1b). 4D-SCED applies defocused pencil beam illumination on the sample and combines a confocal electron optic setup with a pixelated detector to record focused spot-like diffraction patterns. The defocused illumination reduces the dose and generates a homogenous beam-specimen interaction. At the same time, the confocal optics generates spot-like diffraction signals, boosting both the signal-to-noise ratio and signal-to-background ratio even in Poisson noise-limited scenarios [4]. We demonstrated a quasi-in-situ observation of the molecular nanocrystallites' structural evolution during an annealing experiment using a CMOS detector [3] (Fig. 1b). We further discussed new avenues to further reduce dose, improve experimental speed (temporal resolution) and throughput using a fast hybrid pixel detector, and advantage of the frame-based detector over the current generation of event-based detector for these applications [4].
Conclusion
In the study of nano-crystalline structural evolution, the achievable temporal resolution of in-situ 4D-STEM experiments is dose-limited at detection saturation level, independent of sample radiation resistance. Besides calling for further improvements of detectors, we present and discuss several experimental strategies for both beam robust and beam sensitive samples to optimize conditions to spare the meaningful dose to Bragg signal detectability and structural determination.

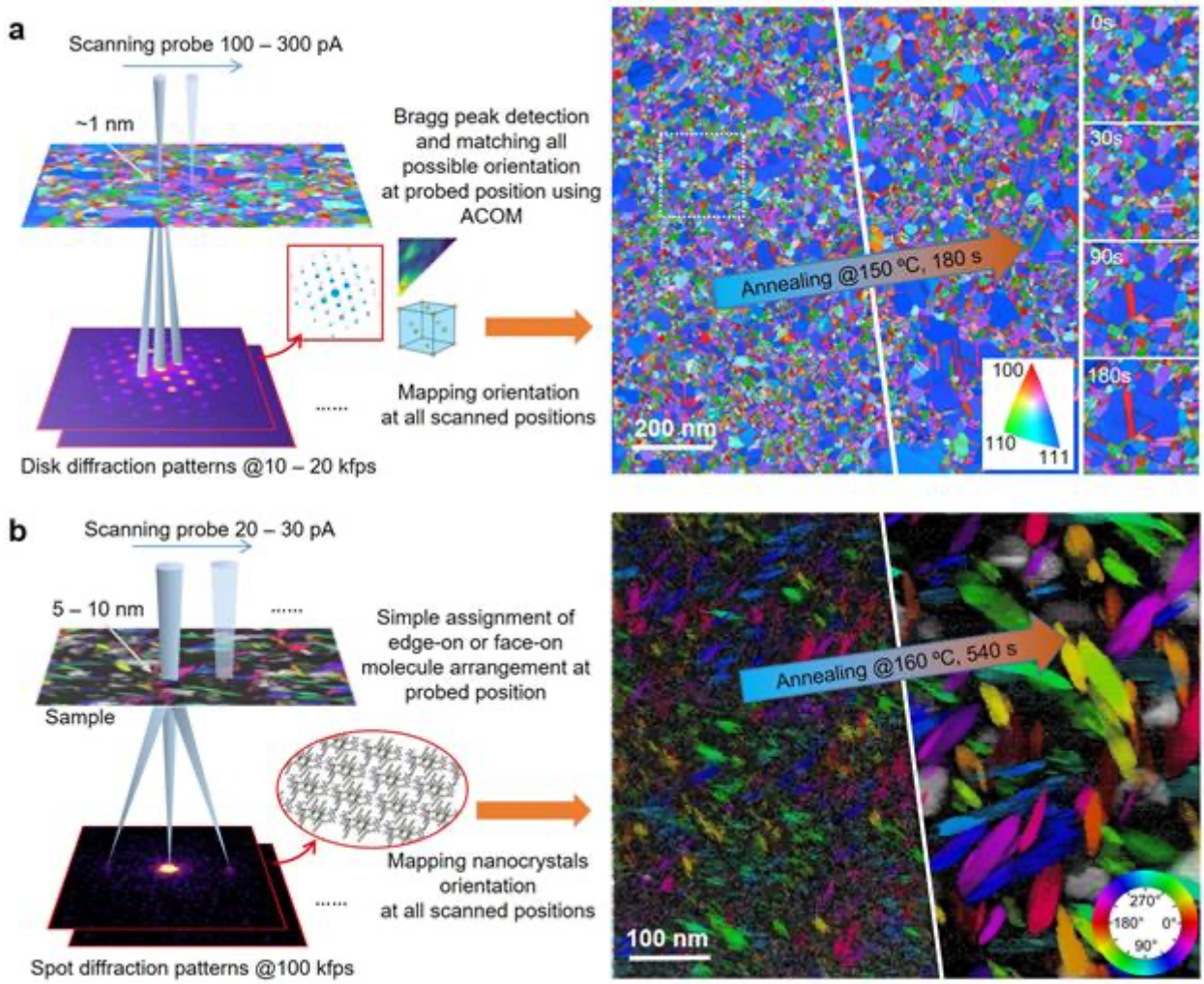

Keywords:

4D-STEM,
in-situ,
texture,
thin film.

Reference:

[1] Ophus, C., et. al., Microsc. Microanal., 28 (2022), 390–403.
[2] Johnstone, D. et. al., J. Appl. Crystallogr., 53 (2020) 1293
[3] Wu, M., et. al., Nat. Comm., 13 (2022), 2911.
[4] Wu, M., et. al., J. of Phys: Mater., 6 (2023), 045008.
[5] Midgley, P., Eggeman, A., IUCrJ. 2 (2015) 126

361

QCBED Measurements of Vacancy Concentrations, Lattice Contraction, and Bonding Electron Densities Surrounding Aluminium Nanovoids

Associate Professor Philip Nakashima[1], Dr Yu-Tsun Shao[2,3], Dr Zezhong Zhang[4,5,6], Dr Andrew Smith[7], Dr Tianyu Liu[8], Professor Nikhil Medhekar[1], Professor Joanne Etheridge[7,9], Professor Laure Bourgeois[1,9], Professor Jian-Min Zuo[10,11]
[1]Department of Materials Science and Engineering, Monash University, Clayton, Australia, [2]Mork Family Department of Chemical Engineering & Materials Science, University of Southern California, Los Angeles, USA, [3]Core Center of Excellence in Nano Imaging, University of Southern California, Los Angeles, USA, [4]Electron Microscopy for Materials Research (EMAT), University of Antwerp, Antwerp, Belgium, [5]NANOlab Center of Excellence, University of Antwerp, Antwerp, Belgium, [6]Department of Materials, University of Oxford, Oxford, United Kingdom, [7]School of Physics and Astronomy, Monash University, Clayton, Australia, [8]Institute of Multidisciplinary Research for Advanced Materials, Tohoku University, Sendai, Japan, [9]Monash Centre for Electron Microscopy, Monash University, Clayton, Australia, [10]Department of Materials Science and Engineering, University of Illinois at Urbana-Champaign, Urbana, USA, [11]Materials Research Laboratory, University of Illinois at Urbana-Champaign, Urbana, USA

IM-06 (3), Lecture Theater 1, august 30, 2024, 14:00 - 16:00

Background incl. aims
We set out to make the first position-resolved measurements of bonding electron density around a nanostructure in an inhomogeneous crystalline material.

All bonding electron density and potential studies to date have only involved homogeneous, single phased materials; however, most materials that serve us have hybridised properties because of the nanostructures that they contain, often by design. We also note that materials defects are ubiquitous and unavoidable, so the assumption that we can derive materials properties from notionally perfect regions of single, homogeneous crystal is limited in scope and "real" applications. This work aims to provide a new capability for interrogating bonding electron densities around nanostructures in nanostructured and inhomogeneous materials. Our first attempt involves nanovoids in nominally pure (99.9999+%) aluminium.

On the way to realising this aim, we have made several discoveries as a result of having to accurately map vacancy concentrations and determine the associated lattice contraction due to vacancies in order to be able to measure the Fourier coefficients (structure factors) of the crystal potential and electron density precisely and accurately (to <0.1% uncertainty).

Methods
Over the last 15 years, we have developed a multislice [1,2] approach to quantitative convergent-beam, electron diffraction (QCBED) refinements. We call this method QCBEDMS. This has facilitated the necessary analyses to generate the results summarised below. For more details regarding the method, please come to the talk – they will not be discussed here.

Results
From 45 CBED patterns collected through many different voids and the surrounding matrix, in different orientations and with different electron energies:

- We measured the volume of a vacancy with 5-fold less uncertainty than previous work.

- Observed that nanovoids in aluminium can "heal" even after significant beam damage.
- We mapped vacancy concentrations around aluminium nanovoids in 3 dimensions.
- We have shown that the bonding electron density around aluminium nanovoids is diluted by the elevated vacancy concentration surrounding these voids.

Conclusion

Our work and the results from it are a precursor to measuring and mapping bonding electron densities around many other types of nanostructures (eg. nano-precipitates) in other nanostructured, inhomogeneous materials. Furthermore, we are confident that our technique can be extended to mapping solute atom concentrations around such structures and that this will go together with accurate bonding electron density measurements within and surrounding these features in other nanostructured materials.

Keywords:

QCBED, multislice, bonding electron densities

Reference:

[1] Cowley, J. M. & Moodie, A. F. The scattering of electrons by atoms and crystals. I. A new theoretical approach. Acta Cryst. 10, 609-619 (1957).

[2] Spence, J. C. H. & Zuo, J. M. Electron Microdiffraction (Plenum Press, 1992).

483

Structure retrieval by parameterised inverse multislice accounting for partial coherence and thermal effects

Prof. Dr. Knut Müller-Caspary[1], Dr. Benedikt Diederichs[1,2], Ziria Herdegen[1], Achim Strauch[1,3]
[1]LMU München, Munich, Germany, [2]HMGU München, Munich, Germany, [3]Forschungszentrum Jülich, Jülich, Germany

IM-06 (3), Lecture Theater 1, august 30, 2024, 14:00 - 16:00

Background
Inverse multislice uses experimental momentum-resolved scanning transmission electron microscopy (4D-STEM) data to reconstruct the individual slice transmission functions (phase gratings) of a specimen. It solves the problem of inverse dynamical scattering, and takes partial coherence effects into account to obtain spatial resolutions in the range of thermal vibrations [1]. Both the incident probes and phase gratings are usually optimized on a pixel-wise grid, involving the determination of 10^6 to 10^7 unknowns. In this work, we present an inverse multislice concept which uses a consequently physical parameterisation of both probes and specimen. A few aberration coefficients, focal spread and source size describe the illumination comprehensively, and the phase gratings are parameterised via atomic types, positions, occupancies and thermal vibrational amplitudes. Consequently, the number of unknowns is reduced by at least four orders of magnitude. This leads to both a more efficient and stable inversion strategy, and the capability of performing inverse frozen phonon (FP) multislice. The latter incorporates thermal diffuse scattering (TDS) and exhibits enhanced sensitivity to temperature and chemistry. We present both the methodological concept and its application to measuring ferroelectric displacements experimentally in $Pb(ZrTi)O_3$ (PZT) with picometre precision [2].

Methods
Inverse multislice starts with an initial guess for the probe and the phase gratings, performs forward multislice so as to calculate a loss with respect to the experimental 4D-STEM data. The update for the subsequent epoch is derived from the gradient of the loss as to the parameters of interest. We developed an efficient implementation of this scheme by (i) expressing the multislice as an artificial neural network following van den Broek [3] within PyTorch, being able to (ii) seamlessly allocate all gradients in a single forward run. We start with conventional, pixel-wise inverse multislice reconstructions, followed by the detection of atomic structure, types and probe parameters to initialise a parametric model. Instead of complex-valued pixels, gradients decisively update real physical parameters, especially atom positions. We then firstly employ the Debye-Waller approach with absorptive potentials for the reconstruction, and secondly switch to a full inverse FP multislice which also inverts TDS using several thermal snapshots while still considering more than 10 probes to account for partial coherence. Our method is verified using FP ground truth 4D-STEM simulations first, before experimental 4D-STEM data of PZT (EMPAD recording on probe-corrected FEI Titan, 200kV) is analysed inversely using 52 slices, corresponding to a thickness of 22nm.

Results
Concerning forward scattering the FP concept involves averaging over multiple configurations of thermal atomic displacements $\vec{u}$ from the equilibrium positions as illustrated in Fig. 1a, being responsible for TDS. Via the mean squared displacement $\langle u^2 \rangle$, TDS is explicitly accounted for in our inverse multislice as forward scattering theory demands. At the same time, our model is also differentiable with respect to the atom positions, as shown in Fig. 1b. Here, we simulated 4D-STEM data of 20nm thick PZT using FP multislice including ferroelectric displacements. For the reconstruction, no polarisation was used as prior by initialising with a centrosymmetric model and

taking projected potentials from literature [4]. For 101 epochs, Fig. 1b shows the optimisation trajectories of the Zr(0.2)Ti(0.8) site treated as a virtual atom obtained by linear interpolation, and one oxygen site. Even though the forward simulation used the discrete random mixture of the Zr(0.2)Ti(0.8) site, the reconstruction with a virtual atom yields a final position between the ground truths (dashed cross) for Zr and Ti, shifted proportionally according to the chemistry of the atomic column. Moreover, the lower graph indicates an exact reproduction of the oxygen site after 101 epochs.
Applying the methodology to experimental 4D-STEM data of PZT results in an atomic structure depicted by its projected potential in Fig. 1c for the reconstructed region, whereas the initial model started with a nonpolar crystal. The polarisation of the final state is visible by eye and free of artefacts such as mistilt which we took into account by a modified Fresnel propagation that was also optimized. The displacements from the symmetry positions are mapped in Fig. 1d, with different markers for the different atom columns and the ferroelectric displacements colour-coded. The high-precision homogeneous polarisation in the scan region becomes obvious, and is confirmed by the statistical evaluation in Fig. 1c (table). The displacements are accurate to a few picometres, can distinguish oxygen from the (ZrTi) site in the same column and fit excellently with literature for the same alloy. We discuss our findings via a quantitative comparison with atom positions retrieved a posteriori from phase gratings retrieved pixel-wise assuming a unimodal specimen. In this case, several unit cells exhibit the wrong polarisation direction.

Conclusion

Inverse multislice taking multimodal states of both illumination and specimen into account is capable of exploiting TDS in the reconstructions. Since TDS is a major contribution in thick specimen for which (inverse) multislice is designed, this opens several possibilities to accurately measure atom positions, atom types and temperature or Debye parameters, whereas sensitivity to the latter parameters will be discussed in our contribution based on simulations.

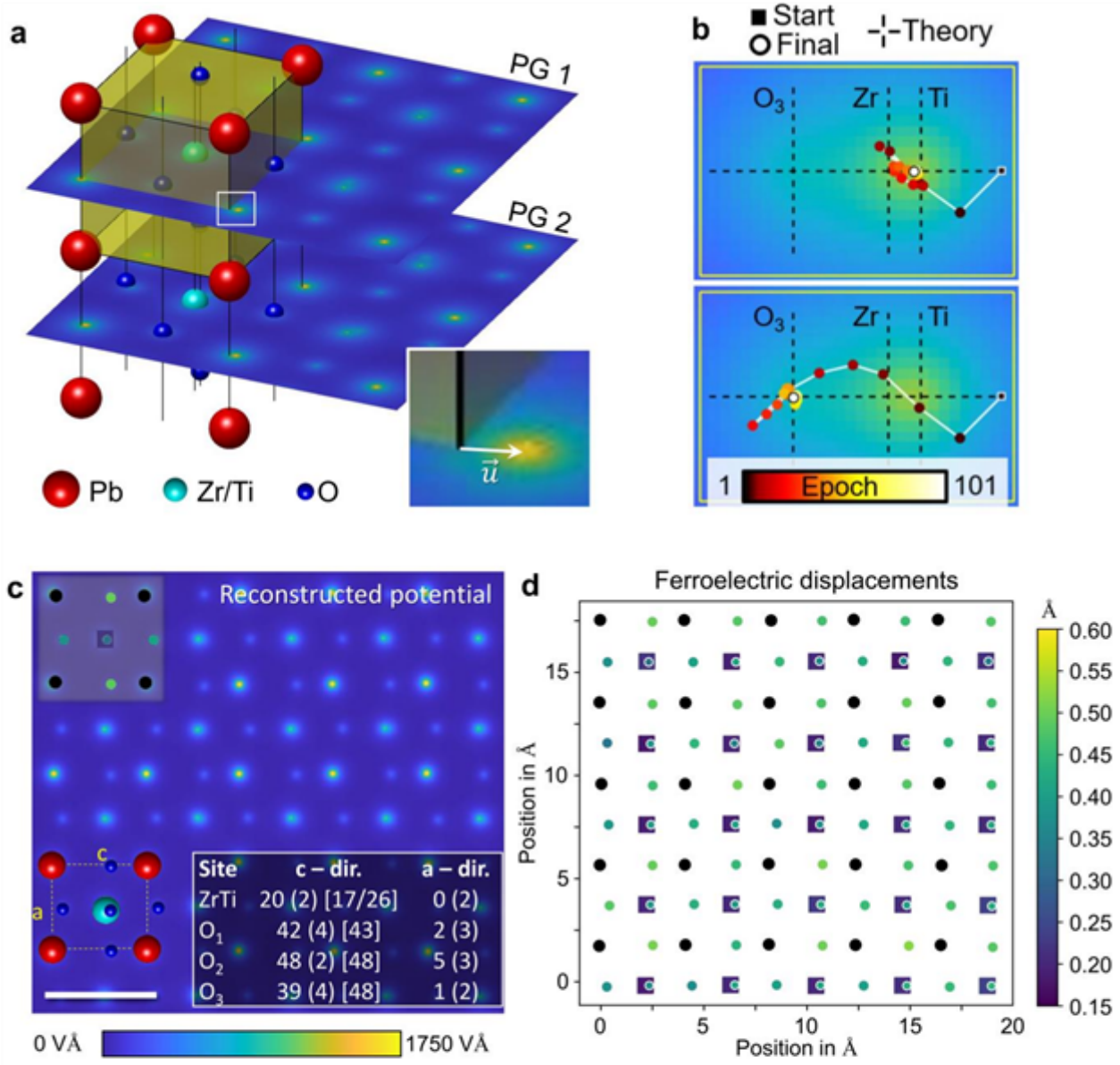

Fig. 1: **a:** Phase gratings (PG) as used in FP multislice with explicit thermal atomic displacements $\vec{u}$. **b:** Optimisation trajectories for a virtual (ZrTi) atom approximating the mixed site, and for a pure oxygen column in ferroelectric PZT. Initial position: centrosymmetric. Dashed cross: ground truth of simulation, which is reproduced accurately by the reconstruction. **c:** Projected potential obtained from experimental 4D-STEM data of PZT with structure and ferroelectric displacement statistics. d: Mapped ferroelectric displacements in reconstructed region from (c) with Pb (black circle), oxygen (coloured circle) and (ZrTi) site (square).

Keywords:

Inverse multislice, Ptychography, 4D-STEM

Reference:

[1] Chen et al. Science 372, 826 (2021).
[2] Diederichs et al. Nat Commun. 15, 101 (2024).
[3] Van den Broek & Koch, Phys, Rev. Lett. 109, 245502 (2012).
[4] Lobato & van Dyck, Act Cryst. A 70, 636 (2014).
[5] Funding from the Bavarian HighTech Agenda (EQAP project), DFG (EXC 2089/1 – 390776260) and Helmholtz (VH-NG1317) is kindly acknowledged.

1117

Towards Single-Pattern Absolute High angular Resolution EBSD without using Simulated Patterns as Reference

Dr. Tijmen Vermeij[1,2], Lloyd Dodsworth[1], Dr. Aimo Winkelmann[3], Dr. René De Kloe[4], Dr. Johan Hoefnagels[1]
[1]Mechanical Engineering, Eindhoven University of Technology, Eindhoven, Netherlands, [2]Laboratory for Mechanics of Materials and Nanostructures, Swiss Federal Laboratories for Materials Science and Technology (EMPA), Thun, Switzerland, [3]AGH University of Science and Technology, Krakow, Poland, [4]EDAX, Tilburg, Netherlands

IM-06 (3), Lecture Theater 1, august 30, 2024, 14:00 - 16:00

Background
Over the years, High angular Resolution EBSD (HR-EBSD) has evolved into a reliable tool for measuring misorientations and relative stresses (elastic strains) in crystalline materials with high sensitivity [1]. However, in the absence of stress-free intragranular reference points, absolute stress measurements are not yet routinely performed, while they could potentially provide new insights in the micromechanics of a range of (poly)crystalline materials.
The extension from relative to absolute cross-correlation based HR-EBSD, by using a simulated EBSD pattern as a reference, is under continuous development in the literature [2]. However, there are limitations by factors such as the inaccurate simulation of EBSD patterns and the uncertainty of the experimental EBSD geometry [3]. Consequently, an absolute HR-EBSD approach without using simulated reference patterns, or any experimental stress-free reference pattern, would be of huge interest to the community.
In the past years, several developments were proposed to extend HR-EBSD from a local cross-correlation based approach to a global full-field correlation [4]. Besides improved accuracy and robustness, such consistent correlation frameworks have shown the potential for non-simulation based absolute HR-EBSD, by exploiting crystal symmetry, simultaneous correlation between multiple (intergranular) patterns and co-correlating the pattern centre [5]. However, experimental validation is non-trivial on polycrystalline materials and excess-deficiency features (band asymmetry) in the patterns were expected to cause problems.

Methods
Therefore, we have continued developments on this framework to reduce the complexity towards an absolute non-simulation-based HR-EBSD correlation of only a single pattern. Specifically, we correlate one area within a pattern to another area of the same pattern by using crystal symmetry operators, as visualized for a single symmetry operator in the figure attached. Using all available symmetry operators, we correlate multiple areas within the same pattern in parallel, using absolute in-plane stress components, absolute orientation, and the pattern centre parameters as degrees of freedom.

Results
In this presentation, we will first show how the framework works and how it performs on idealized simulated patterns. Further testing on single experimental stress-free patterns, acquired with a direct electron EBSD camera, will show how excess-deficiency features can significantly degrade the experimental accuracy, as verified on dedicated dynamically simulated patterns. Therefore, the method is extended with an integrated excess-deficiency correction approach which shows how non-simulation based absolute HR-EBSD is finally within reach.

Conclusion

In summary, we advance absolute HR-EBSD while avoiding the use of simulated patterns as a reference. Through single-pattern correlation in an advanced DIC framework, we show the potential for measuring absolute elastic strains at high resolution.

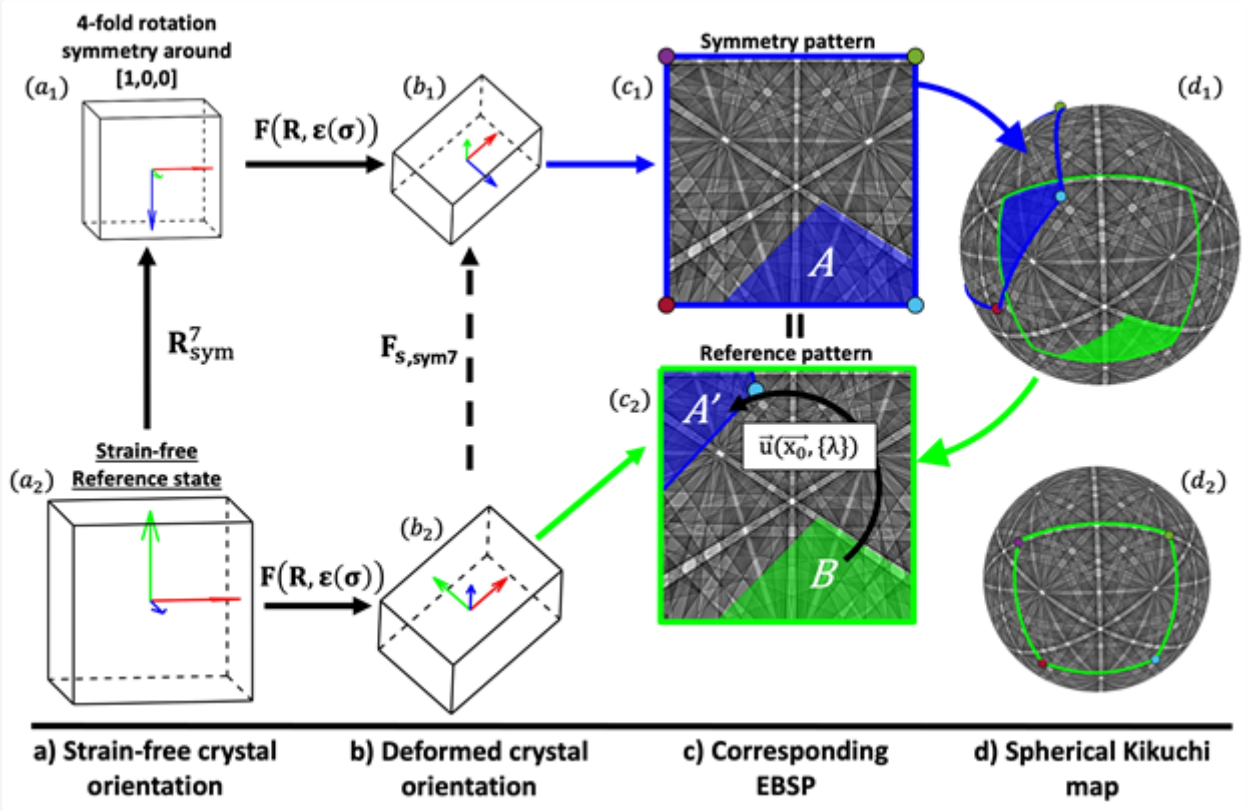

Keywords:

HR-EBSD, EBSD, absolute stress, DIC

Reference:

[1] A.J. Wilkinson, G. Meaden & D.J. Dingley. Ultramicroscopy 106 (2006) 307-313.
[2] T. Tanaka & A.J. Wilkinson. Ultramicroscopy 202 (2019) 87-99.
[3] T.B. Britton, C. Maurice, R. Fortunier, J.H. Driver, A.P. Day, G. Meaden, D.J. Dingley, K. Mingard & A.J. Wilkinson. Ultramicroscopy 110 (2010) 1443-1453.
[4] T. Vermeij & J.P.M. Hoefnagels. Ultramicroscopy 191 (2018) 44-50.
[5] T. Vermeij, M. De Graef & J.P.M. Hoefnagels. Scripta Materialia 162 (2019) 266-271.

38

HeXI: The High-energy Electron Xtallography Instrument at Diamond Light Source

Pedro Nunes[1], Mark Lunnon[1], Bodvar Olafsson[1], Andrew Foster[1], Richard Littlewood[1], Graham Duller[1], Gwyndaf Evans[1,2], Alistair Siebert[1]
[1]Diamond Light Source, Harwell, United Kingdom, [2]The Rosalind Franklin Institute, Harwell, United Kingdom

Poster Group 2

The HeXI project, funded by the Wellcome Trust “Electrifying Life Sciences” grant and Diamond Light Source, aims to build a dedicated electron diffractometer to investigate the potential of Mega-electron volt (MeV) electrons for the determination of molecular structures from nanometre sized crystals. The HeXI instrument will leverage the increased penetration of MeV electrons and the high precision goniometry, cryo-sample transfer systems and sample preparation methods developed at Diamond to target crystal thicknesses between 300 nm and ~1 µm to determine the molecular structures of proteins and pharmacologically relevant molecules. The ability to acquire high-fidelity sweep and serial diffraction data from ≤1-micron thick crystals will bridge the current crystal size gap between samples amenable to electron diffraction performed on commercial Transmission Electron Microscopes (TEMs) using <300 nm crystals and microfocus X-ray diffraction of >3 µm crystals at microfocus beamlines

Keywords:

Megavolt Electron Diffraction

55

Using Virtual Detectors as a Compression Tool for Electron Ptychography

Anton Gladyshev[1,2], Mr. Marcel Schloz[1,2], Mr. Johannes Müller[1,2], Dr. Benedikt Haas[1,2], Prof. PhD Christoph Koch[1,2]
[1]Humboldt-Universität zu Berlin , Berlin, Germany, [2]Center for the Science of Materials Berlin, Berlin, Germany

Poster Group 2

Background incl. aims

Far-field iterative electron ptychography [1,2,3] is a phase retrieval technique offering atomic scale imaging in scanning transmission electron microscopy (STEM) [4,5]. It fits an electrostatic potential of a specimen to a set of diffraction patterns collected while illuminating overlapping areas of its surface with a convergent beam [1,2,3,5]. Despite its rapid development, ptychography suffers from several practical challenges, particularly from the massive amount of data that is required to achieve a high degree of redundancy to solve the phase problem [2]. Our study addresses this limitation by proposing a lossy compression method for diffraction patterns [2] utilising virtual STEM detectors [2,4].

Methods

A 92 Å thick atomistic model of a silicon crystal containing a 60° edge dislocation dissociated into a stacking fault bounded by a 30° and 90° partial dislocation [5] was used to simulate a 4D-STEM [1] dataset with qstem [5], at an accelerating voltage of 60 kV, convergence semi-angle of 30 mrad and a scan step of 1 Å, including thermal diffuse scattering, an effective source of size 0.5 Å and a finite electron dose of 104 e-/Å^2. To perform electron ptychography we utilize an in-house written gradient-based optimization code [3] and use 4 slices of the transmission function in order to account for multiple scattering [1,2,5].

Our compression approach relies on virtual detectors [2,4]. With a single 4D-STEM detector they allow for a simultaneous recording of multiple signals, such as virtual annular dark- and bright-field (vADF and vABF), or centre of mass (COM) signals. In contrast to physical detectors, the virtual ones offer a flexibility to adjust their shapes to closely mimic actual diffraction patterns, facilitating a more efficient compression [2]. In an uncompressed scenario [1,2,3] the goal of an iterative ptychographic algorithm is to minimize the summed squared error (SSE) between the 4D-STEM dataset and the diffraction patterns generated by algorithm [1,2,3]. With a compressed data we modify the algorithm to predict the signals instead of the diffraction patterns via an additional known convolution layer [2] and aim to minimize the SSE between them and the measured signals of virtual detectors.

Results

In Figure 1 we compare three sets of virtual detectors for the bright field of the diffraction patterns: first 36 Zernike polynomials, 45 binning squares each 7x7 px wide and 15 virtual detectors generated via the Gram-Schmidt algorithm [2] from the diffraction patterns acquired at the positions indicated by the x-markers in the panel c). The dark field of the diffraction patterns was described via a single vADF detector in all three cases. For each compression option we show 6 bright field virtual detectors in panels e)-v) and compute the Fourier ring correlation with the projected potential used for the simulation of the dataset.

Figure 1 Comparison of ptychographically reconstructed projected phases of a silicon crystal from compressed 4D-STEM data. a), b) and c) show the results for first 36 Zernike polynomials, 45 binning detectors and 15 data-dependent virtual detectors, respectively. For each of three options we show 6

virtual detectors in e)-v). For data-dependent detectors we denote the scan positions used to generate them via lime-colored x-markers in c). The projected electrostatic potential used for a simulation of the dataset is presented in d). Further we compare the Fourier ring correlations between the reference potential and three reconstructions in w).

Conclusions

The diffraction patterns in the initial dataset were 500x500 px wide. Our findings reveal that through the application of virtual detectors, including Zernike polynomials, binning squares, and detectors generated via the Gram-Schmidt algorithm, we can achieve a data compression ratio [2] of 5,000 to 15,000. Most importantly, our results demonstrate that atomic resolution in ptychographic reconstructions can be maintained even under conditions of partial spatial coherence and limited electron dose. The proposed compression approach takes the specific geometry of diffraction patterns into account and retains a sufficient amount of the "intact" information [2]. No specific constraints, e.g. a regularization, were used, but as previously shown [1], this could improve the quality of the reconstructions.

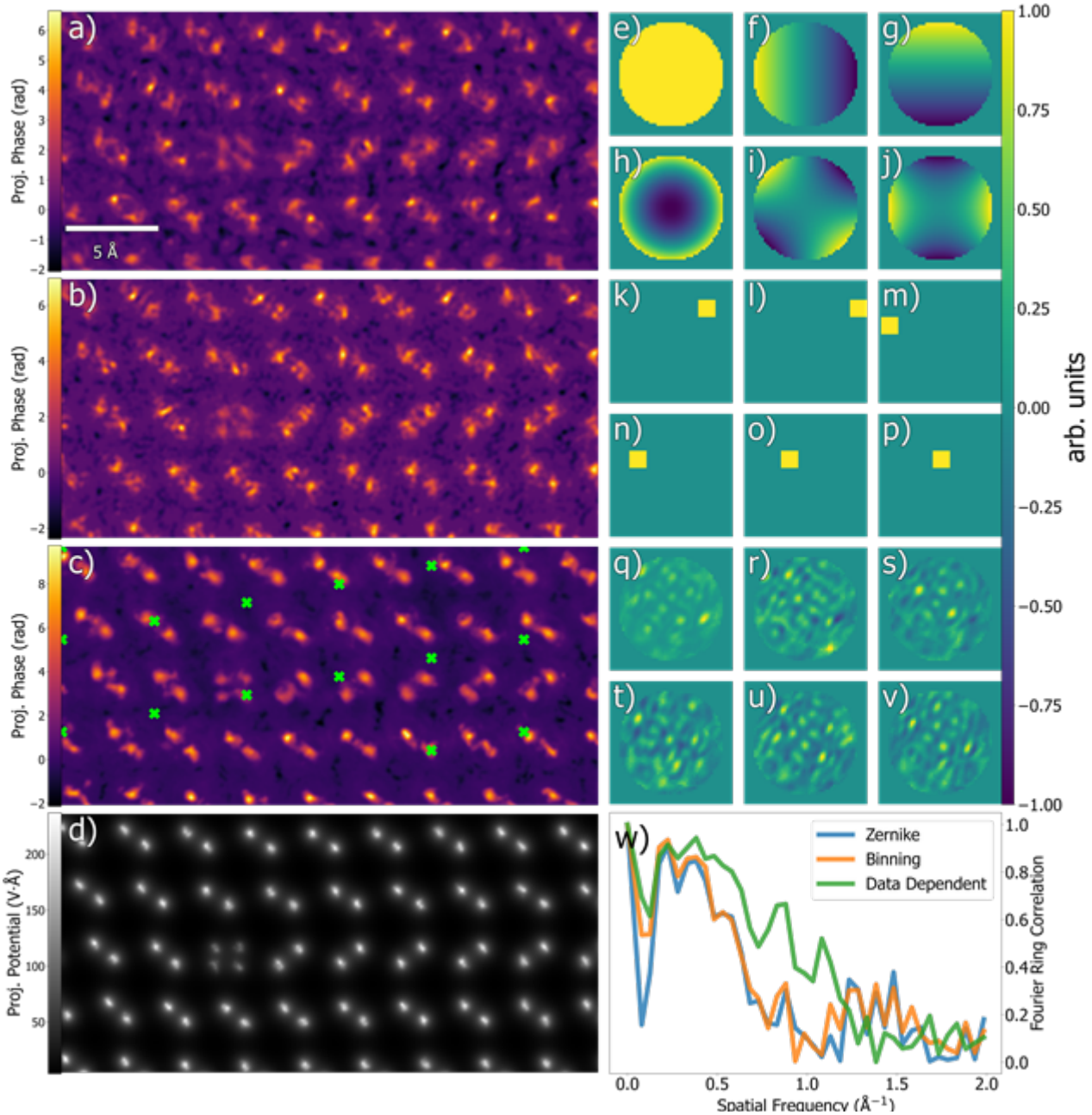

Keywords:

4D-STEM, Compression, Virtual Detectors, Ptychography

Reference:

[1] Schloz, M. et al. (2020). Optics Express. doi:10.1364/OE.396925
[2] Gladyshev, A. et al. (2022). arXiv. doi:arXiv:2211.07372
[3] Gladyshev, A. et al. (2023). arXiv. doi:arXiv:2309.12017
[4] Haas, B. et al. (2021). Microscopy and Microanalysis. doi:10.1017/S1431927621003779
[5] Spence, J. C. H. et al. (2006). Philosophical Magazine. doi:10.1080/14786430600776322

113

Determining alloy concentration by analyzing dynamic diffraction at strained semiconductor interfaces

Frederik Otto[1], Dr. Laura Niermann[1], Dr. Tore Niermann[1], Prof. Dr. Michael Lehmann[1]
[1]Technische Universität Berlin, Berlin, Germany

Poster Group 2

Background incl. aims
In the realm of semiconductor devices, particularly in the context of quantum well lasers, the optical properties are shaped by bandgaps and band offsets derived from precisely engineered alloy concentrations in ternary semiconductors, exemplified by InGaAs quantum wells in GaAs. While S/TEM possesses the necessary spatial resolution for resolving sharp interfaces, EDX typically lacks precision in determining the alloy concentration. However, during epitaxial growth on a substrate, lattice mismatch induces stress at the interface, resulting in localized lattice deformations known as strain. When preparing a thin transmission electron microscopy (TEM) lamella of a strained interface, the stress supporting this strain lacks support on the top and bottom of the lamella, leading to stress relaxation. For a compressively strained layer, this corresponds to the lamella bulging outwards at the interface. The magnitude of this relaxation is unique to the strain at the interface cause by the lattice mismatch, and hence by the alloy concentration in the layer.
The aim of this study is to deduce the alloy concentration of compressively strained InGaAs quantum wells in a GaAs matrix through a detailed analysis of stress relaxation at the lamella's surfaces. This is accomplished by evaluating patterns inside the diffraction discs using scanning convergent electron beam diffraction (SCBED). These patterns, manifestations of multiple electron scattering or dynamic diffraction, exhibit high sensitivity to small changes in displacement in electron beam direction and consequently, to stress relaxation at the lamella’s surfaces. Alloy concentrations are determined by matching beam simulations of relaxed lamellas with varying parameters to the experimental data.
Methods
We prepare a TEM-lamella containing InGaAs layers with known In-concentration in GaAs close to the [100] zone axis using FIB. Deriving information involves detailed reproduction of measured features through simulations to infer the original lamella state. For computational efficiency, we tilt specimen along a quantum well layer into [002] systematic row conditions. Full 2D diffraction patterns (256x256 pixels) are recorded at each scan position within a 256x256 scan window. The resulting 4D dataset can be reduced to a 2D-representation, named as x-q plot, by considering the problem’s symmetry. This reduction involves focusing on one spatial coordinate x orthogonal to the layer. Additionally, only one reciprocal coordinate q along the systematic row, into which the specimen was tilted, is considered. The convergence angle is chosen to achieve non-overlapping discs.
To model the experimental data in simulations, we employ a two-step forward calculation process: Initially, we model the initial stress and the resulting relaxation by doing finite element calculations, providing the layer width, elastic constants and lattice mismatch as inputs. The resulting displacement is then incorporated into beam simulations, numerically propagating the Darwin-Howie-Wheelan (DHW) equation. The simulations are fine-tuned to align with experimental conditions, accounting for tilt, specimen bending, and lamella thickness.
Results
Leaveraging the nominal alloy concentration of a 5 nm wide In0.23Ga0.77As quantum well within GaAs, we successfully replicate dynamic diffraction features in simulations, yielding three key outcomes, as illustrated in Fig. 1. Firstly, our measurement reveals distinct features discernible in the x-q plot, unveiling changes in dynamic diffraction, even at considerable distances of multiple quantum well widths from the interface (Fig. 1 a). Secondly, comparing these findings with DHW

beam simulations that omit surface relaxation highlights the absence of these long-ranging features, conclusively attributing them to surface relaxation (Fig. 1 b, c). Lastly, by manipulating the initial lamella alloy concentration, we can modulate the influence of surface relaxation. Minimizing the discrepancy between the measurement and simulations for the Indium concentration allows us to faithfully reproduce the nominal Indium concentration. These results are validated using STEM-EDX and dark-field imaging of a chemically sensitive reflection. We further discuss the method's limitations concerning specimen thickness, quantum well width, and alloy concentration.

Conclusion

Our study successfully identifies the nominal alloy concentration of a compressively strained InGaAs quantum wells in GaAs through a detailed analysis of stress relaxation at the TEM-lamellas surfaces. This accomplishment involves precisely replicating dynamic diffraction features within diffraction discs through simulations. These simulations account for surface relaxation by incorporating the displacement from finite-element calculations of the strained interface for a given specimen thickness. The process of minimizing discrepancies between measurement and simulation by adjusting the alloy concentration opens a novel avenue of discerning semiconductor alloy concentrations at strained interfaces by analyzing the impact of surface relaxation on dynamic diffraction.

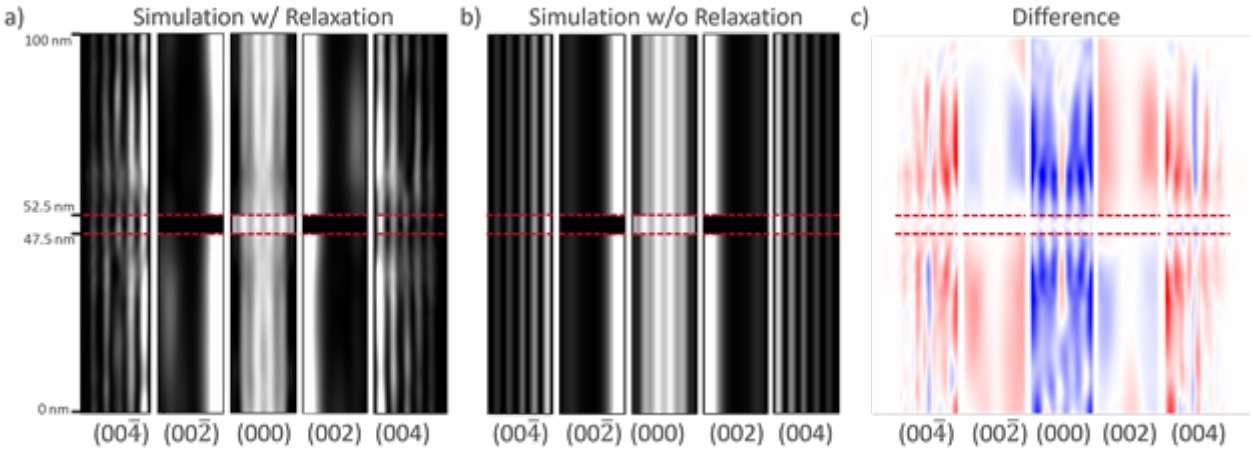

Keywords:

Strain, Relaxation, composition-determination, dynamic-diffraction, 4D-STEM

120

Depth Dependence of Electron Channeling Contrast Imaging in Gallium Nitride

Etienne Lavallee[1,2], Mr. Antoine Guitton[2], Mr. Peter Imrich[1], Ms. Claire Chisholm[1]
[1]KAI Kompetenzzentrum Automobil-und Industrieelektronik GmbH, 9524 Villach, Austria, [2]Université de Lorraine, CNRS, Arts et Métiers, LEM3, Metz, France

Poster Group 2

Background incl. aims
Interest for Gallium Nitride (GaN) and wide band-gap semiconductors has been growing the last few decades as a green-energy solution for electronic power devices and digital transition. Their enhanced electrical properties such as reduction of power losses or lower energy consumption tends to make them more suitable for power electronics applications over silicon. However, it is unclear whether leakage currents or device failures are related to crystalline defects, such as Threading Dislocations (TD), for which defect densities in GaN are orders of magnitude higher than in silicon. Detailed characterization of the defect nature and estimation of their density is, therefore, relevant to understand and improve GaN power devices. In this context, Electron Channeling Contrast Imaging (ECCI) can provide valuable insights. ECCI is a non-destructive method that offers the capability to provide Transmission Electron Microscopy (TEM)-like diffraction contrast imaging inside a Scanning Electron Microscope (SEM) on bulk samples. ECC is generated from electrons that channel down the crystal planes. Strain and defects cause distortion of the crystal lattice, resulting in changes in Backscattered Electron (BSE) intensity, thereby producing contrast in the image.
Diffraction contrast in bulk material is widely assumed to be generated from the near-surface layers (from tens to hundreds of nanometers) by electron channeling but there is currently no consensus about the depth from which the collected information originates. Therefore, it is critical to understand the depth dependence of the method to ensure measurements are made in the layer of interest.
The present study provides an experimental measurement of the signal from which the information in ECCI arises. This estimation aims to sharpen the statistical dislocation density estimation through series of measurements at different accelerating voltage and to establish a model for information emission while imaging GaN by ECCI.

Methods
The layer of interest, the GaN layer, lies between an AlxGa1-xN barrier layer and a series of strain-relief layers called the superlattice, for which the composition differs from the first one. As such, misfit dislocations, due to lattice mismatch, stand at the interface between the GaN and the superlattice. A Focused Ion Beam (FIB) was used to create wedges of different angles across these layers to vary the GaN layer thickness. The incident electron beam energy of the SEM was varied and the final depth the misfit dislocations were visible was recorded. Comparisons between multi-beam and 2-beam diffraction conditions was also performed.

Results
First results show ECCI probing depth can be tuned as a function of incident electron beam energy and that there are discrepancies between multi-beam and 2-beam diffraction conditions as well as the theorized channeling extinction distance and the experimentally measured probing range.

Conclusion

The key expected outcomes are an increase in estimated dislocation density accuracy in GaN and a better understanding of ECCI micrographs. The dataset is expected useful for complementary dislocation related fields of study such as layer growth or electrical characterization.

Acknowledgments

Funded by the European Union under grant agreement no. 101091621. Views and opinions are however those of the author(s) only and do not necessarily reflect those of the European Union. Neither the European Union nor the granting authority can be held responsible for them.
The authors would also like to acknowledge Dr. Aidan Taylor for assistance and expertise during sample preparation.

Keywords:

ECCI, GaN, SEM, Crystallography

201

Three-dimensional classification of dislocations from single projections

Dr. Tore Niermann[1], Ms. Laura Niermann[1], Mr. Michael Lehmann[1]
[1]Technische Universität Berlin, Institut für Optik und Atomare Physik, Berlin, Germany

Poster Group 2

Background incl. aims
Many material properties are governed by dislocations and their interactions. Examples range from the strengthening of metals and alloys to efficiency in semiconductor laser devices. Thus, knowledge of the three-dimensional topology of dislocation networks is crucial for material engineering. A two-dimensional projection of dislocation networks can be readily obtained by conventional (scanning-) transmission electron microscopy (S/TEM) images. Here we show a way to reveal the three-dimensional location of dislocations and simultaneously classify their type from a single 4D-STEM measurement [1].
Methods
Under systematic row conditions, where the systematic row is oriented non-parallel to the dislocation's Burgers vector, the 4D-STEM dataset can be represented by a reduced 2D dataset, with a spatial dimension x perpendicular to the dislocation line and a diffraction dimension q in the direction of the systematic row. Due to dynamical diffraction effects, such (x, q)-datasets exhibit sufficient information to uniquely identify the dislocation type and its three-dimensional depth within the S/TEM lamella. This identification is facilitated by comparison of the experimental (x, q)-data to a database with calculated (x, q)-data, where the relevant parameters Burger's vector, dislocation depth, lamella thickness, and beam tilt were varied. The column approximation is sufficiently accurate for the calculation task, which allows a numerically efficient calculation of the database by a forward propagation of the Darwin-Howie-Whelan equations [2].
Results
For an exemplary dislocation the results are shown in the figure. The investigated dislocation is a threading screw dislocation with a line vector of [0001] found within a GaN buffer grown on a sapphire substrate. The data was obtained under (0002) systematic row conditions. In the left-hand panel the experimentally obtained (x, q)-data for this dislocation is displayed. The panel in the middle shows the best matching calculation for the data, which was obtained for a Burgers vector of [000-1], a lamella thickness of 132 nm, and a depth of the dislocation core of 55 nm behind the entrance surface. The right-hand panel shows the mean squared error evaluated during the comparison, which is the average squared difference between the experimental data and the individual (x, q)-data from the database. Even though local minima are found for several specimen thicknesses and dislocation depths, the global minimum can be easily identified.
Conclusion
The ability to three-dimensionally locate a dislocation within a specimen and simultaneously classify its type provides an extremely powerful way for the investigation of dislocation networks. A 3D classification is possible from a single 4D-STEM measurement within the limitations of the g·b criterion. In comparison to tomographic methods a single 4D-STEM measurement can be performed much faster and with less dose, which enables the investigation of dislocation networks in beam-sensitive materials or in dynamic conditions, like during an in-situ heating/cooling experiment.

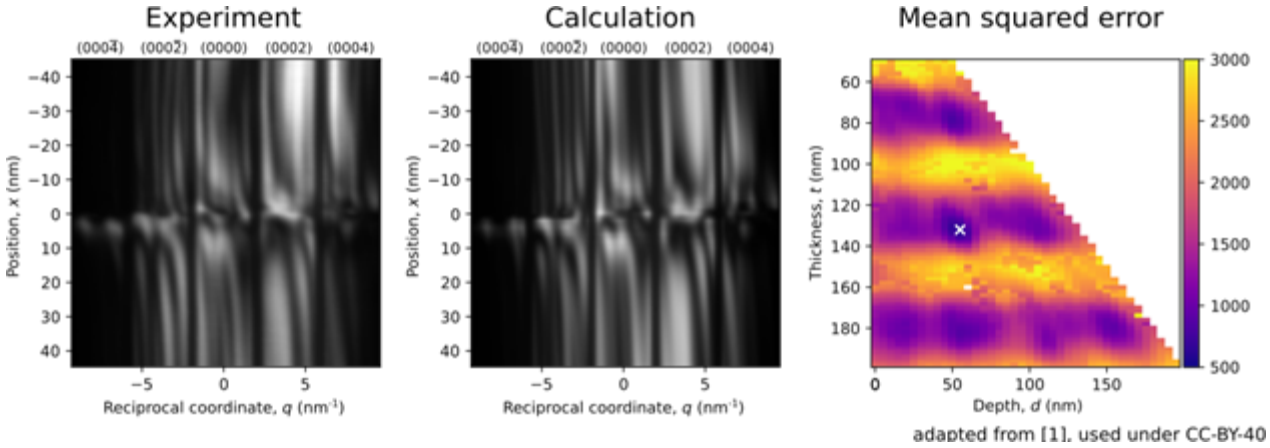

adapted from [1], used under CC-BY-40

Keywords:

4D-STEM, Dislocations, Dynamical diffraction

Reference:

[1] T. Niermann, L. Niermann, M. Lehmann; Nature Communications 15 (2024), 1356
[2] A. Howie, Z. Basinski, Phil. Mag. 17 (1968), 1039

229

Gigabytes to Megabytes – Rapidly analyzing in-situ videos to track lattice spacing changes

Ben Miller[1], Cory Czarnik[1]
[1]Gatan, Inc., Pleasanton, USA

Poster Group 2

Background incl. aims
Recently, counted direct detection cameras which are virtually noise-free have enabled very faint diffraction spots to be detected at high spatial frequencies. These same cameras provide sharp detail, enabling spots to be precisely located. This combination of a large range and high resolution in reciprocal space requires large images to be captured. When samples are also changing over time, the capacity to capture an entire video dataset of the dynamic behavior is also valuable. This leads to three-dimensional datasets with billions of pixels that may be tens of gigabytes in size. These may be information-rich, but are impossible to visualize or analyze without some processing. In this work, we use a Python script to process each diffraction pattern in an in-situ video dataset to produce a series of radial profiles over time. This reduces the dimensionality, making them more amenable to visualization, easier to analyze, and significantly smaller. It also provides a more directly interpretable result in minutes that can be used to determine whether good data has been captured while the user is still sitting at the microscope.
Methods
The Python script used in this work processes each diffraction pattern in an in-situ video dataset to produce a series of radial profiles over time. It is freely available online[1] and runs within the Gatan DigitalMicrograph software, which facilitates immediate application of the processing to diffraction datasets just collected at the microscope. The script does not merely calculate a radial average, since this will tend to miss faint spots, especially those at large spatial frequency, where there may be thousands of pixels at a specified radius, but only a few with real diffraction signal. Even if the detector was perfect, contributing no noise to the pattern, shot noise from the diffuse scatter in the pattern at that radius would often contribute more to the average than the real signal. Instead the script calculates a radial maximum, and subtracts the radial average, reducing the impact of any uniformly distributed background intensity. It also masks the center of the pattern and optionally filters it with a median filter prior to calculating the profiles. The script applies this processing to every frame in an in-situ video dataset captured by a Gatan in-situ camera, and produces two equivalent outputs. The first output is a 1D profile over time, which can be played back with the same In-Situ Player used to play back the original data, and is automatically synced with the original data if this is also displayed. The second output, as shown in Figure 1, is a 2D visualization where the horizontal axis is time, and the profiles are displayed vertically with the center of each pattern at the top. While this abstract is focused on the application of this script to diffraction patterns, it should be noted that a similar approach can be applied to high resolution TEM videos by first computing the FFT of each frame.
Results
This script reduces the dimensionality of datasets from 3D to 2D, reducing data size and facilitating visualization and analysis. For a diffraction dataset with 1k x 1k patterns (1 million pixels) a single radial profile with minimal loss of resolution is 500 pixels, so the reduction in data size is roughly a factor of 2000. If the same dataset has 1,000 frames with a bit depth of 32, the data size will be reduced from around 3.7 GB to 1.9 MB. This takes about 3 minutes on the Gatan camera computer, making it possible to run during a TEM session. In many cases, this can immediately inform the user about whether they've collected the data they need. For almost all datasets, it is easier and faster to perform further processing or analysis on the 2D data, rather than the full 3D dataset.

We have applied this diffraction processing to 2 classes of in-situ videos. First, this has been applied to monitor the damage of beam-sensitive materials over time, including metal-organic frameworks (MOFs) and zeolites. If the electron dose rate is known, this can rapidly quantify the amount of dose required to degrade or destroy the sample. Second, the same script has been applied to in-situ videos of reversible phase changes, making it easy to determine the exact timing of the phase change, and to correlate this with the in-situ conditions.
It should be noted that not all changes observed in diffraction patterns over time can be attributed to beam damage or phase changes. Sample drift in x-y or in the z direction, or rotation of small crystals can lead to changes in the pattern which are difficult to distinguish changes that are the result of more interesting phenomena. Care must be taken by the user to correctly interpret the changes observed, and a full discussion of this is outside the scope of this work.
Conclusions
In-situ diffraction data captured by modern cameras is information-rich, but can also be very large and must be processed. Rapid processing and visualization can be performed using Python in DigitalMicrograph to reduce dimensionality and data size prior to performing detailed analysis. A freely available script has been written to perform this analysis, and applied to video datasets of beam damage and phase transformations.

Figure: Examples of 2D visualizations of in-situ diffraction datasets. For each dataset, the profiles go from the center of the pattern at the top toward the edge of the pattern at the bottom. Left: Datasets recording the effects of beam damage for 2D MOF-2 and for ZSM-5. The MOF sample was damaged in seconds, while the zeolite dataset was recorded for over an hour. Right: Datasets recording temperature-induced reversible phase transformations: Sn nanoparticles being heated repeatedly above and below the melting point, VO2 heated above and below its metal-to-insulator transition, with varying ramp rates.

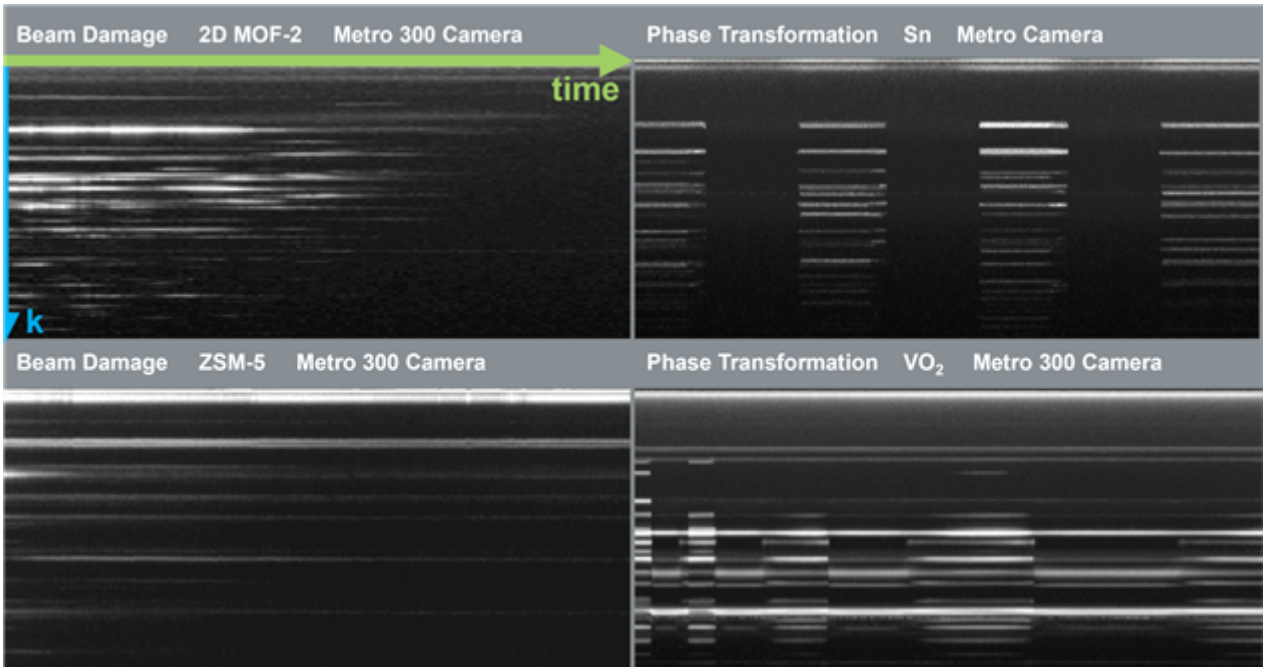

Keywords:

Diffraction, Python, Processing, In-Situ, Continuous

Reference:

[1] https://www.gatan.com/resources/scripts-library?field_script_type_value%5B%5D=python_gatan Accessed Mar 2024

261

Texture analysis of radiation sensitive organic films: Comparative study by electron diffraction tomography and GIWAXS

Irene Kraus[1], Dr. Mingjian Wu[1], Dr. Stefanie Rechberger[1], Dr. Johannes Will[1], Dr. Santanu Maiti[2], Andreas Kuhlmann[3,4], Marten Huck[3,4], Marc Steinberger[5], Prof. Dr. Christoph Brabec[5], Prof. Dr. Hans-Georg Steinrück[3,4], Prof. Dr. Tobias Unruh[2], Prof. Dr. rer. nat. habil. Erdmann Spiecker[1]
[1]Institute of Micro- and Nanostructure Research (IMN) & Center for Nanoanalysis and Electron Microscopy (CENEM), FAU Erlangen-Nürnberg, Erlangen, Germany, [2]Institute for Crystallography and Structural Physics (ICSP), FAU Erlangen-Nürnberg, Erlangen, Germany, [3]Institute for a Sustainable Hydrogen Economy (INW), Forschungszentrum Jülich GmbH, Jülich, Germany, [4]Institute of Physical Chemistry, RWTH Aachen University, Aachen, Germany, [5]Institute Materials for Electronics and Energy Technology (i-MEET), FAU Erlangen-Nürnberg, Erlangen, Germany

Poster Group 2

Background incl. aims
Texture describes the preferred orientation of grains in crystalline materials. For characterization of texture, the reciprocal space is conventionally investigated in diffraction experiments using electrons, X-rays or neutrons as probes. In polycrystalline thin films texture is an important characteristic of the microstructure determining anisotropic properties like, e.g., charge carrier transport in bulk heterojunction (BHJ) organic solar cells (OSC). Gracing incidence wide angle X-ray scattering (GIWAXS) is a well-established method for texture analysis of OSCs, however, real space information is only indirectly accessible as averaging measure (e.g. grain size or coherence length). In contrast, electrons as probe in transmission electron microscopes (TEM) provide direct access to both real and reciprocal space while additionally delivering analytical signals for local chemical analysis. However, due to the challenge of radiation damage, electron diffraction is not well explored for OSCs. In this work we show that electron diffraction tomography (EDT) can be used to investigate the reciprocal space of polycrystalline thin films in 3D, providing information on texture comparable to results obtained with GIWAXS.
Methods
We chose two radiation sensitive BHJ OSC active layers as model sample systems. Both OSCs contain $PC_{71}BM$ as fullerene acceptor, but differ in that the donor component is a small molecule (DRCN5T) in one case and the classical polymer P3HT in the other. Large-area plan-view samples of the active layer were prepared by floating off the spin-coated film from the substrate and transferring it to a TEM grid. Real space information on the nanomorphology of the donor and acceptor phases was obtained using STEM-EELS or EFTEM as exemplary shown for the DRCN5T/$PC_{71}BM$ system in Fig. 1a. For EDT we acquired tilt series of zero-loss energy filtered SAED patterns across a tilt range of ±70° using a single-axis tomography holder (Fig. 1b). Energy filtering is necessary to suppress inelastic scattering background in particular at small scattering angles, which is critical to reveal crystallographic information on the small molecule/polymer crystallites with their nm-sized unit cells. To minimize effects of radiation damage, each diffraction pattern was acquired at a fresh sample area with electron dose well below the evaluated critical dose. From the SAED tilt series the 3D diffraction space was reconstructed with a home-developed code for 3D reciprocal space filling which is based on polar transformations (Fig. 1c). Furthermore, azimuthal averaging of the volume around qz axis was performed to obtain qr-qz reciprocal space maps for direct comparison with GIWAXS data.
Results
The qr-qz reciprocal space maps derived from EDT and GIWAXS are exemplarily depicted side-by-side in Fig. 1d for the DRCN5T/$PC_{71}BM$ film. They show excellent agreement, indicating that not only GIWAXS but also EDT is perfectly suited for texture analysis of such radiation sensitive organic films.

Moreover, direct comparison of different line profiles extracted from the reciprocal space maps reveal even quantitative matching of EDT and GIWAXS data. Interestingly, the EDT data show a better signal-to-noise ratio, in particular regarding the in-plane reciprocal information, which is difficult to access with GIWAXS. From the reciprocal space maps, it can be seen that the π-stacking of the small molecules in the DRCN5T crystallites exhibit preferred edge-on and face-on orientation in the fibre like nanomorphology revealed by STEM-EELS. Quantitative evaluation of the diffraction peak characteristics yields comparable structural information in terms of crystal coherence length, mosaicity, etc..

Conclusion

In summary, we demonstrate that the texture of radiation sensitive OSC thin films can be investigated using EDT yielding results in quantitative agreement with GIWAXS. Combining EDT with real space characterization using high-resolution and analytical TEM methods provides great opportunities for a more comprehensive and in-depth analysis of OSC thin films. Furthermore, the application of the presented methodology to state-of-the-art, non-fullerene OSC systems consisting of PM6:Y6 is in progress and will be covered in the conference contribution.

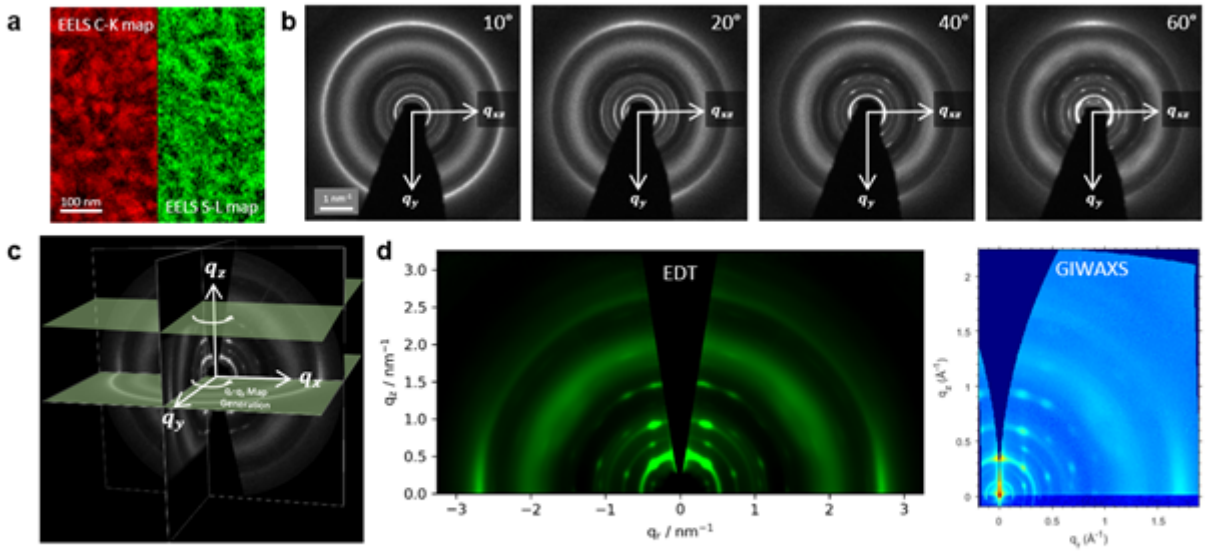

Figure 1: Characterization of DRCN5T:$PC_{71}BM$ BHJ OSC. (a) STEM-EELS dataset showing the nanomorphology. (b) Exemplary EF-SAED patterns out of the acquired tilt series. (c) Reconstructed 3D reciprocal space featuring the azimuthal integration for obtaining (d) the q_r-q_z map for comparison to GIWAXS measurements (left: EDT data, right: GIWAXS data).

Keywords:

Thin-film texture, EDT, OSC, GIWAXS

275

Electron channeling pattern imaging – a novel approach for the determination of wafer offcut angles

Han Han[1], Mr. Libor Strakos[2], Mr. Clément Porret[1], Ms. Valérie Depauw[1], Mr. Tomas Vystavel[2], Mr. Olivier Richard[1], Ms. Eva Grieten[1], Mr. Thomas Hantschel[1]
[1]imec, Leuven, Belgium, [2]Thermo Fischer Scientific, Brno, Czech Republic

Poster Group 2

Background incl. aims
The epitaxial growth of semiconductor multilayers can benefit from the use of wafer substrates with different offcut angles. The offcut angle of a wafer refers to the angle between the wafer surface normal and the chosen zone axis. These offcuts can be precisely controlled on monocrystalline wafers such as silicon or sapphire according to the growth needs. A possible application consists in tuning the strain in the epitaxial stacks by growing the layers on single-crystal wafers with precisely controlled offcuts. However, improper wafer offcuts can lead to the undesired formation of grains, anti-phase boundaries and uncontrolled growth modes. These offcuts must therefore be accurately controlled. To characterize wafer offcuts, methods based on high-resolution X-ray diffraction (XRD) [1] and electron backscatter diffraction (EBSD) [2] can be used to characterize the wafer offcuts with sub 0.1° angular resolution. However, such measurements are complex and time-consuming (several hours). Therefore, the availability of a fast and accurate method for wafer offcut angle determination is highly desirable to enable efficient quality checks of incoming wafers and to support the growth of high-quality materials for advanced semiconductor devices. In this contribution we propose a novel workflow based on applying electron channeling pattern imaging (ECPI) techniques and successfully utilized this method to measure wafer offcut angles.

Methods
ECP is based on the diffraction of backscattered electrons (BSE) inside crystalline materials [3]. The variation of the BSE yield as a function of the incident beam direction results in a distinctive band pattern on the sample surface. This generates a set of electron channeling bands (ECB) appearing as dark lines, which forms the ECP superposed on the BSE image. For monocrystalline samples, the ECP is determined by the crystal structure and orientation. While ECP represents the reciprocal space projection onto the detector plane, the sample rotation causes the respective rotation of the ECP. The beam center can be determined by the sample rotation. Having a sample with an offcut angle deviated from the zone axis means that the ECP rotation center is not fixed to the nearest zone axis. Upon sample rotation, the ECP center forms a circular trajectory as the sample is rigidly fixed with the zone axis. As a result, the precise wafer offcuts can be directly measured from the analysis of ECP images.

Results
In this work, we successfully applied this method to Si(001) wafers with and without offcut angles. After sample loading into the chamber, the sample surface normal is first properly aligned to the primary electron beam. For the zone axis (offcut angle < 3°) present on one ECP image, a rotation series is needed to determine the wafer offcuts. During the sample rotation the whole ECP including the zone axis moves around the surface normal along a circular path. The resulting radius of the zone axis trace is determined as the wafer offcut angles. In case the zone axis is not present in the field of view, additional tilts are required to determine the zone axis position and thus the wafer offcut. Following this approach, the achieved angular resolution is 0.1°, which agrees well with reference XRD results. With the routine procedure established in this work, the results can be obtained within 1

hour. Compared to the XRD and EBSD methods, it is faster and provides an acceptable accuracy, without requiring any specific sample preparation.

Conclusion

We demonstrate a new approach based on ECP images to determine wafer offcuts. The wafer offcut angle is characterized rapidly with an angular resolution of 0.1º. As a fast, accurate, and easy-to-use solution, the technique has wide applications, especially in the semiconductor field.

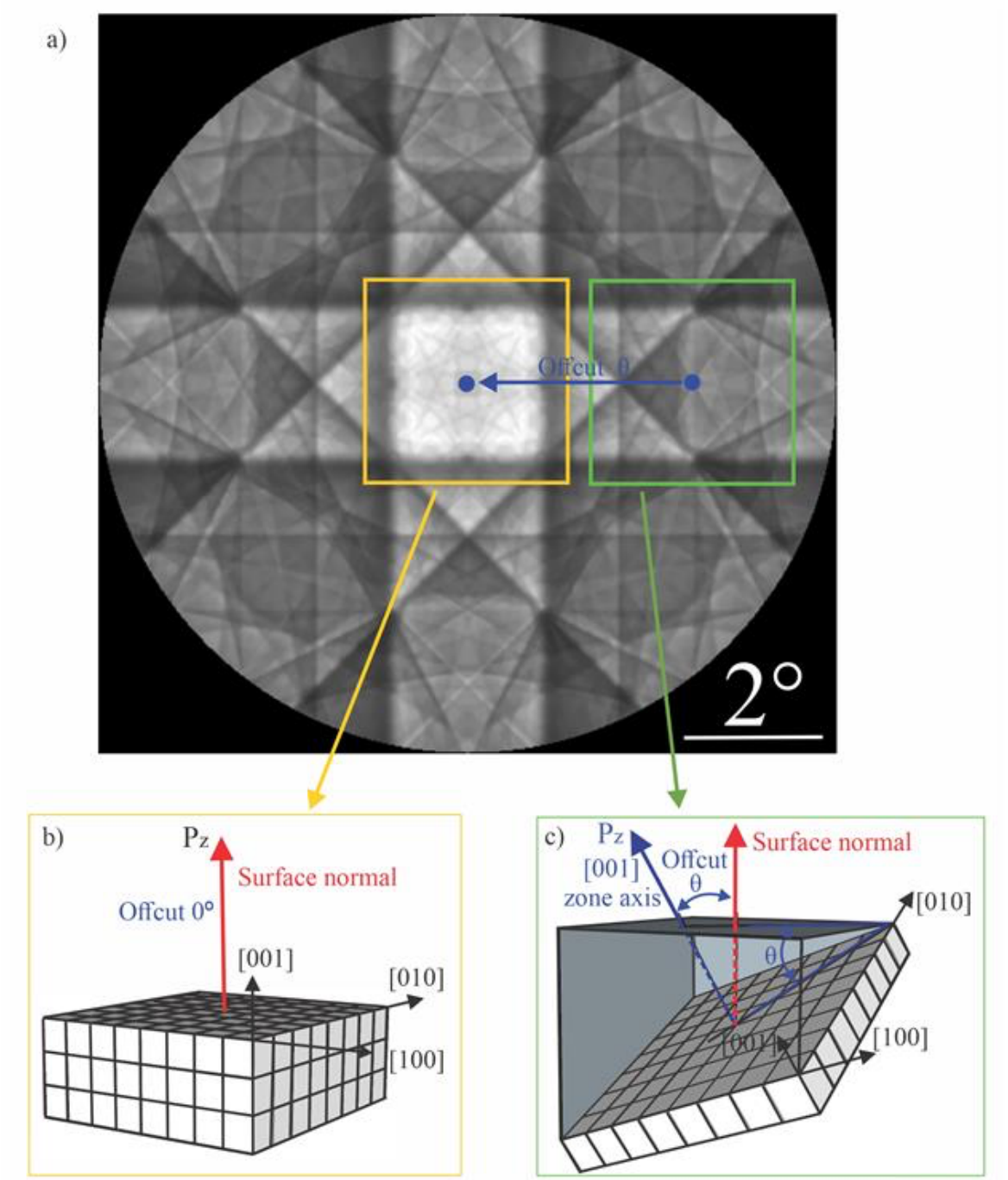

Fig.1 Schematic illustration showing the principle to determine wafer offcuts using ECPI. (a) Simulated ECP on a Si(001) wafer. (b) sample without offcut and (c) sample with offcut. For the sample without offcut (b), the ECPI is marked by the blue box on (a). The surface normal is identical to the [001] zone axis. For the sample with offcut (c), the corresponding ECPI is marked by the red box on (a). The surface normal stays at the ECPI center whereas the [001] zone axis is shifted away from the surface normal. The ECPI center C is determined by the sample rotation. The angular distance in-between is defined as the offcut angle θ.

Keywords:

Wafer offcut, misorientation, ECPI

Reference:

[1] L.D. Doucette, M. Pereira da Cunha, R. J. Lad, Rev. Sci. Instrum., 76, 036106 (2005)
[2] F.J. Humphreys, Y. Huang, I. Brough and C. Harris, J. Microsc., 195, 212-216 (1999)
[3] G. R. Booker, A. M. B. Shaw, M. J. Whelan, P.B. Hirsch, Philos. Mag., 16:144, 1185-1191 (1967)

314

Measuring electric fields with 4D-STEM: Demonstration of pitfalls by the example of GaN and SiGe

Tim Grieb[1,2], Christoph Mahr[1,2], Florian F. Krause[1,2], Knut Müller-Caspary[3], Marco Schowalter[1,2], Martin Eickhoff[1,2], Andreas Rosenauer[1,2]
[1]Institute of Solid State Physics, University of Bremen, Bremen, Germany, [2]MAPEX Center for Materials and Processes, University of Bremen, Bremen, Germany, [3]Department of Chemistry and Centre for NanoScience, Ludwig-Maximilians-Universität München, Munich, Germany

Poster Group 2

Background
The development of fast pixel-based detectors in (scanning) transmission electron microscopy ((S)TEM) has resulted in 4D-STEM becoming almost a standard tool [1]. The computationally simplest analysis of 4D-STEM data is the calculation of the center of mass (COM) of the intensity in the diffraction pattern (the so-called COM or first-moment method) [2]. The COM corresponds to the expectation value of the net momentum transferred to a beam electron during the interaction with the sample. The momentum transfer is caused by a magnetic or electric field [3]. However, it is anything but easy to draw conclusions about an electric field in the sample from a measured COM. In this contribution, we use the example of AlN/GaN as well as of SiGe/Si to demonstrate effects that influence the measured COM and which may lead to artifacts in the measured electric field. A knowledge of these effects is important for a correct interpretation of the COM measurement [4,5]. We focus primarily on two aims: (i) Deriving the difference of polarization induced fields in GaN and AlN and (ii) measuring the relative mean inner crystal potentials (MIPs) using the electric field at the interface between different materials.
Methods
The investigations are performed by multislice simulations and by experimental 4D-STEM. In the experimental case, an FEI/Thermo Fisher Titan 80/300 and a Thermo Fisher Spectra 300 were used.
Results
Figure 1a shows the projected electric field obtained from a simulated COM measurement [4] along a line profile of an unrealistic, non-atomistic supercell in which a layer with the MIP of AlN is embedded in a material with a MIP corresponding to that of GaN. The x-axis shows the line-scan position, the y-axis shows the simulated sample thickness.
Apparently, the beam electrons at both interfaces experience a momentum transfer towards GaN, i.e. towards the material with the higher MIP. This is intuitively understandable, with the interpretation that an electric field exists - due to the (mean inner) potential difference - that deflects the electrons.
If one now considers the complex propagation and interaction of the beam electrons inside the specimen using an atom-based supercell, one gets a completely different picture shown in Figure 1b: the strength with which the beam electrons are deflected at the interface between GaN and AlN is not just higher - it points in the opposite direction. It can be shown that this simulation result agrees with experimental measurements.
In addition to this example, we will also address the influence of sample geometry (inclined surfaces) and examine what effect beam convergence has and how strongly nanobeam-electron diffraction (NBED) is influenced by it.
Conclusion
The interaction of the beam electrons in the STEM with the sample is strongly influenced, for example, by dynamic scattering. Thus, there are also effects on the measured COM of the diffracted intensity in 4D-STEM image series. Caution is therefore advised when interpreting these COM results

(e.g. for quantifying electric fields). For complex and especially small-scale structures, comparison with simulations is a must.

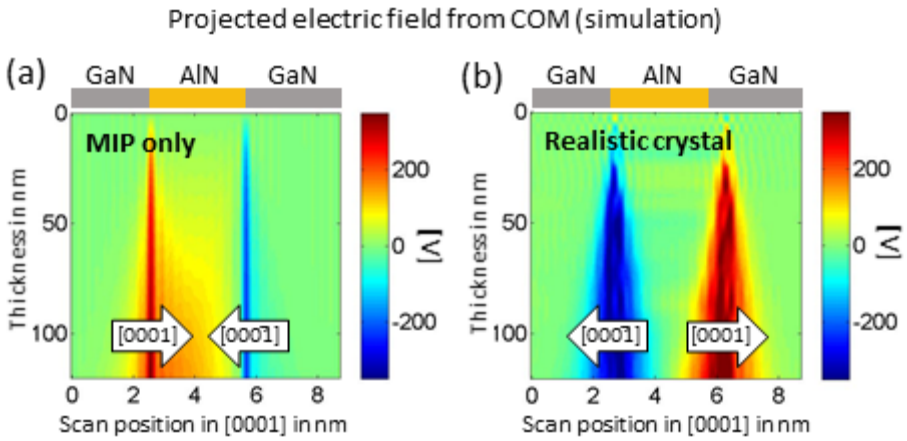

Projected electric field for a simulated 4D-STEM line profile along the [0001] direction. **(a)** For an unrealistic, non-atomistic supercell in which a layer with the mean inner potential (MIP) of AlN is embedded in a material with a MIP corresponding to that of GaN. **(b)** For a realistic, atom-based supercell in which a layer of AlN is embedded in GaN.

Keywords:

4D-STEM, COM, electric fields

Reference:

[1] C. Ophus, Microanal. 25 (2019) 563–582
[2] K. Müller-Caspary et al., Nature Commun. 5 (2014) 56531–56538
[3] K. Müller-Caspary et al., Ultramicroscopy 178 (2017) 62–80
[4] Tim Grieb et al., Ultramicroscopy 228 (2021) 113321
[5] Christoph Mahr at al., Ultramicroscopy 236 (2022) 113503

322

Retrieving sub-angstrom resolution from low order dynamical diffraction intensities

Grigory Kornilov[1], Sam Fairman[1], Sherjeel Shabih[1], Dr. Benedikt Haas[1], Dr. Niklas Dellby[2], Adnan Hammud[3], Dr. Zbigniew Galazka[4], Prof. Christoph Koch[1]
[1]Department of Physics, Humboldt-Universität zu Berlin, Berlin, Germany, [2]Bruker AXS (formerly Nion Co. R&D), Kirkland, USA, [3]Fritz Haber Institute of the Max Planck Society, Berlin, Germany, [4]Leibniz-Institut für Kristallzüchtung, Berlin, Germany

Poster Group 2

Background incl. aims
While dynamical scattering has typically been viewed as a hindrance when attempting to retrieve an unknown crystal structure from electron diffraction data, it can also be of direct benefit since it encodes phase information in the intensity of the electron wave function exiting the crystal [1]. For example, recent advances in 3D electron diffraction have utilized dynamical effects to complement and significantly improve kinematical refinement methods [2]. Building on prior work by Feng et al. [3] we have developed a structure retrieval method which, using experimental large-angle-rocking-beam electron diffraction (LARBED) data, is not only capable of reconstructing complex crystal structures, but also shows that dynamical scattering can be directly used to increase the resolution of a reconstruction beyond what would be achievable under assumption of purely kinematical conditions.

Methods
The approach by Feng et al. [3], which was demonstrated on a rather simple structure (SrTiO3), used a conjugate gradient method to minimize the sum of squared differences between an experimental LARBED pattern and one simulated via the Bloch wave formalism from reconstructed structure factors. We expanded on this method by switching to the adaptive moment estimation (ADAM) optimization algorithm as well as introducing analytical calculation of gradients of the scattering matrix. Significant improvements were achieved by utilizing a series expansion of the scattering matrix [4] to develop a weighting scheme which selectively prioritizes matching those diffraction intensities which have a dominating linear dependence on the structure factors of the crystal. Experimental measurements were performed using a Dectris ELA detector mounted to the end of the IRIS spectrometer of a Nion HERMES microscope, allowing zero-loss filtering with the energy-selecting EELS beam trap. The results presented below were achieved using a roughly 40nm thick lamella of β-Ga2O3 which was prepared with the FIB technique from a bulk crystal grown by the Czochralski method [5].

Results
Figure a) shows the 2D projected potential of β-Ga2O3 in [010] zone axis, generated from reconstructed structure factors, with the theoretical structure overlaid on top. The structure factors were refined from 1129 diffraction patterns of an experimental LARBED tilt series, collected with an accelerating voltage of 200 kV and a maximum tilt angle of 100 mrad. Figure b) shows the Fourier transform of the reconstructed potential with the red circle indicating the range of visible frequency components (image is not to scale with a)). Figure c) shows the mean of all experimental diffraction patterns collected in the LARBED measurement. While many excited beams are visible, only the first 8 (indicated by green circles) were actually used in the reconstruction of the crystal structure. Our method reaches a sub-angstrom resolution of 1.39 Å-1, which is over 5 times finer than the maximum resolution of 0.27 Å-1 which one obtains when only using the structure factors corresponding to these 8 beams, as in kinematic scattering theory. The reconstructed potential

shows good agreement with reference data, further validating this result. In addition to the crystal structure, a specimen thickness of 36.9 nm was also retrieved. The reconstruction was performed ab-initio, i.e. without initializing it with any reasonable starting guess. Besides a small regularization term in the loss function to aid convergence, no further constraints were placed on reconstructed structure factors and no prior information about the crystal, except for its lattice parameters (which can also be extracted from the diffraction data), were used.

Conclusion

In summary, we have directly utilized experimental dynamical diffraction data to perform an ab-initio reconstruction of a crystal at a much higher resolution than would be possible with purely kinematical methods. While we show the best result in this text, our method has successfully been tested on experimental data from further crystals, such as BaTiO3 and Al2O3. An interesting consequence of these findings is that it may be possible to reconstruct a 3D structure from 2D rocking curve data, since there is no fundamental difference in how structure factors corresponding to different reciprocal lattice vectors influence the diffraction pattern produced by the crystal. Preliminary testing on simulated data appears to be promising in this regard and will be further discussed.

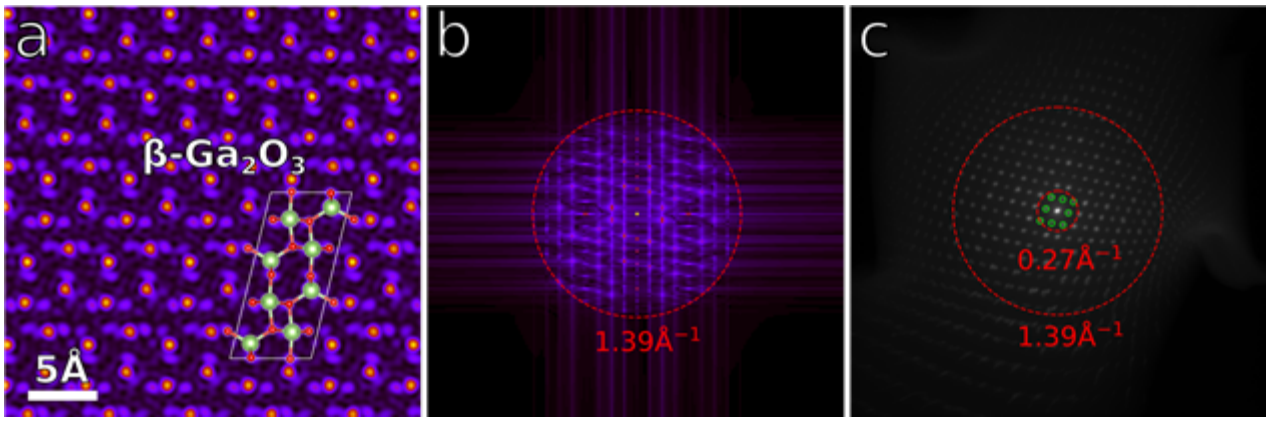

Keywords:

dynamical scattering, crystallography, electron diffraction

Reference:

[1] J. Zuo, M. Kim, M. O'Keeffe, J. C. H. Spence, Nature 401 (1999) 49–52, doi: 10.1038/43403
[2] P. B. Klar, Y. Krysiak, H. Xu et al., Nat. Chem. 15 (2023) 848–855, doi: 10.1038/s41557-023-01186-1
[3] F. Wang et. al., Phys. Rev. Lett. 117 (2016) 015501, doi: 10.1103/PhysRevLett.117.015501
[4] C. T. Koch, J. C. H. Spence, J. Phys. A36 (2003) 3, doi: 10.1088/0305-4470/36/3/314
[5] Z. Galazka, J. Appl. Phys. 131 (2022) 031103, doi: 10.1063/5.0076962

330

Fully Integrated Pixelated 4D-STEM Detector for Scanning Electron Microscopes

Pavel Stejskal[1], Rastislav Motúz[2], Michal Horák[3], Tomáš Šikola[4]
[1]AdvaScope, Brno, Czech Republic, [2]TESCAN Group, Brno, Czech Republic, [3]Brno University of Technology, CEITEC, Brno, Czech Republic, [4]Brno University of Technology, Institute of Physical Engineering, Brno, Czech Republic

Poster Group 2

Four dimensional scanning transmission electron microscopy (4D STEM) refers to a technique where the electron beam scans across a 2 dimensional array on the sample while a detector positioned below the sample records a 2 dimensional pattern for each point in the array, thus creating a 4 dimensional dataset. 4D STEM is a common technique in TEM and is used for virtual imaging, orientation and strain mapping, and differential phase contrast. This work focuses on developments in detector design, centred on miniaturization and low energy sensitivity, which enable a 4D STEM detector to be used in scanning electron microscopy(SEM).
Presented is a 4D STEM solution based on a Timepix 3 hybrid pixelated detector. This detector consists of a matrix of 256 x 256 smart digital pixels (pixel pitch 55 µm), each containing advanced electronics for signal processing including digital registers. The digitisation is performed immediately for each detected electron recording complex information (position, energy and time) which suppresses unwanted signals and therefore selects only relevant events. This principle significantly improves image quality, reduces noise and increases the resolution and contrast in the acquired images. For 4D STEM applications the main advantages of this approach is the so-called data-driven readout, where every single detected event is streamed directly out of the chip, thus allowing dwell times of hundreds of nanoseconds, effectively removing the traditional bottleneck arising from the requirement to store a full pattern for each point in the array.
Figure 1 shows a map of 1536 x 1024 pixels of a stainless steel specimen, acquired in only 80 s. The full dataset with individual diffractograms along with the subsequent virtual diffraction image is shown. In this example, the high contrast arises from the noisless operation of the detector paired with the low energy sensitivity and the virtually unlimited dynamic range.
With a full integration of the detector into a microscope vacuum chamber the complete workflow from lamella preparation to 4D STEM imaging can now be realised. This approach significantly improve the performance capabilities achievable within SEM.

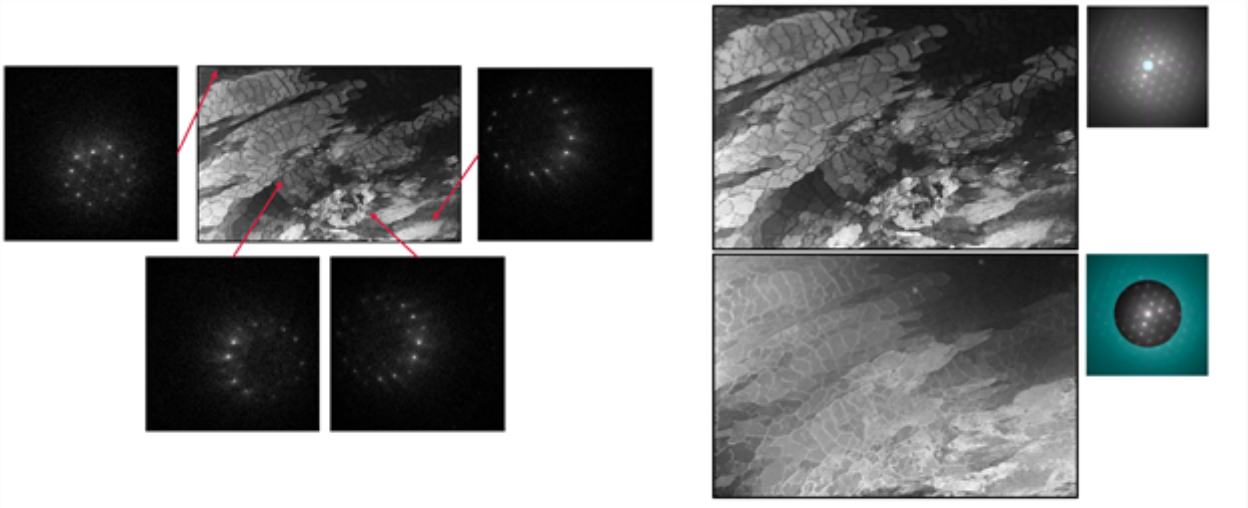

a) individual diffractograms for different locations b) reconstructed SEM images with bright field and HAADF masks applied

Figure 1: 4D-STEM image of a stainless steel sample, 1536 × 1024, 30 kV, 13 pA with a frame time 80 s.

Keywords:

4D-STEM, Timepix, diffraction imaging

Reference:

1. Ophus, Colin: “Four-Dimensional Scanning Transmission Electron Microscopy (4D-STEM): From Scanning Nanodiffraction to Ptychography and Beyond” doi: 10.1017/s1431927619000497
2. Tureček, D., Jakůbek, J. and Soukup, P.: "USB 3.0 readout and time-walk correction method for Timepix3 detector", doi:10.1088/1748-0221/11/12/C12065
3. "Four-dimensional scanning transmission electron microscopy in a FIB-SEM instrument", ID: FW06010396, national TAČR grant

422

Determination of Magnetic Symmetries by Electron Diffraction

Oleksandr Zaiets[1,2], Carsten Timm[3], Jan Rusz[4], Subakti Subakti[1], Axel Lubk[1,2]
[1]Leibniz Institute for Solid State and Materials Research Dresden, Dresden, Germany, [2]Institute of Solid State and Materials Physics, TU Dresden, Dresden, Germany, [3]Institute of Theoretical Physics, TU Dresden, Dresden, Germany, [4]Department of Physics and Astronomy, Uppsala University, Uppsala, Sweden

Poster Group 2

Background incl. aims
Neumann's principle states that symmetries of physical properties (e.g., dielectric / piezoelectric / elastic tensor) derive from structural point (space) symmetry groups of the crystal lattice. The same can be applied for magnetism: the symmetry of magnetic properties (e.g., anomalous Hall effect, multiferroicity, altermagnetism) is determined by the magnetic point (space) group symmetry of the magnetic crystal. Consequently, the ability to determine such symmetries is crucial for the prediction of physical properties of new materials. Currently, the only probe for magnetic point and space group symmetries was neutron diffraction, requiring rather large samples and scarce beam time to be carried out.
It is well known, on the other hand, that convergent beam electron-beam diffraction methods can be used to determine spatial symmetries of crystalline samples, due to the direct relationship between the diffraction groups (symmetry group of convergent electron diffraction patterns) and the point (space) group of the sample [1]. In this work we employ group theory and electron scattering simulations to demonstrate an extension of CBED toward capable to determine magnetic point groups. The method would be applicable in Transmission Electron Microscopes with spatial resolution in the range of 10 nanometers.
Methods
Magnetic electron diffraction groups are composed of standard electron diffraction groups [1] plus time (magnetization) reversal symmetry. We used group theory to obtain and classify all 125 possible magnetic electron diffraction groups obtained by this procedure. The cornerstones for such a theory are the commutation of time-reversal with all other symmetry transformations and its antiunitary character. In a second step we establish the relations between the 122 crystallographic magnetic point groups and the electron diffraction groups for different zone axis orientations of the sample in the electron diffraction experiment.
The verify the theory, dynamic electron scattering simulations for samples with different magnetic point group symmetries and crystal orientations were conducted to obtain convergent beam electron diffraction patterns with magnetic Bragg discs.
Results
We provide the group theory for convergent beam electron diffraction of magnetic crystals and give a complete mapping of magnetic point groups to corresponding diffraction groups for all possible crystal orientations. We conduct electron scattering simulations for selected antiferromagnetic samples (NiO, etc.) in order to verify the group theoretical considerations. It is shown that obtained symmetries from simulated electron diffraction images correspond to the expected magnetic point groups of the samples.
Conclusion
This work proposes convergent beam electron diffraction as an alternative of neutron diffraction for unambiguous determination of magnetic point group symmetry. With a given map of magnetic point groups to corresponding electron diffraction groups one can determine the latter from a finite series of diffraction experiments at different crystal orientations. Simplicity, accuracy and relatively small

spatial resolution of a proposed method makes it an intriguing candidate for magnetic symmetry detection and investigation.

Keywords:

magnetic symmetry groups, diffraction groups

Reference:

[1] B. F. Buxton, J. A. Eades, John Wickham Steeds, G. M. Rackham, and Frederick Charles Frank. The symmetry of electron diffraction zone axis patterns. Philosophical Transactions of the Royal Society of London. Series A, Mathematical and Physical Sciences, 281(1301):171-194, 1976.

emc2024 COPENHAGEN

432

4D-STEM/PNBD: Fast and easy powder electron diffraction in SEM

Miroslav Slouf[1], Ms. Pavlina Sikorova[2], Mr. Radim Skoupy[2], Mr. Martin Slouf[3], Mrs. Ewa Pavlova[1], Mr. David Rendl[4], Mr. Filip Sroubek[4], Mr. Vladislav Krzyzanek[2]
[1]Institute of Macromolecular Chemistry CAS, Praha, Czech Republic, [2]Institute of Scientific Instruments CAS, Brno, Czech Republic, [3]LiveSystems Ltd., Praha, Czech Republic, [4]Institute of Information Theory and Automation CAS, Praha, Czech Republic

Poster Group 2

Background: We have developed a new method, named 4D-STEM/PNBD (i.e., four-dimensional scanning transmission electron microscopy/powder nanobeam diffraction), which can convert a modern SEM microscope to a simple, fast, and user-friendly powder electron diffractometer [1, 2]. The only hardware requirement is that the SEM microscope must be equipped with a 2D-array detector of transmitted electrons (also referred to as 2D-array STEM detector or pixelated STEM). In 4D-STEM/PNBD, we reduce a huge and complex 4D-STEM-in-SEM dataset to a single 2D powder diffraction pattern (as shown in the attached figure). The final powder diffraction patterns are equivalent to those from TEM/SAED as documented in our previous studies [1-3]. They can be compared to theoretically calculated powder X-ray diffraction patterns (PXRD) in order to identify the investigated nanocrystals [2, 3]. This contribution deals with the recent improvements of our method, which should make it even more user-friendly and robust [3, 4].

Materials and methods: We performed TEM/SAED (selected area electron diffraction) and 4D-STEM/PNBD measurements on three types of nanocrystalline samples on an electron-transparent carbon film. The samples differed by signal-to-noise ratio (SNR), where signal and noise are represented by the intensity of diffraction peaks and the amorphous background, respectively. The samples could be grouped as follows: (i) Au nanoislands with high SNR, (ii) GdF3 and TbF3 nanocrystals with good SNR, and (iii) magnetic iron oxide nanoclusters with or without amorphous silica shell with intermediate SNR. The 4D-STEM/PNBD calculations were performed with recent version of our open-source Python libraries STEMDIFF (conversion of 4D datasets to 2D powder diffraction patterns; https://pypi.org/project/stemdiff) and EDIFF (conversion of 2D-diffraction patterns to 1D radially averaged diffraction profiles and their comparison with theoretically calculated PXRD; https://pypi.org/project/ediff).

Results and discussion: Our initial studies [1-3] showed that the 4D-STEM/PNBD works very well for reasonably small, highly diffracting crystals with low absorption. If the crystals are thicker and/or surrounded by amorphous matrix, the extraction of 2D powder diffractogram can become difficult or impossible. This results from the lower-energy electrons in SEM ($E < 30$ keV), which suffer from higher absorption and inelastic scattering than the higher-energy electrons in TEM ($E > 100$ keV). The better 4D-STEM-in-SEM datasets and, subsequently, the higher-quality 2D powder diffractograms can be obtained with better hardware (i.e. better SEM microscope and/or pixelated STEM detector), better experimental parameters (optimized scanning speed, dwell time etc.), and better software (i.e. data processing). For given hardware and optimized experimental conditions, the decisive factor is the data processing. Consequently, we made several improvements of our STEMDIFF software. At first, we introduced better, multi-criteria filtering of the raw 4D-STEM-in-SEM dataset. The better filtering allows us to select the highly-diffracting locations and ignore the rest, which contain high noise. Moreover, it enables us to get the better estimate of the point-spread-function (PSF) of the primary beam, which can improve the quality of the individual diffractograms by means of 2D-PSF deconvolution. At second, we increased the speed of the above-mentioned time-consuming 2D-PSF deconvolution step ca 5x by introducing multicore processing. Last but not the least, we improved

the user interface and extended the original software package STEMDIFF (the conversion of 4D-datasets to 2D diffractograms) with a sister package EDIFF (the conversion of 2D diffractograms to 1D profiles and their comparison with theoretically calculated PXRD patterns). The recent versions of STEMDIFF and EDIFF employ the well-established Jupyter notebooks as interactive templates for complete data processing (4D → 2D → 1D) without any third-party software. The notebooks are written and documented in such a way that the data could be processed in step-by-step way by any SEM user without detailed knowledge of diffraction theory. The above-listed improvements enabled us to process not only the 4D-STEM-in-SEM datasets of strongly diffracting samples with high SNR (such as Au nanoislands), but also samples with intermediate SNR (such as iron oxide nanoclusters enveloped with amorphous silica). The samples with low and poor SNR remain as a challenge for our ongoing work, which comprises advanced 2D-PSF deconvolution methods and automated, machine learning-based noise reduction.

Conclusion: The 4D-STEM/PNBD method brings a simple, fast, and easy-to-use electron diffraction technique to SEM users. The classical SEM microscopes offer imaging modes (such as SE or BSE) and spectroscopy modes (such as EDX). The modern SEM microscopes equipped with pixelated STEM detectors add also the third mode – the electron diffraction. The pixelated detectors can be installed in a common SEM port like any other detector. The 4D-STEM datasets are easy-to-collect, but difficult-to-process – at least for non-crystallographers. Our STEMDIFF package reduces a complex 4D-STEM dataset to a simple 2D diffractogram. The sister EDIFF package enables a fast conversion of 2D diffractogram to radially averaged 1D diffraction profile and its comparison with theoretically calculated PXRD diffraction pattern. Both packages aim to be as user-friendly as possible, so that the new 4D-STEM/PNBD method could be employed by all users of SEM microscopes.

Acknowledgement: Project TN02000020 (TA CR) and Thermo Fisher Scientific company for a high-resolution SEM with pixelated detector installed at ISI CAS.

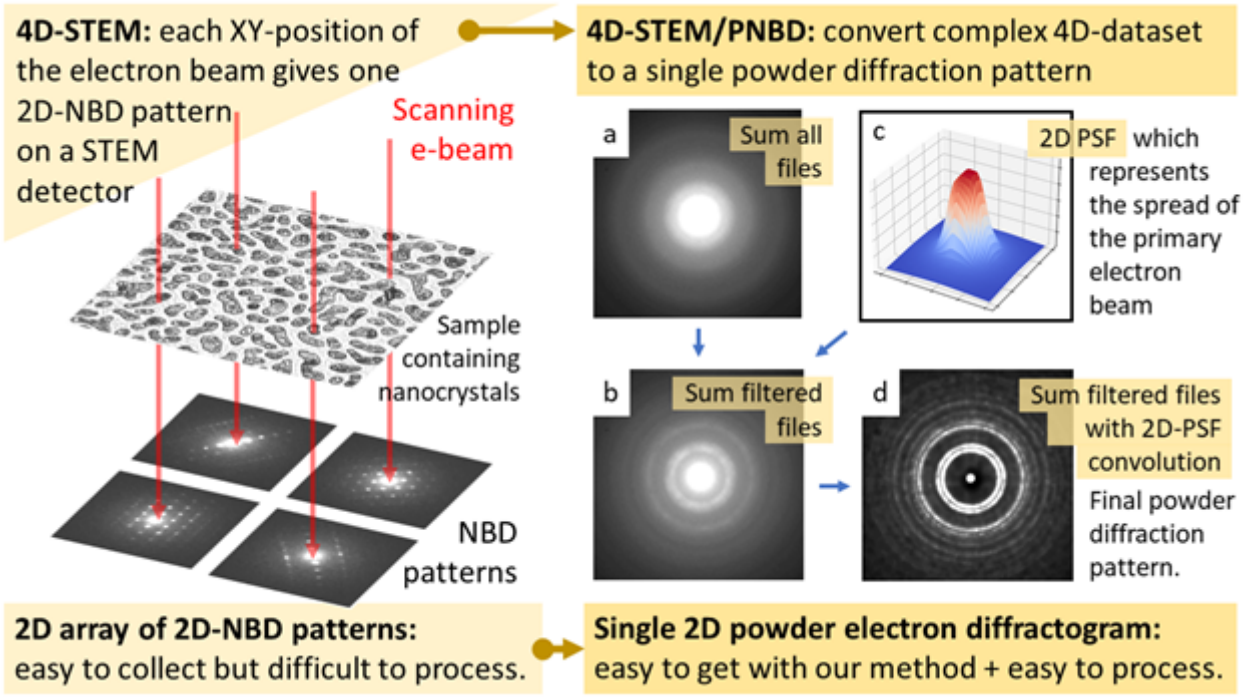

Keywords:

4D-STEM-in-SEM, powder electron diffraction, nanocrystals

Reference:

[1] Slouf M et al.: Nanomaterials 11 (2021) 962.
[2] Slouf M et al.: Materials 14 (2021) 7550.
[3] Skoupy R et al.: Small Methods 7 (2023) 2300258.
[4] Pilatova J et al.: mBio 14 (2023) 03279-22.

438

Scanning electron diffraction reveals the nanoscale ordering of cellulose in a hierarchically structured hybrid material

Mathias Nero[1], Dr Hasan Ali[2], Professor Yuanyuan Li[3], Dr Tom Willhammar[1]
[1]Stockholm University, Stockholm, Sweden, [2]Uppsala University, Uppsala, Sweden, [3]Royal Institute of Technology, Stockholm, Sweden

Poster Group 2

Background
Biopolymers are electron beam-sensitive materials with low scattering power, which poses a significant challenge for nanoscale characterization. One promising technique to overcome these issues is scanning electron diffraction (SED), utilizing the strong interaction between electrons and matter. In SED, the sample is raster scanned using a near-parallel electron probe while simultaneously capturing a diffraction pattern at each beam position. These patterns provide highly localized crystalline information from the sample, including strain, phase, and orientation, later characterized through post-acquisition data analysis.
Cellulose, with its unique properties and crystalline structure, has emerged as a promising resource for sustainable composite materials. Controlling its hierarchical organization is an essential consideration in cellulose utilization. The aligned orientation of the highly anisotropic cellulose nanofibers is vital to macroscale mechanical properties. Fundamental insights into the intrinsic arrangement of cellulose enhance its exploitation in composites with new and improved properties.

Methods
The wood-based composite material was sectioned using ultramicrotomy in two orthogonal directions, longitudinally and transversely, relative to the elongated wood cell structure. The microscope was configured with a convergence angle of 0.1 mrad, resulting in a probe diameter of less than 10 nm. SED data was acquired using a beam current of 2 pA with a dwell time of 5 ms to minimize beam damage. Cellulose orientation and degree of alignment in each beam position were determined through post-acquisition data processing. 360 virtual detectors were arranged in an annular pattern around the unscattered beam, with a radius corresponding to the scattering angle of the most prominent 200-reflection of cellulose to optimize the signal-to-noise ratio.

Results
In this study, we employed SED to unveil the hierarchical assembly of cellulose nanofibers in transparent wood, a composite material prepared by infiltrating wood with polymerized methyl methacrylate (PMMA)[1]. Our results reveal a well-ordered hierarchical arrangement of nanofibers in the secondary cell wall with a spatial resolution of 15 nm[2]. In the inner regions, the nanofibers are aligned parallel to the cell elongation, including the innermost part closest to the lumen. In the outer part, the nanofibers transition to a tangential orientation. Based on the quantitative SED data, we can conclude that this reorientation occurs smoothly over 1.5 µm. Despite the change in direction, cellulose nanofibers stay well-aligned. Uniform cellulose orientation in the inner part and a plateau in the outermost part support a layered cell wall structure.
Furthermore, wood cells sectioned longitudinally exhibit clockwise or counterclockwise nanofiber rotation towards the outer part. This rotation difference is caused by sectioning the cells at different depths and is consistent with a helical arrangement of nanofibers with a gradually changing pitch.
Peak width analysis of transversely sectioned transparent wood discloses a higher degree of nanofiber alignment in the outer part of the cell wall than in the inner part.
Preserving the anisotropic organization of cellulose in this new biocomposite retains the mechanical properties of wood.

Conclusions

This work demonstrates the potential of Scanning Electron Diffraction in characterizing biobased composite materials. Combining sensitive detectors and innovative data analysis enables the detection of very subtle signals from the sample. SED provides quantitative crystal information with exceptionally high spatial resolution from a relatively large field of view (20x20 µm).

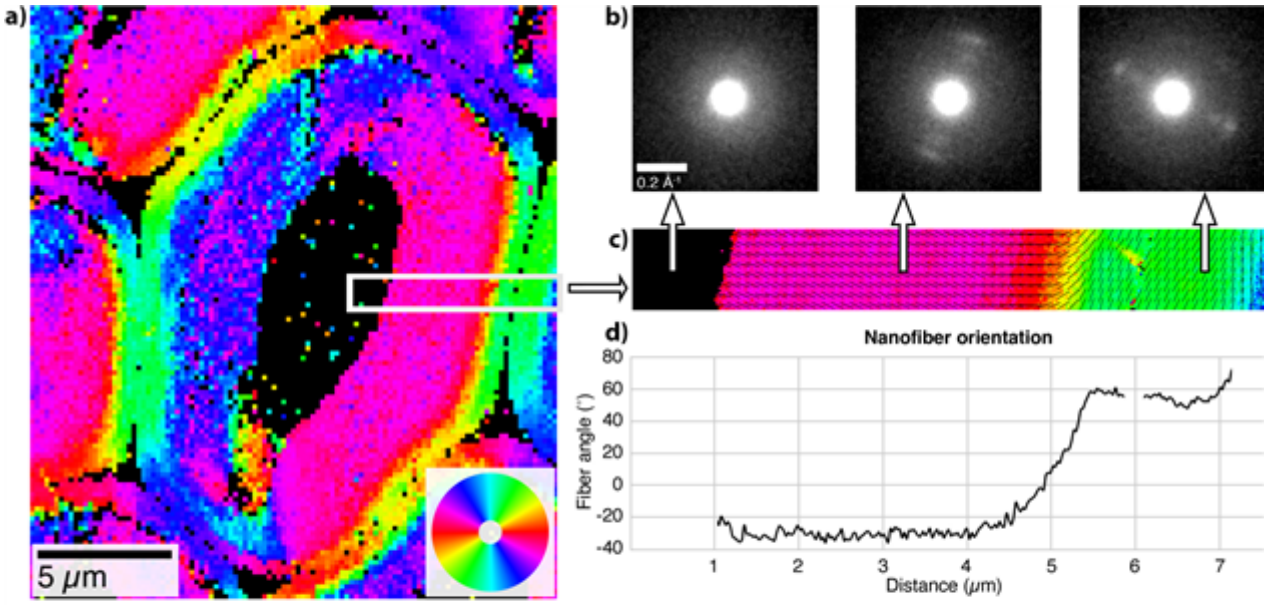

Organization of cellulose nanofibers within transversely sectioned transparent wood in an entire fiber cell (a). Colors in the figure correspond to the nanofiber orientations according to the color wheel, with black indicating areas lacking cellulose. The enlarged view (c) reveals the aligned orientation of nanofiber within the secondary cell wall captured with a step size of 30 nm. Representative diffraction patterns (b) show the rotation and absence of Bragg's reflection in selected areas. The line scan (d) reveals the smooth oriental transition of nanofibers in c with a plateau in the outermost part of the cell wall, indicating a layer of uniformly oriented fibrils.

Keywords:

scanning electron diffraction, hierarchical structures

Reference:

[1] Y. Li, X. Yang, Q. Fu, R. Rojas, M. Yan, and L. Berglund, 'Towards centimeter thick transparent wood through interface manipulation', J Mater Chem A Mater, vol. 6, no. 3, pp. 1094–1101, 2018, doi: 10.1039/c7ta09973h.

[2] M. Nero, H. Ali, Y. Li, and T. Willhammar, 'The Nanoscale Ordering of Cellulose in a Hierarchically Structured Hybrid Material Revealed Using Scanning Electron Diffraction', Small Methods, Dec. 2023, doi: 10.1002/smtd.202301304.

455

Improving Transmission Kikuchi Diffraction workflows

Dr. Mark Coleman[1], Mr Kim Larsen[1]
[1]Oxford Instruments NanoAnalysis, High Wycombe, United Kingdom

Poster Group 2

Transmission Kikuchi diffraction (TKD) is an increasingly popular technique in the scanning electron microscope (SEM) for the characterization of nanoscale structures in wide range of materials [1-3]. The convenience of being able to utilize a conventional commercial electron backscatter diffraction (EBSD) system in a field emission SEM or focused ion beam (FIB) SEM has made TKD a particularly attractive alternative to orientation mapping techniques in the transmission electron microscope (TEM).

Improvements to focused ion beam instruments and sample preparation methods [4], have added analysis capabilities but not significantly improved the overall workflow or data quality. Methods such as the large area preparation method have made it possible to apply many standard approaches used for EBSD, however there is scope for TKD specific improvements. related to data processing during data acquisition, offline reprocessing and the geometry in which data is being acquired.

We will discuss the latest improvements to TKD workflows, improving the acquisition of high-resolution data, making the end-to-end workflow easier, and improving data processing to obtain better data quality in relation to TKD analysis.

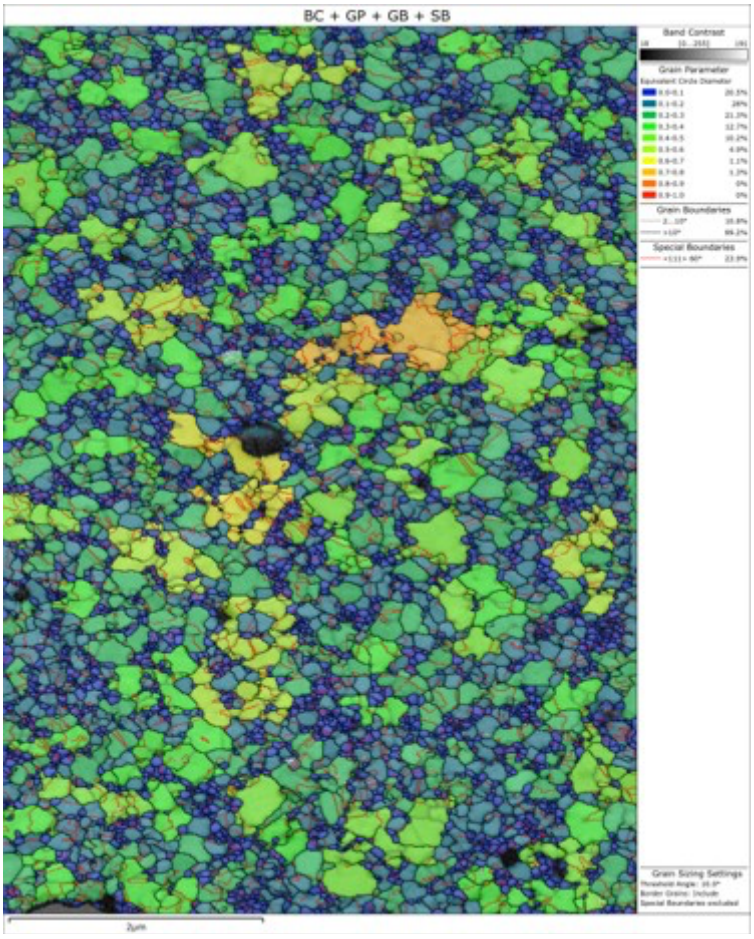

Keywords:

TKD, EBSD, FIB, FIB-SEM

Reference:

[1] R.R. Keller and R.H. Geiss, J. Microscopy, 245 (2012), p. 245-251.
[2] P.W. Trimby, Ultramicroscopy, 120 (2012), p. 16-24
[3] G. Sneddon et al., Materials Science and Engineering R: Reports, 110 (2016), p. 1-12.
[4] P.W. Trimby et al., Microscopy and Microanalysis, 27(S1) (2021), p. 1596-1598.

460

Characterization of the crystal structure of In-Ga-Zn-O materials via Precession Electron Diffraction

Marta Antonella Agati[1], Pradyumna Kumar Parida[1], Olivier Richard[1], Athanassios S. Galanis[2], Harold Dekkers[1], Eva Grieten[1], Paola Favia[1]
[1]IMEC, Leuven, Belgium, [2]NanoMegas, Brussels, Belgium

Poster Group 2

Indium-Gallium-Zinc-Oxide (IGZO) compounds have been regarded as attractive material for the channel in transparent thin-film transistors (TFTs), with low leakage in the off-state and high mobility. IGZO-based materials belong to the class of high band-gap semiconductors and their crystallographic properties are the key characteristic determining the final performances of the electronic devices. Amorphous IGZO, for example, is easy to grow and has good electron mobility, in contrast to other semiconductors such as Si and Ge in the amorphous state. However, in the perspective of the fabrication of electronic devices, amorphous IGZO TFTs suffer from electrical instability. Crystalline IGZO mostly exists in two polytypes having spaces group R$\bar{3}$m (160) and P63/mmc (194), and has showed improved electrical performances. There is also an intermediate crystal phase where the periodicity is kept only in the c-axis, while being structureless in the a and b-axis. This phase is called CAAC (c-axis aligned crystalline) IGZO and it is less prone to defect formation. More sophisticated configurations have been employed in TFTs: for example, a double layer design, constituted of amorphous and CAAC-IGZO, has shown good device stability [1]. To further enrich the family of IGZO compounds, a new a spinel polytype has been recently demonstrated, which can be grown via PVD using intermediate conditions derived from the growth of amorphous and CAAC-IGZO, and exploiting a Ga2ZnO4 (GZO) layer as a seed [2].
In such a complex panorama, there is a need for an appropriate technique to characterize the huge diversity of crystal phases in IGZO-based TFTs. To this end, we referred to Precession Electron Diffraction (PED) [3] executed via a Transmission Electron Microscope (TEM) in scanning (STEM) mode. In fact, standard electron diffraction, due to sample thickness, is significantly affected by multiple/dynamic scattering, which leads to diffracted intensities not easy to be interpreted. PED was introduced to solve this issue and analyze crystal structures with better sensitivity. In PED, the electron beam is rocked at a fixed angle to the optic axis above the sample, forming a hollow cone, and then it is de-rocked below the sample. It can be demonstrated that the final diffraction pattern has many more reflections than in the case of an unprecessed beam, having intensities unaffected by dynamic scattering. We applied scanning PED to the study of IGZO thin (about 20 nm) films having spinel structure and grown on GZO layers having different thickness (from 2 to 10 nm). We prove the possibility to correctly identify materials with similar electron diffraction patterns, such are IGZO and GZO, using PED and Phase & Orientation mapping of the scanned area (ASTAR, NanoMEGAS) [4]. We demonstrate that high sensitivity can be achieved to properly resolve even narrow GZO layers, as thin as 2 nm, from the above IGZO. This can be inferred from Figure 1, which shows the combination of phase map and indexation for two different IGZO samples, grown on GZO having thickness of 10 nm (a) and 2 nm (b), respectively. Moreover, phase and orientation mapping allowed us to study the grains structural properties in IGZO grown on GZO layer with different thickness. We show that, as expected, IGZO grows epitaxially on the GZO seed layer. Moreover, IGZO grain growth is related to the thickness of the underlying GZO layers: size of the IGZO grains is coarse when GZO has higher thickness, while columnar growth of narrower and IGZO grains is reached when thin GZO is used. For GZO having 2 nm thickness, IGZO and GZO present texture, with growth of IGZO/GZO along the <111> direction. Finally, we study the case where thermal annealing in a hydrogen atmosphere reduces the IGZO film and induces the formation of In-rich grains dispersed in the IGZO matrix. In this context, we study the crystal structure of these grains and their matrix.

This study is preliminary to the characterization of TFTs devices employing complex design and based on IGZO compounds as channel material. In general, these results can open the way to the study of different devices, where the common feature relies in the close link between the crystallographic structure and the final performances.

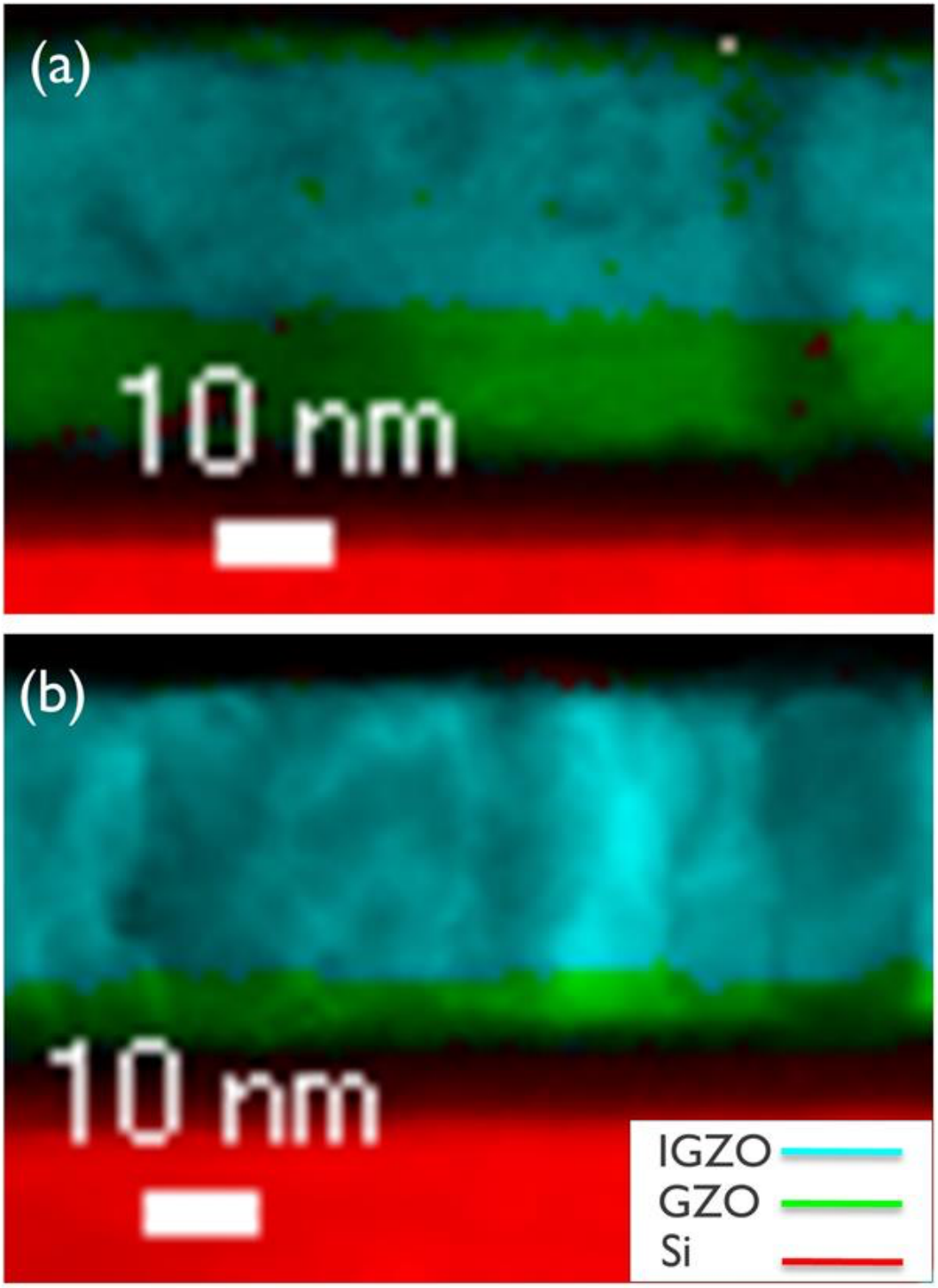

Figure 1. Combination of Phase Map and Index Map for (a) IGZO grown on 10-nm GZO and (b) IGZO grown on 2-nm GZO.

Keywords:

In−Ga−Zn oxide, Precession Electron Microscopy

Reference:

[1] S. Subhechha et al, “First demonstration of sub-12 nm Lg gate last IGZO-TFTs with oxygen tunnel architecture for front gate devices”. 2021 Symposium on VLSI Technology, pp. 1-2.
[2] H. F. W. Dekkers et al, “Deposition, Characterization, and Performance of Spinel InGaZnO4”. 2022 ACS Appl. Electron. Mater. (4), pp. 1238–1249.
[3] R. Vincent and P. Midgley. “Double conical beam-rocking system for measurement of integrated electron diffraction intensities”. 1994 Ultramicroscopy (53), pp. 271-282.
[4] E. F. Rauch et al, “Automated nanocrystal orientation and phase mapping in the transmission electron microscope on the basis of precession electron diffraction” 2010 Z. Kristallogr. (225), pp. 103-109.

525

Assessing the Accuracy of Strain Mapping using 4D-STEM

Petr Vacek[1], Paul Midgley[1]
[1]Department of Materials Science and Metallurgy, University of Cambridge, 27 Charles Babbage Road, Cambridge, United Kingdom

Poster Group 2

Background

With the advent of sensitive direct electron detectors, coupled with ever-greater computational power, 4D-STEM has grown rapidly in popularity [1,2]. In particular, scanning electron diffraction (SED), a variant of 4D-STEM, is based on acquiring a set of diffraction patterns with low convergence (near-parallel) probes for each scan position such that subsequent computational data processing can retrieve nanoscale information regarding phase identification, crystallographic orientation, internal electric and magnetic fields and strains. This work assesses the impact of different acquisition conditions to identify optimal imaging conditions for 2D strain mapping.

Methods

A simulated strain distribution (quantum well phantom with an (unstrained) primitive unit cell of 5Å) that included areas with uniaxial and biaxial normal strain, shear strain, lattice rotation, and their combination, was used to generate a SED dataset for strain mapping. The simulated diffraction patterns, 'recorded' on detectors with four different pixel sizes, were generated using the kinematical diffraction module in Py4DSTEM python library [3], and a custom plotting code based on the pyxem python library [4]. The maximum extent of the simulated diffraction pattern on each detector (with the origin at the detector centre) is +/- 1.25 Å-1. Kinematical simulations can be justified here because strain mapping often uses precession electron diffraction, providing integrated 'near-kinematical' intensities and, importantly, integrates over any contrast seen within the diffraction disk ('rocking curve' contrast); such contrast is known to have a deleterious impact on the accuracy of strain mapping [5]. Noise is added to the diffraction data accounting for the statistical nature of electron arrival and to account for a background noise that represents readout noise of the detector. Strain analysis was performed on the SED dataset using both cross-correlation (CC) and centre-of-mass (COM) algorithms and the results compared with the strain phantom (ground truth) to assess the effect of each parameter on the accuracy of strain mapping. A diagram of the workflow is illustrated in Figure 1(a).

Results

The effect of number of detector pixels, signal to noise ratio (SNR), order of reflection / magnitude of g-vector, and probe convergence was investigated. In general, as expected, the higher the number of detector pixels, the higher the strain mapping accuracy. This is illustrated in Figure 1(b), where we see a significant improvement in the sum of squares of errors in strain mapping between 128 and 256 detector pixels, while increasing the number of pixels still further is beneficial, in the case studied it has diminishing returns. Increasing the order of the reflection, and thus increasing the g-vector magnitude will, in general lead to a lower SNR for each disc. For strain mapping it is intuitively the case that we would wish to use reflections with high SNR and large g-vector magnitudes (reflections of high order). However, lower order reflections tend to have higher SNR and therefore it is important to find a balance between SNR and g-vector magnitudes. The effect of beam convergence depends on which peak-finding algorithm is used. It is advantageous to use COM algorithms for probes with low convergence, where it is difficult to fit the peak position due to the lack of pixels to accurately represent a circle. CC works best for higher convergence angles where the pixelation of the detector does not affect the fitting precision. CC also requires lower SNR to work precisely

compared to the COM algorithm. The optimised conditions taken from the simulation were used to acquire an experimental strain mapping dataset of SiGe quantum wells in a MAG*I*CAL sample using CMOS camera (ThermoFisher Ceta) and hybrid pixel direct electron camera (Quantum Detectors Merlin) to evaluate the findings from the simulations in an experimental setting, see Figure 1(c).

Conclusions

We have assessed the accuracy of strain mapping using SED, a 4D-STEM variant, by considering key parameters such as the number of detector pixels and the SNR of the reflection used for strain mapping. A clear optimum is found that balances the SNR and g-vector magnitude for a strain phantom. We find it is advantageous to use a centre of mass algorithm for low convergence probes and a cross correlation algorithm for larger convergence probes. Using these findings we were able to reconstruct a high fidelity experimental strain map from a SiGe quantum well data set. The authors thank the EPSRC for funding under grant numbers EP/V007785/1, and EP/R008779/1.

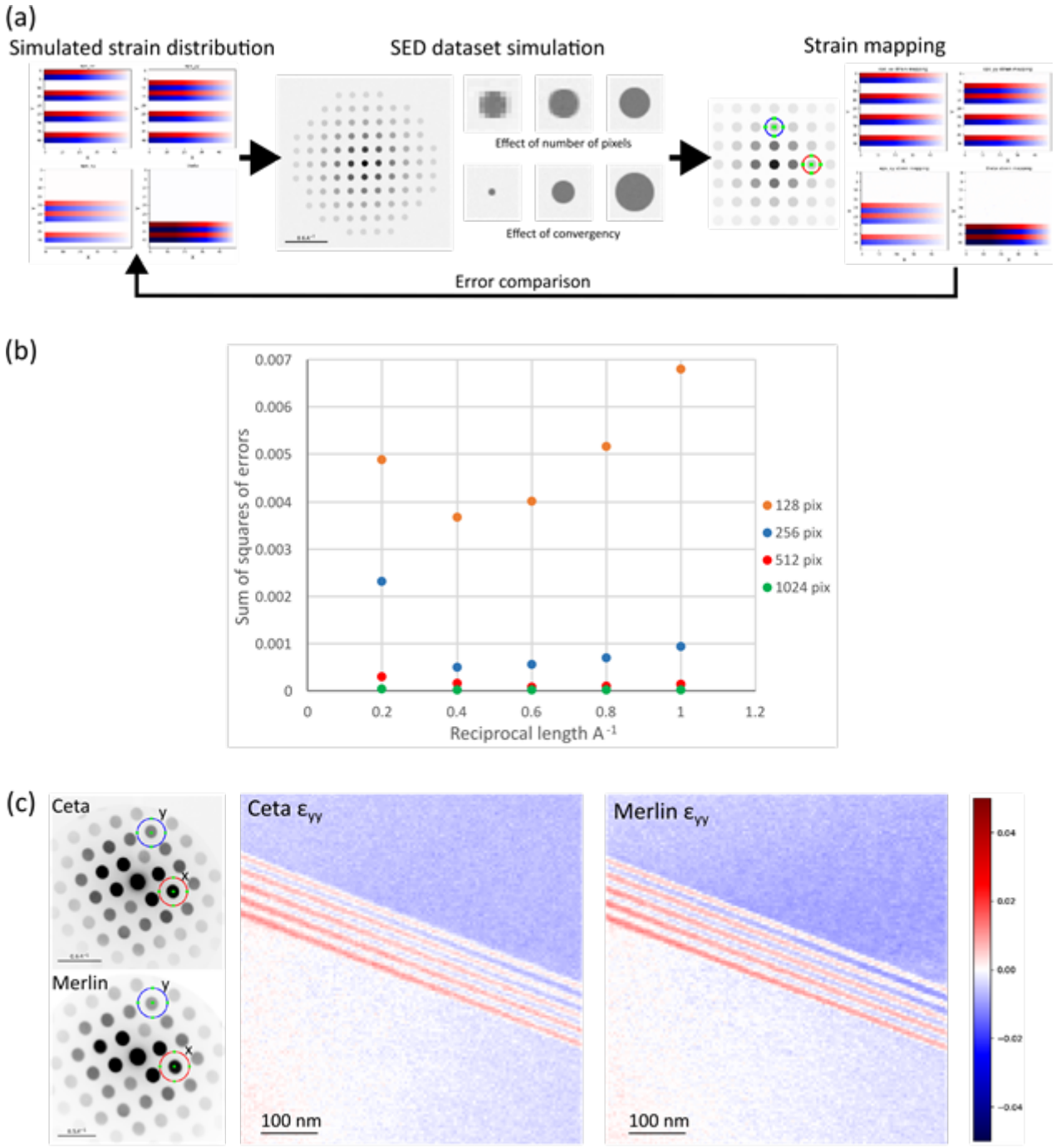

Figure 1: (a) Illustration of the workflow, starting with simulated strain distribution, which is used for SED dataset simulation, and the SED dataset is subsequently used for strain analysis. The results from the strain mapping are then compared to the initial strain distribution. (b) Comparison, using a cross-correlation algorithm, of the sum of squares of errors in ε_{xx}, ε_{yy}, ε_{xy}, and lattice rotation for different number of detector pixels and order of reflection used for strain mapping. (c) Comparison between ε_{yy} strain maps in an experimental SiGe QW structure taken using Ceta and Merlin cameras.

Keywords:

Strain mapping, scanning electron diffraction

Reference:

[1] P.A. Midgley, A.S. Eggeman, Precession electron diffraction – a topical review, IUCrJ 2 (2015) 126–136. https://doi.org/10.1107/S2052252514022283.

[2] C. Ophus, Four-Dimensional Scanning Transmission Electron Microscopy (4D-STEM): From Scanning Nanodiffraction to Ptychography and Beyond, Microsc Microanal 25 (2019) 563–582. https://doi.org/10.1017/S1431927619000497.

[3] B.H. Savitzky, S.E. Zeltmann, L.A. Hughes, et al., py4DSTEM: A Software Package for Four-Dimensional Scanning Transmission Electron Microscopy Data Analysis, Microsc Microanal 27 (2021) 712–743. https://doi.org/10.1017/S1431927621000477.
[4] Duncan Johnstone, Phillip Crout, Magnus Nord, et al., pyxem/pyxem: v0.17.0, (2024). https://doi.org/10.5281/ZENODO.10551678.
[5] C. Mahr, K. Müller-Caspary, T. Grieb, et al., Theoretical study of precision and accuracy of strain analysis by nano-beam electron diffraction, Ultramicroscopy 158 (2015) 38–48. https://doi.org/10.1016/j.ultramic.2015.06.011.

542

Study of Lithiation Dynamics in Cathode Materials by in situ TEM Electrochemical Liquid Technics.

Student Kevyn Gallegos-Moncayo[1], Justine Jean[1,2], PhD Nicolas Folastre[1], PhD Arash Jamali[1,2], PhD Arnaud Demortière[1,2,3]
[1]CNRS-LRCS, Amiens, France, [2]RS2E-French Research Network on Electrochemical Energy Storage, Amiens, France, [3]ALISTORE- European Research Institute, Amiens, France

Poster Group 2

Lithium-ion (LIB) batteries' technology has evolved rapidly to be on par to the increasing demands of the market. The EV (Electric Vehicle) market requires batteries presenting high safety, higher energy density and duration. For instances, one of the cathode materials suitable for EV application is NMC 811, however, its accelerated degradation leads to a short battery life. For the further development of EV suited batteries, the understanding of NMC 811 degradation dynamics is crucial.
For a proper study of the dynamics of (de)lithiation in NMC 811 cathode material, an in-situ analysis at the primary particle scale is proposed. The electrochemical liquid TEM analysis configuration [1] allows the performance of battery cycling inside the TEM for imaging at different SoC (state of charge), inducing less of perturbations during data acquisition and imaging analysis. The information obtained could reveal the behavior of lithium inside the crystallographic, as well as other phenomena that lead to battery degradation.
One of the main causes of degradation in NMC 811 is due to the formation of a passivation layer during cycling, the CEI (cathode electrolyte interface) [2]. The CEI formation take place during the first cycles of the batterie, at the interface between the active material and the electrolyte, organic and inorganic compounds (LiF, LiOH, Li2Co3, etc.) are formed, consuming active Li which leads to the reduction of the batter capacity and degradation of the electrolyte. The CEI layer is not stable, dissolution and reformation of it occurs during each cycle, reducing the batterie life. STEM-EDX and 4D-STEM microscopy technics can be used to follow the formation of the CEI.
4D-STEM technique allows us to obtain structural information based on electron diffraction pattern collections (50k patterns) with a spatial resolution of 1-2 nm. [3-5]. Using this method, it is possible to reconstruct it via pattern matching, a phase mapping of the present inorganic components in a CEI as has already being done for ex situ analysis of NMC 811 (figure 1) [2]. Coupling 4D-STEM and STEM-EDX analysis for different SoC (State of Charge) will allow us to follow the behavior of the CEI layer and determine the dynamics behind it.
The obtained information could lead to the comprehension of the strains present at the primary particle level that could eventually lead to the fracture of secondary particles and the degradation of the material as reported several times in literature.

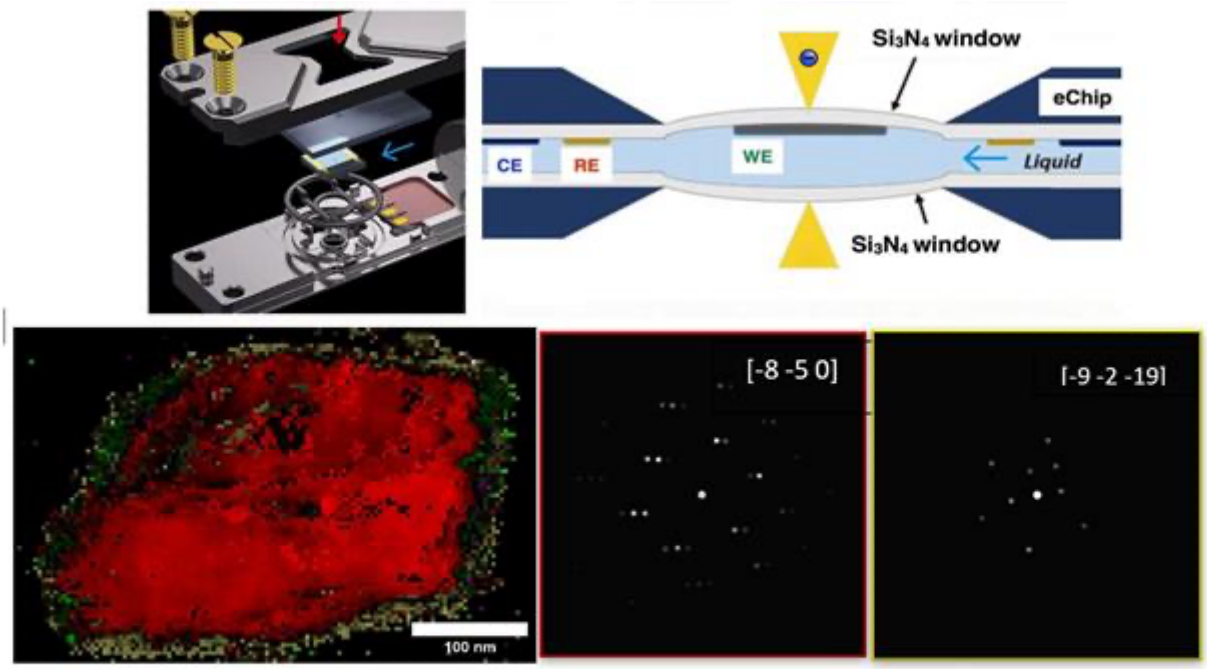

Figure 1 : a) Poseidon sample holder and schematics of liquid electrochemistry cell, b) 4D-STEM ex situ analysis for a NMC811 particle cycled in coin cell, Diffraction pattern corresponding to c) NMC 811 and d) LiF, after pattern matching determination.

Keywords:

In-situ, 4D-STEM, NMC, CEI

Reference:

[1] Fan Wu, Nan Yao, Nano Energy, 11 (2015), p 196-210. Doi:10.1016/j.nanoen.2014.11.004

[2] Symmetry 2024, 16, 301. https://doi.org/10.3390/sym16030301

[3]Katharina Märker, Philip J. Reeves, Chemistry of Materials, 31 (2019), p. 2545-2554. Doi: 10.1021/acs.chemmater.9b00140

[4] Bhatia, A., Cretu, S., Hallot, M., Folastre, N., Berthe, M. , Troadec, D.Demortière, A. (2022) . Small Methods, 6(2), 2100891.

[5] Folastre, N., Cherednichenko, K., Cadiou, F., Bugnet, M., Rauch, E., Olchowka, J., Demortière, A. (2021). Microscopy and Microanalysis, 27(S1), 3446-3447.

[6] Gomez-Perez, A., Galanis, A., Das, P., Nicolopoulos, S., Demortière, A.(2021).Microscopy & Microanalysis,27(S1),2234-2235.

568

eCHORD crystalline orientation maps: channeling contrast at interfaces

Dr. Hdr Cyril Langlois[1], Dr. Gabriel Denhez L'Hôte[1], M. Thierry Douillard[1], Dr. Matthieu Bugnet[1], Dr. Claire Maurice[2]
[1]INSA Lyon, MATEIS laboratory, Lyon, France, [2]Ecole des Mines Saint-Etienne, LGF laboratory, Saint Etienne, France

Poster Group 2

Background incl. aims
Every signal acquired by a scanning electron microscope (SEM) originates from a certain interaction volume below the surface, making localization of the received information challenging. For orientation maps obtained by EBSD, the Kikuchi patterns acquired at the interface between two grains contain contributions from both crystals. This impacts the precise localization of the interfaces on the generated map and thus, influences the spatial resolution when dealing with objects of a size comparable to the interaction volume [1]. For EBSD, this interaction volume can be hardly reduced, as Kikuchi patterns significantly weaken at accelerating voltages of 5kV and lower.
The same “blending” effects are expected in eCHORD orientation maps obtained using SEM since the channeling contrast also arises from a certain interaction volume beneath the sample surface [2, 3]. However, at such low accelerating voltages, electron channeling contrast can still be accomplished, hence orientation maps with a reduced interaction volume could potentially be obtained via the eCHORD approach.

Methods
When considering the orientation maps obtained using the eCHORD approach [2, 3], the raw data comprises of an image series captured by rotating the region of interest (ROI) within the SEM, with the sample being tilted at approximately 10-15°. Such an image series constitutes a datacube from which intensity profiles can be extracted, one for each beam position on the ROI, representing the variation of the backscattered electron (BSE) signal as the sample rotates. Similar to Kikuchi patterns, these intensity profiles are also influenced by the respective contributions of two neighbouring crystals. To evaluate how this effect affects the eCHORD orientation maps, acquisitions were carried out on a copper thin film of 3 µm thickness exhibiting submicronic twins with 80 nm in thickness. The acquisition conditions are outlined as follows: 120 images (2048*1536) were captured using a frame time of 20.3s per image, at an accelerating voltage of 5kV, with a sample tilt of 15°, and utilizing a below-the-lens BSE detector. It is worth noting that an accelerating voltage of 5kV is now a routine condition for eCHORD experiments.

Results
Experimental evidences of a hybridisation effect are presented, showing that the intensity profile at a given interface is a blend between the intensity profiles of the two neighbouring grains. In addition to the interaction volume, various other factors explaining these hybridisation effects are presented and discussed: CHORD geometrical setup, image alignment, denoising, and indexing by pattern matching. Numerical simulations were also performed to quantitatively assess the effect of this hybridisation on the results of indexing intensity profiles, leading to a proposed adjustment in the indexing algorithm for the eCHORD method. This adjustment involves deriving the experimental as well as the theoretical profiles of the CHORD database prior to indexation, aiming to limit the effect of hybridisation on the final orientation maps. We demonstrate that this new algorithm has beneficial effects on indexation quality in general, compensating for differences between simulated and experimental profiles.

Conclusion

An effect of hybridization at interfaces has been observed in eCHORD orientation maps, which is limited by the adjustment of the indexing algorithm, thus demonstrating its robustness against degraded data.

This work represents an intermediary step in a more comprehensive approach aiming to enhance the spatial resolution in orientation maps obtained by eCHORD. This is achieved through the reduction of the accelerating voltage, improving the acquisition procedure, and by enhancing the post-treatment operations.

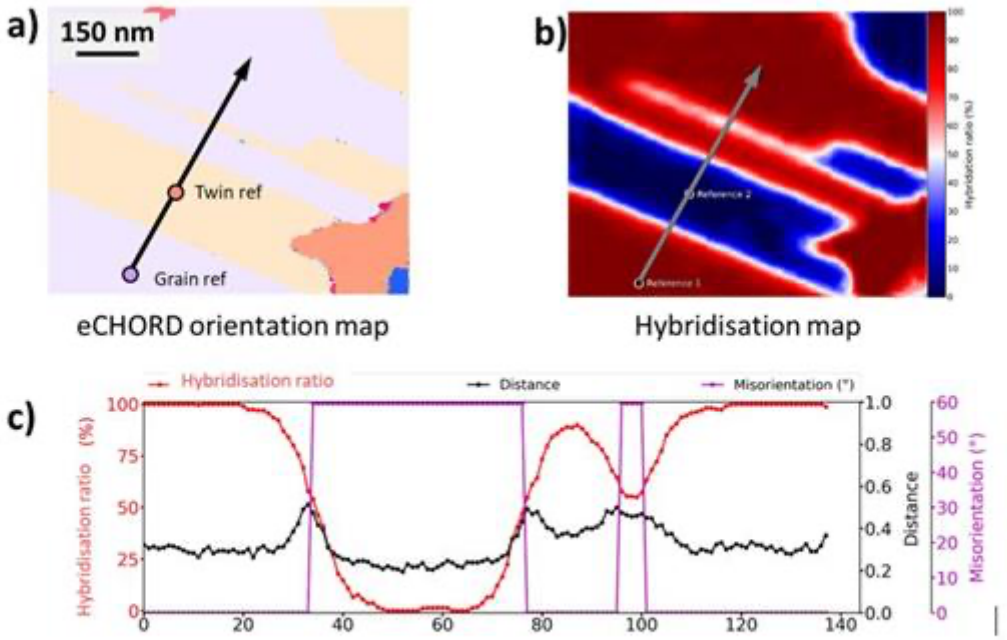

Figure 1: a) Detail of an eCHORD orientation map at 5kV, tilt 15°kV. b) Hybridisation map from references in the grain and in the twin, c) Evolution of the hybridisation ratio (red), pattern matching quality ("Distance", black), and misorientation compared to grain orientation (purple).

Keywords:

eCHORD, orientation mapping, interfaces, SpatialResolution,

Reference:

[1] Brodu E, Winkelmann A, Seefeldt M. (2022) A Pattern Processing Method to Map Nanoscale Phases by EBSD. Microscopy and Microanalysis 28(3) 716-722. doi:10.1017/S1431927622000526

[2] Lafond C., Douillard T., Cazottes S., Steyer P. and Langlois C. (2018) Electron CHanneling ORientation Determination (eCHORD): An original approach to crystalline orientation mapping. Ultramicroscopy, 186, 146-149. doi:10.1016/j.ultramic.2017.12.019

[3] Lafond C., Douillard T., Saad H., Deville S. Meille S., Steyer Ph., Cazottes S., Langlois C. (2021), eCHORD orientation mapping of bio-inspired alumina down to 1 kV, Materialia 20 101207. doi: 10.1016/j.mtla.2021.101207

607

Multi-Dimensional Data Restoration from Subsampled EBSD Data

Zoe Broad[1], Jack Wells[2], Daniel Nicholls[3], Alex W. Robinson[3], Amirafshar Moshtaghpour[4], Robert Masters[5], Louise Hughes[5], Angus I. Kirkland[4], Nigel D. Browning[1,3]
[1]Department of Mechanical, Materials and Aerospace Engineering, University of Liverpool, Liverpool, UK, [2]Distributed Algorithms Centre for Doctoral Training, University of Liverpool, Liverpool, UK, [3]SenseAI Innovations Ltd, Liverpool, UK, [4]Rosalind Franklin Institute, Didcot, UK, [5]Oxford Instruments NanoAnalysis, High Wycombe, UK

Poster Group 2

Background incl. aims

Electron backscatter diffraction (EBSD) is a popular technique for the identification of sample morphology, providing information about the crystal orientation and grain boundaries present [1]. Although detector technology has significantly improved, analysis times can be long, on the order of hours, depending on sample type and size. Additionally, long dwell times are often needed to enable sufficient signal to be collected, making the technique unviable for beam sensitive samples.

Recently, compressive sensing techniques have been applied to electron microscopy, wherein low-dose and fast acquisition methods are enabled through the use of subsampling. To date, subsampling has been successfully applied in STEM and FIB-SEM [2-4].

EBSD datasets are 4-dimensional (4-D), meaning multiple applications of subsampling and reconstruction are possible. Demonstrated here is the application of probe subsampling in EBSD datasets. For reconstruction 2-D, 3-D and 4-D data volumes were investigated.

Methods

A low noise Ni-superalloy dataset consisting of 416 x 512 probe locations was used, with a mask applied to simulate 25% subsampling. The reconstruction methods investigated used 2-D, 3-D and 4-D data volumes to reconstruct the full dataset.

Probe location maps are formed by taking each pixel from the full set of EBSD patterns at a single probe location, forming an image similar to a pattern quality map. 2-D reconstruction consists of inpainting the probe positions on an image by image basis. In 3-D reconstruction the dataset is vectorised. In 4-D reconstruction the data is inpainted in the position it was acquired in.

Results

The results of inpainting the 2-D and 3-D data volumes are shown in Figure 1 (Reconstruction quality of 25% sampled EBSD datasets using 2-D or 3-D data volumes for inpainting).

For 2-D inpainting a minor decrease in hit rate is observed, dropping from 99.80% to 99.53%. The band contrast map is less defined at grain boundaries than in the fully sampled dataset and an overall smoother map being output with the surface texture being lost.

For 3-D inpainting the hit rate drops to 97.87%. This is evident in the IPF Z map, where significant zero solution pixels can be seen around the grain boundaries. By using a 3-D data volume for inpainting there is a greater overlap of EBSD patterns between grains which results in a less distinct

EBSD pattern being inpainted. Despite this, the band contrast map is slightly sharper than the 2-D reconstruction, although some grain boundaries are no longer evident.

Although 4-D reconstruction shows promising results on a heavily cropped dataset (8x10 pixels), the memory currently required for this method limits its applicability. Due to this cropping, the datasets cannot be indexed in AZtec and hit rate is not recorded. Further work looking into optimising the datasets and inpainting parameters may help to improve this.

Conclusion

Pre-indexing reconstruction has been demonstrated. 2-D reconstruction is thus far the most effective method, with 3-D reconstruction through probe positions providing valid but slightly lower quality reconstructed patterns. Although the output quality of 4-D reconstruction is good it is currently unfeasible given the memory requirements.

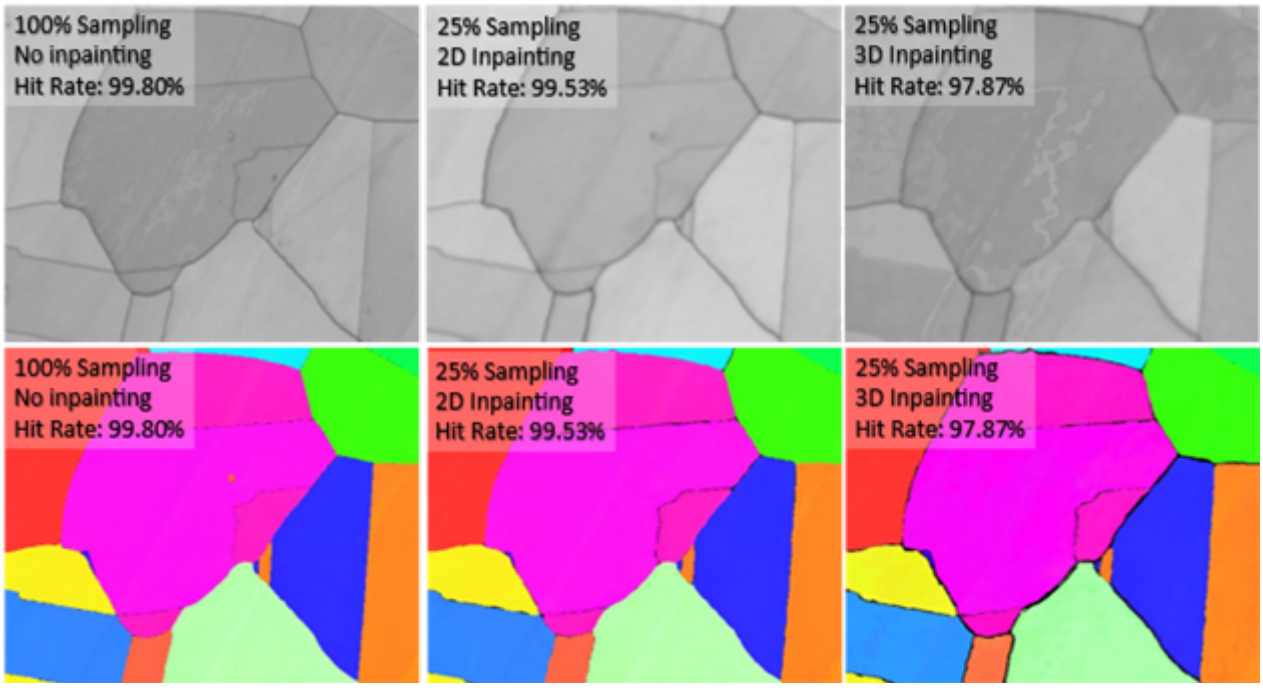

Keywords:

EBSD, SEM, compressive sensing

Reference:

[1] A. J. Schwartz, M. Kumar, B. L. Adams, and D. P. Field, Electron backscatter diffraction in materials science, 2nd ed. New York: Springer, 2009.
[2] Z. Saghi, M. Benning, R. Leary, M. Macias-Montero, A. Borras, and P. A. Midgley, “Reduced-dose and high- speed acquisition strategies for multi-dimensional electron microscopy,” Advanced Structural and Chemical Imaging, vol. 1, no. 1, pp. 1–10, 2015.
[3] N. D. Browning, J. Castagna, A. I. Kirkland, A. Moshtaghpour, D. Nicholls, A. W. Robinson, J. Wells, and Y. Zheng., “The advantages of sub-sampling and inpainting for scanning transmission electron microscopy,” Applied Physics Letters, vol. 122(5), p. 050501, 2023.
[4] D. Nicholls, M. Kobylynska, Z. Broad, J. Wells, A. Robinson, D. McGrouther, A. Moshtaghpour, A. I. Kirkland, R. A. Fleck, and N. D. Browning, “The potential of subsampling and inpainting for fast low-dose cryo fib-sem imaging,” Microscopy and Microanalysis, p. ozae005, 2024.

653

Tilted multislice approach for quantitative STEM simulation

Xian Li[1], Changlin Zheng[1]
[1]State Key Laboratory of Surface Physics and Department of Physics, Fudan University, Shanghai, China

Poster Group 2

Background incl. aims
Scanning transmission electron microscopy (STEM) is a powerful tool for studying materials down to the atomic scale. Although qualitative STEM imaging offers plentiful information about atom locations and identification, quantitative analysis is becoming increasingly valuable for insights into composition, atom counting and thickness determination [1]. However, due to the strong dynamical scattering in crystals, directly solving the inverse problem from scattered electron intensity in STEM is nearly impossible. As a result, STEM imaging simulation is crucial for quantitative STEM analysis. In this study, we develop a new multislice algorithm that can be applied to nonorthogonal crystal structures, a task generally challenging in conventional multislice simulation [2].
Methods
For nonorthogonal unit cells, such as a triclinic unit cell, we first use an iterative algorithm to find a new unit cell. We aim to make the angles between the three new basis vectors as close to 90° as possible, while the c-axis keeps along the electron beam direction. The nonorthogonal supercell is then divided into a series of tilted slices parallel to the a-b vector plane. The Coloumb potential of the crystal is then projected onto the tilted slices based on a nonorthogonal mesh, and a tilted Fresnel propagation is performed between subsequent slices. The generated STEM image based on nonorthogonal mesh is then re-mapped into conventional format. By using this tilting-slice operation, we can effeiciently model the electron dynamical scattering in nonorthogonal structures.
Results
We implemented the method in our in-house STEM simulation code and performed high angle annular dark field (HAADF) STEM simulations on Gd2B4O9 [0 0 1], as shown in Figure 1.
Conclusion
We develop a tilted multislice approach to simulate focused electron beam propagation in nonorthogonal structures. This effectively extends quantitative STEM analysis to compound materials with more complex structures.

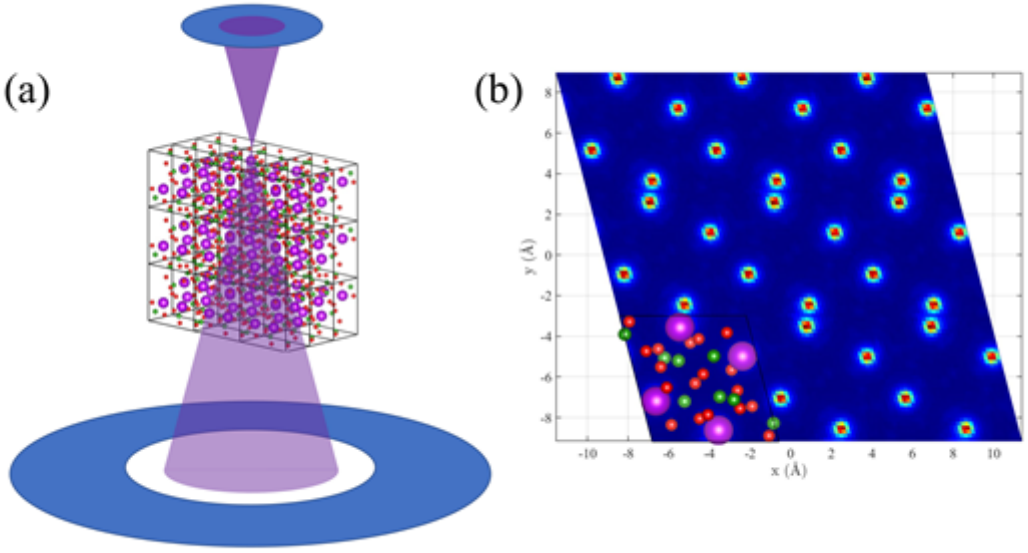

Keywords:

Quantitative STEM, multislice, nonorthogonal crystal

Reference:

[1] J. M. LeBeau, S. D. Findlay, L. J. Allen, and S. Stemmer, Quantitative Atomic Resolution Scanning Transmission Electron Microscopy, Physical Review Letters 100, 206101 (2008).
[2] E. J. Kirkland, Advanced Computing in Electron Microscopy, 2nd ed. (Springer, 2012).

655

4DSTEM-in-SEM by placing a pixelated detector below the sample

Johannes Müller[1], Christoph T. Koch[1]
[1]Department of Physics & IRIS Adlershof, Humboldt-Universität zu Berlin, Berlin, Germany

Poster Group 2

Background

Four-dimensional scanning transmission electron microscopy (4DSTEM) is a powerful diffraction-based technique to probe local crystallinity, orientation, strain, and many more properties of electron-transparent samples [1]. Furthermore, various open source Python packages exist to analyze the large amounts of data generated by 4DSTEM, for instance LiberTEM, py4DSTEM, and pyxem. 4DSTEM can also be employed in scanning electron microscopes (SEMs) for example by placing an electron-sensitive pixelated detector (camera) below the sample similar to on-axis transmission Kikuchi systems [2-5]. The lower accelerating voltage of SEMs leads to strong scattering even from monolayers. 4DSTEM-in-SEM is ideally suited to characterize 2D-like materials due to their inherent thickness of a few nms.
Compared to dedicated (scanning) transmission electron microscopes ((S)TEMs), the large sample chamber of SEMs with their various flanges as well as the large area around the sample give enough space to integrate cameras and other equipment into the sample chamber without compromising on the SEM's original functionality. The large field of view of SEMs of several mm² combined with their resolution in the sub-nm range are ideal to map properties on different length scales. Furthermore, using SEMs as a base platform allows for simpler, more easily customizable, and more economical experimental setups. On the other hand, the lower accelerating voltage of SEMs require thinner samples and the native spatial resolution doesn't allow STEM-imaging at atomic resolution.

Methods

We built two transmission diffraction substages that fit between the pole piece and the SEM stage, and can be mounted on top of the original SEM stage. One substage utilizes a fiber-coupled scintillator-based CMOS camera and the other substage a Medipix 3 hybrid-pixel detector with single electron sensitivity (X-Spectrum GmbH, Germany). Both substages with their corresponding cameras are shown in Fig. 1 a) and b). The compact 2.5x2.5x1.1cm³ CMOS camera is integrated inside a hexapod stage and mounted to a linear stage, enabling us to physically adjust the distance between camera and sample (the camera length). The camera length is limited to the distance between the sample and the camera because there are no active lenses after the sample. The substages have sample holders for standard TEM grids and are kept inside an external vacuum chamber when not inserted into the SEM to reduce carbon contamination.
Hardware synchronization between each camera, the GeminiSEM 500 (Zeiss), our in-house scan generator, and the electrostatic beam blanker makes it possible to only expose the sample during a camera frame and to utilize the maximum possible frame rate of each camera. The scan generator also acquires the signals of the SEM's secondary electron (SE) detectors during a 4DSTEM scan. We integrated all hard- and software in-house, providing full control over the 4DSTEM-in-SEM systems allowing us to explore new and existing methods.

Results

Fig. 1 c) shows maps of the in-plane orientation and the coverage of both components of a C60/MoS2 van der Waals heterostructure [5]. The in-plane orientation map of MoS2 obtained by gold-mediated exfoliation shown in Fig. 1 d) reveals the single crystallinity of the MoS2 over several mm² [5]. The data shown in Figs. 1 c) and d) were obtained using the above-mentioned CMOS camera-based system and are exemplary applications of 4DSTEM-in-SEM.

Conclusion

4DSTEM-in-SEM is feasible and adds to the SEM's wide range of applications. The large scan area of several mm² and the nm sized spatial resolution of SEMs is ideal to employ 4DSTEM in SEMs to characterize low-dimensional materials and thin bulk samples. Furthermore, SEMs are an excellent platform for method development due to their simplicity compared to dedicated (S)TEMs, their spacious sample chamber, the convenient access to the sample area, and their good imaging performance.

Acknowledgements

We acknowledge financial support by the ScienceCampus GraFOx of the Leibniz Association, the German Research Foundation (Projektnummer 414984028 - SFB 1404), and by the Volkswagen Foundation (Initiative: "Experiment!").

We wish to thank Max Heyl, Thorsten Schulz, Kristiane Elsner, Steffen Rühl, and Hélène Seiler for their contribution to the sample preparation.

We thank Julian Schmehr from X-Spectrum for lending us the Medipix 3 detector. We thank Harald Niebel, Björn Gamm, Markus Boese from Carl Zeiss Microscopy GmbH for help with controlling the SEM. We thank the mechanical workshop at the Department of Physics of Humboldt-Universität zu Berlin for the machined parts.

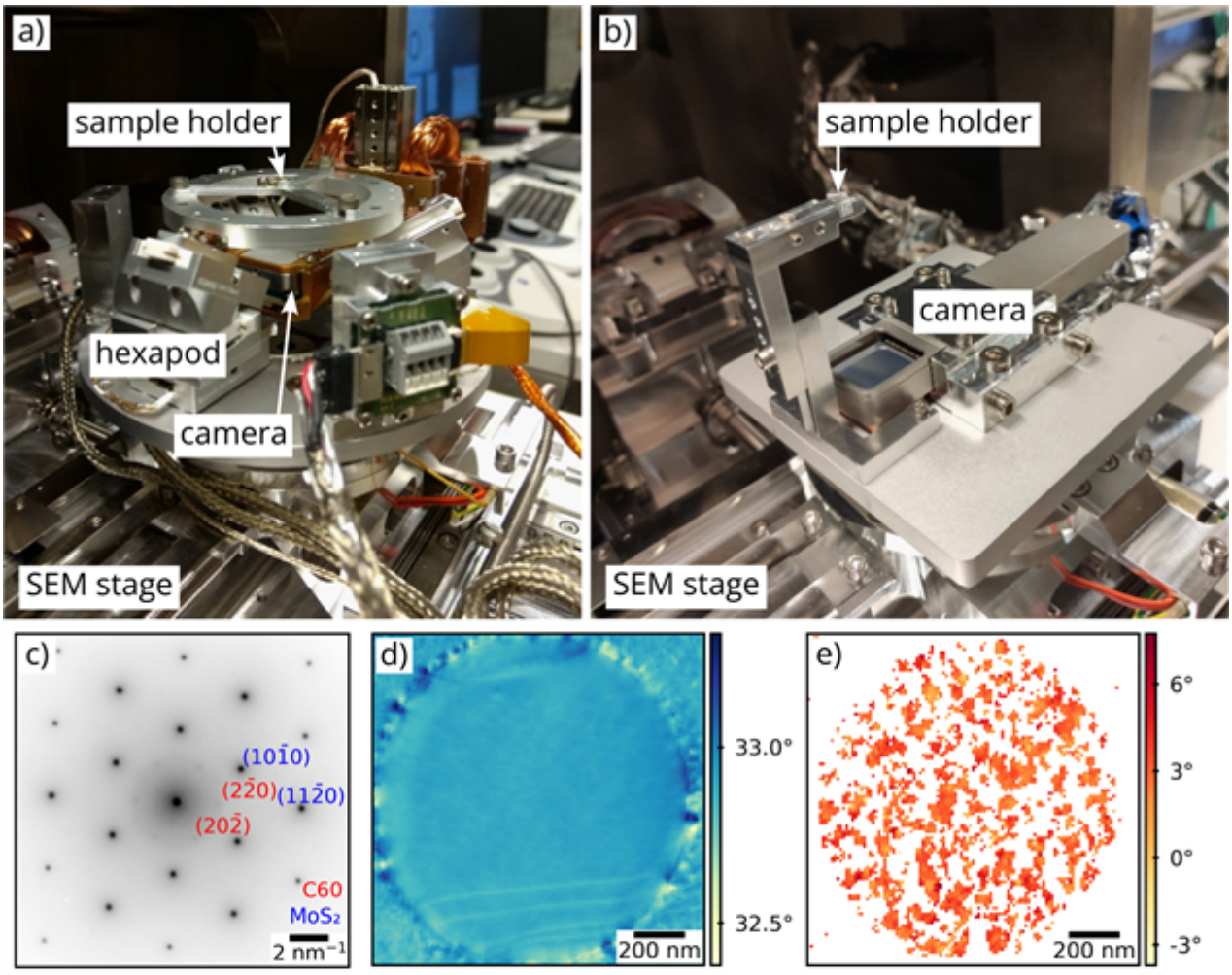

Fig. 1. a) Substage with the fiber-coupled scintillator-based camera inside the hexpod. b) Substage with a Medipix 3-based camera. Both substages are mounted on top of the GeminiSEM 500 sample stage. c) to e) Results of a C60/MoS2 van der Waals heterostructure suspended over a hole of a Quantifoil TEM grid membrane [5]. c) Logsum of all diffraction patterns of the 4DSTEM dataset with indexed diffraction peaks. d) and e) in-plane orientation of the MoS2 and C60 lattice respectively revealing a preferred alignment of both lattices.

Keywords:

4D-STEM, 4D-STEM-in-SEM, transmission-electron-diffraction, 2D-materials

Reference:

[1] C Ophus, Microscopy and Microanalysis 25 (2019), p. 563.
https://doi.org/10.1017/S1431927619000497
[2] P Schweizer et al., Ultramicroscopy 213 (2020), p. 112956.
https://doi.org/10.1016/j.ultramic.2020.112956
[3] B W Caplins et al., Ultramicroscopy 219 (2020), p. 113137.
https://doi.org/10.1016/j.ultramic.2020.113137
[4] Wide field of view crystal orientation mapping of layered materials,
http://arxiv.org/abs/2011.01875 (accessed June 4, 2023)
[5] J Müller et al., physica status solidi (a) 221 (2024), p. 2300148.
https://doi.org/10.1002/pssa.202300148

698

Low dose and in situ 4D-STEM powered by real-time sparse-array analytics on an event-driven detector

Penghan Lu[1], Yucheng Zou[1], Tingting Yang[1], Janghyun Jo[1], Deli Kong[1], Dieter Weber[1], Alexander Clausen[1], Matthew Bryan[2], Dmitry Byelov[3], Giuseppe Spano[3], Thorbjörn Schönbeck[3], Rafal E. Dunin-Borkowski[1]
[1]Ernst Ruska-Centre for Microscopy and Spectroscopy with Electrons, Forschungszentrum Juelich, Juelich, Germany, [2]Université Grenoble-Alpes, CEA, Leti, , France, [3]Amsterdam Scientific Instruments, Amsterdam, The Netherlands

Poster Group 2

Background incl. aims
Four-dimensional scanning transmission electron microscopy (4D STEM) measures 2D reciprocal space scattering information from an electron probe laterally shifted across a 2D real space specimen area [1]. This high-dimensional dataset allows much richer information to be retrieved than conventional STEM, ranging from crystallographic orientation and phase, strain, short and medium range ordering, to differential phase contrast (DPC), ptychography as well as other new imaging modes. The past decade has particularly witnessed the advance of this technique because of the introduction of fast direct electron-counting detectors. These detectors usually run at 1-10 kHz continuous readout, which corresponds to 1000-100 µs pixel dwell time in 4D STEM measurements, while the conventional STEM usually runs in few µs pixel dwell time. Such a 2-3 order-of-magnitude gap in speed would limit the application of the versatile 4D STEM measurements to at least two fields, including low-dose atomic-resolution high-contrast imaging of sensitive specimens as well as in situ time-resolved studies of dynamic behaviour upon external stimuli.
Methods
In order to tackle this challenge, we installed an event-driven CheeTah T3 detector with 2x2 chips (in total 512x512 pixels) from Amsterdam Scientific Instruments (ASI) on a monochromated and probe-corrected Thermo Fisher Scientific Titan STEM for 4D STEM applications. This detector retrieves precise timing of scanning line trigger signal from the microscope with the same clock as the electron impact events on the detector, which facilitates a reliable assignment of the electron events to each scanned pixel. Thanks to its 1.56 ns Time of Arrival resolution, this detector also permits recording electron events continuously in an effectively much higher frame rate for 4D STEM. Due to its inherent sparse nature, this high-dimensional data can be compressed and computed in real time efficiently in the compressed sparse row (CSR) format based on the collaborative development between ASI and LiberTEM team [2].
Results
4D STEM measurements at effectively MHz frame rate with live image reconstruction has been demonstrated based on these developments (see one example in the enclosed figure). This unique workflow enables the user to navigate the specimen, adjust focus or astigmatism, and eventually visualise sensitive specimens or dynamics without changing between different detectors or optical modes. A few application examples will be discussed during this presentation. This includes, but not limited to,
- Fast and low-dose phase-contrast imaging at nanometer to atomic resolution based on integrated centre-of-mass imaging, ptychography, and other 4D STEM modes,
- In situ 4D STEM measurement of both electromagnetic fields and strain/orientation/phase on magnetic and semiconductor specimens under tensile loading and unloading conditions,
- In situ 4D STEM mapping of electron-beam-induced charging on dielectrics and vitrified ice.
Conclusions

Effectively MHz frame rate event-driven detector has been successfully demonstrated for low dose and in situ time-resolved 4D STEM characterization. Sparse-array data format was implemented for real-time feedback and efficient analysis with compact data size. Versatile applications on low dose imaging of sensitive specimens and time-resolved studies of dynamic processes will be presented during this contribution. Further improvement and other potential applications for this workflow will also be discussed.

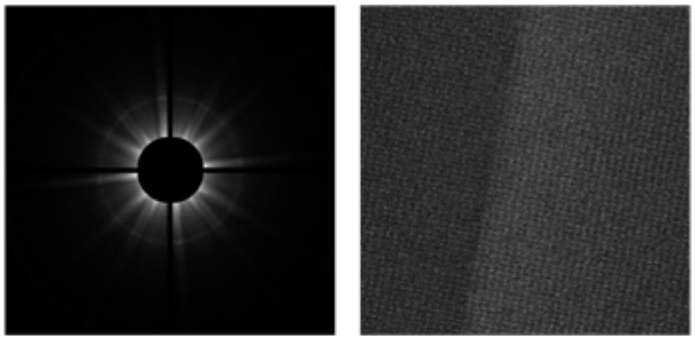

$SrTiO_3$ / $LaSrMnO_3$ interface
PACBED and virtual ADF image
Digital block BF and LAADF area
Probe current: 20 pA
Pixel dwell time: 1 us
Scanning step size: 17 pm
Scanning size: 1024 * 1024
Dose: $4.3*10^3$ e-/A^2

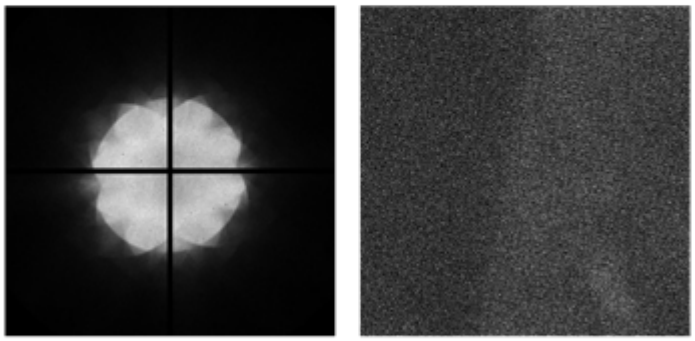

$SrTiO_3$ / $LaSrMnO_3$ interface
PACBED and virtual ADF image
No digital block
Probe current: 2.4 pA
Pixel dwell time: 1 us
Scanning step size: 17 pm
Scanning size: 1024 * 1024
Dose: $5.1*10^2$ e-/A^2

Due to the limited maximum event rate, when using BF for analysis, the probe current has to be low. Dose-efficient imaging methods such as iCoM or ptychography would help. Multi-frame or sub-area averaging will be also useful.

Keywords:

4D-STEM, low-dose, in-situ, event-driven detector

Reference:

[1] C. Ophus, Microscopy and Microanalysis 25, 563 (2019).
[2] A. Clausen et al., Zenodo 10.5281/zenodo.8252548 (2023).

703

ePattern: an adaptive 4D-STEM Pattern Registration Algorithm to Optimize ACOM Pattern Matching

Dr. Arnaud Demortière[1,2], Dr. Nicolas Folastre,[1,2], Junhao Cao[1,2], Dr. Arash Jamali[1], Fayçal Adrar[1,2]
[1]Laboratoire de Réactivité et Chimie des Solides (LRCS) CNRS UMR7314, Amiens, France, [2]Réseau sur le Stockage Electrochimique de l'Energie (RS2E) CNRS FR3459. , Amiens, France

Poster Group 2

The technique known as four-dimensional scanning transmission electron microscopy (4D-STEM)1 has recently emerged as a potent tool for the local characterization of crystalline structures in various materials, including cathode materials for lithium-ion batteries and perovskite materials for photovoltaics.
This 4D-STEM data analysis method based on the ACOM system of NanoMegas (Astar)2,3 uses pattern matching of a scanning nano-diffraction dataset with libraries of diffraction patterns simulated from known structures extracted from CIF files. This method enables to construct crystalline phase and orientation maps to determine crystallinity4,5, microstructures6, structural deformation7, and grain boundaries8 using scanning nano-diffraction with precession mode in a nanometer resolution9,10. However, the utilization of new detectors specifically designed for electron diffraction patterns and other advanced techniques necessitates the continuous adaptation of methodologies to address the challenges associated with crystalline materials.

The goal of the data preparation methods proposed here is to improve the quality of Astar pattern-matching using a dataset of diffraction patterns acquired with a CMOS Oneview camera. The high sensitivity of the CMOS camera and the data filtering developed here modify the diffraction images leading to a compromise between improving image quality and optimizing template-matching results11.

Our strategy employs a data reduction technique that utilizes registration methods to identify electron diffraction spots within patterns. By doing so, we are able to filter and capture the diffraction signal and subsequently reconstruct the patterns. These reconstructed patterns are then inputted into the Astar suite pattern-matching software. This process allows us to record the essential information of each reflection in a dataset, including intensity, size, and position, with a high level of accuracy (sub-pixelar) for the position, typically on the order of 10-3px. Additionally, this technique achieves a significant reduction in data size, typically by a factor of 103. This means that the essential information of the diffraction pattern is stored on a disk with 100 to 1000 times less space required. The adaptative nature of this method not only reduces noise and compresses nanodiffraction scanning data for ACOM and strain mapping analysis but also extends its applicability to other techniques such as 3D electron diffraction (3DED).

To evaluate our approach, we employ dedicated metrics that clearly demonstrate a substantial improvement in phase recognition. Our results indicate that this data preparation method not only enhances the quality of the resulting image but also boosts confidence levels in the analysis of crystal orientation and phase determination outcomes. Furthermore, it helps mitigate the potential impact of user bias that may arise when manipulating parameters during the application of this method.

Firstly, modifications on inside diffraction patterns are estimated through image quality metrics such as peak signal-over-noise (PSNR), structural similarity index measure (SSIM), and root-mean-square error (RMSE). Secondly, the quality of the pattern-matching process on filtered and reconstructed

images obtained by the proposed experimental data preparation method is evaluated using index and orientation reliability, as defined in the Astar software. We demonstrate that the experimental data preparation helps to improve the pattern-matching quality result, as it reduces noise overfitting, improves structural similarity index measure, and increases the orientation reliability.

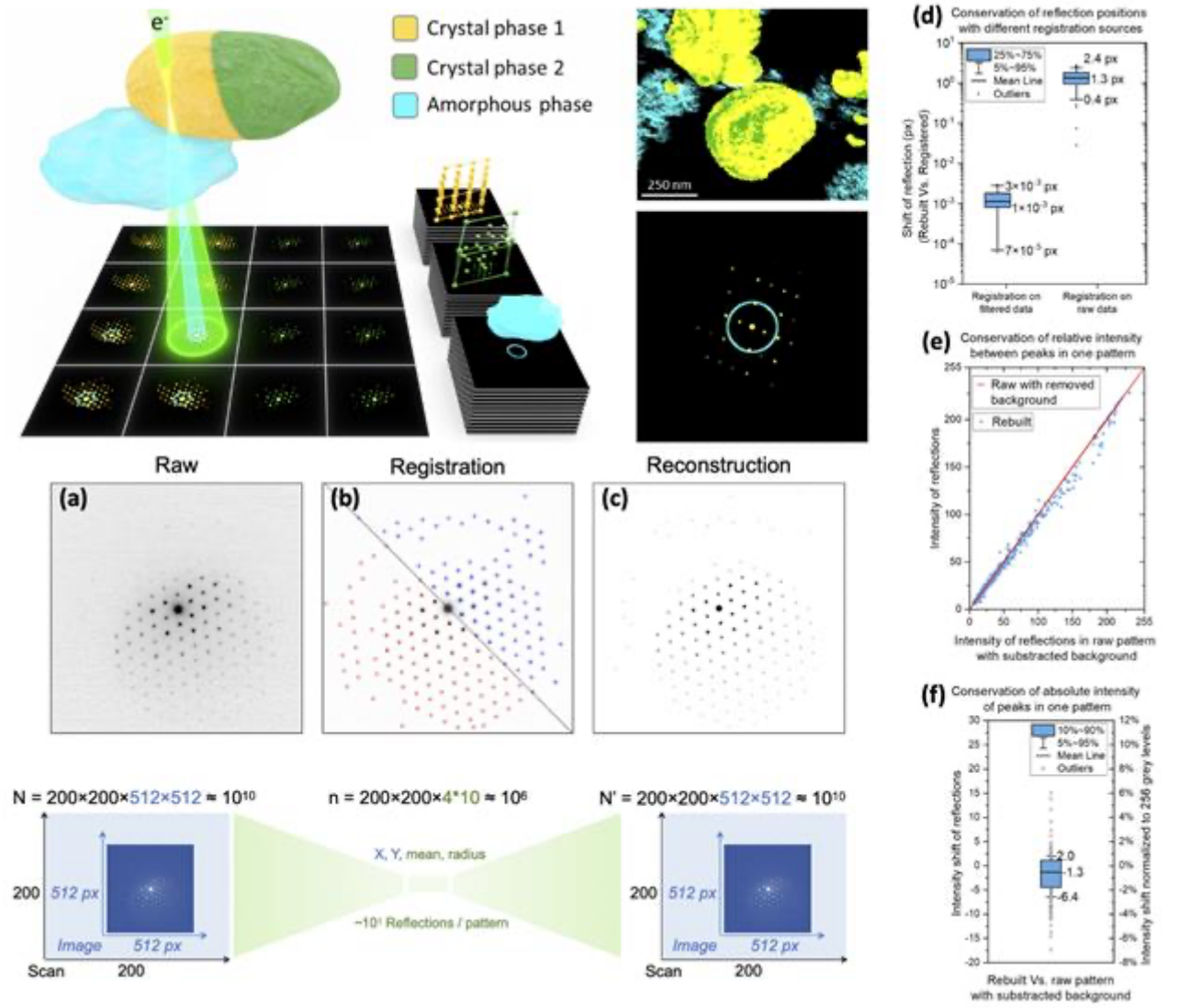

Keywords:

4D-STEM ACOM, ePattern software, diffraction-pattern

Reference:

[1] Ophus, C. Microsc. Microanal. 563–582 (2019) doi:10.1017/S1431927619000497.
[2] Rauch, E. F. & Véron, M. Automated crystal orientation and phase mapping in TEM. Mater. Charact. 98, 1–9 (2014).
[3] Rauch, E. F., Harrison, P. & Véron, M. Symmetry (Basel). 13, 1–12 (2021).
[4] McCartan, S. J. et al ceramic. J. Am. Ceram. Soc. 104, 2388–2397 (2021).
[5] Bhatia, A. et al. Small Methods 6, (2022).
[6] Sunde, J. K., Marioara, C. D. & Holmestad, R. Mater. Charact. 160, 110087 (2020).
[7] Londoño-Calderon, A. et al. J. Phys. Chem. C 125, 3396–3405 (2021).
[8] Bustillo, K. C. et al. Acc. Chem. Res. 54, 2543–2551 (2021).
[9] Nicolopoulos, S. et alScanning 2019, (2019).
[10] Ponce, A., Aguilar, J. A., Tate, J. & Yacamán, M. J. Nanoscale Adv. 3, 311–325 (2021).
[11] Folastre, et al. (2023). arXiv preprint arXiv:2305.02124 (Nature Scientific Report)

726

Evaluating spherical models of EBSD patterns for forward modelling indexing

Dr René De Kloe[1], William Lenthe[2], Stuart Wright[2], Matt Nowell[2]
[1]EDAX-Gatan, Tilburg, The Netherlands, [2]EDAX-Gatan, Pleasanton, USA

Poster Group 2

The application of full pattern matching-based forward modelling indexing techniques of EBSD and transmission EBSD patterns has shown significant improvements over conventional indexing methods that are based on the detection of individual bands in the EBSD patterns [1,2]. Forward modelling provides superior robustness on poor quality patterns, improved orientation precision, and can resolve common indexing challenges including pseudo-symmetry, non-centrosymmetric point groups (polarity), and overlapping patterns. Furthermore, new GPU implementations of spherical harmonic indexing and real space orientation refinement can both achieve speeds of thousands of patterns per second on modest hardware making its application accessible for routine EBSD analyses.
A remaining challenge for these indexing methods, both dictionary indexing and spherical indexing, is that they rely on detailed knowledge of the crystal structure of the phase(s) that are being indexed. The dynamic simulations that are the basis of the forward-model indexing methods are critically dependent on the crystal symmetry, atomic positions, occupancy, and electron scattering parameters. This is especially important in more complex phases such as solid solutions, intermetallic phases, and minerals. In many cases this detailed information is not available.
Alternative master patterns that do not require the same detailed knowledge of the crystal structure can be created using a kinematical model or using actual EBSD patterns. For these methods the information that is already available in the more basic EBSD structure files that are used for Hough transform-based indexing is sufficient. With the lattice parameters, the point group symmetry, a list of expected reflectors or bands, and the relative intensity of the bands in the EBSD patterns a kinematic spherical intensity model can be constructed. Alternatively, Kikuchi spheres may be created using actual EBSD patterns, provided that their phase and orientation is known by conventional EBSD indexing [3]. These spheres can then be applied as experimental master patterns for spherical indexing.
The advantage of using the experimental master patterns is that the required calculation time is less than 1 minute while dynamic simulations may take multiple hours to generate. Experimental patterns will also exhibit the same contrast range as the experimental patterns which may change with specific pattern image processing methods. With a closer match between the experimental patterns and the master pattern, improved indexing results may be expected. In this presentation the requirements for successful generation of master pattern simulations for pattern matching will be discussed together with application examples.

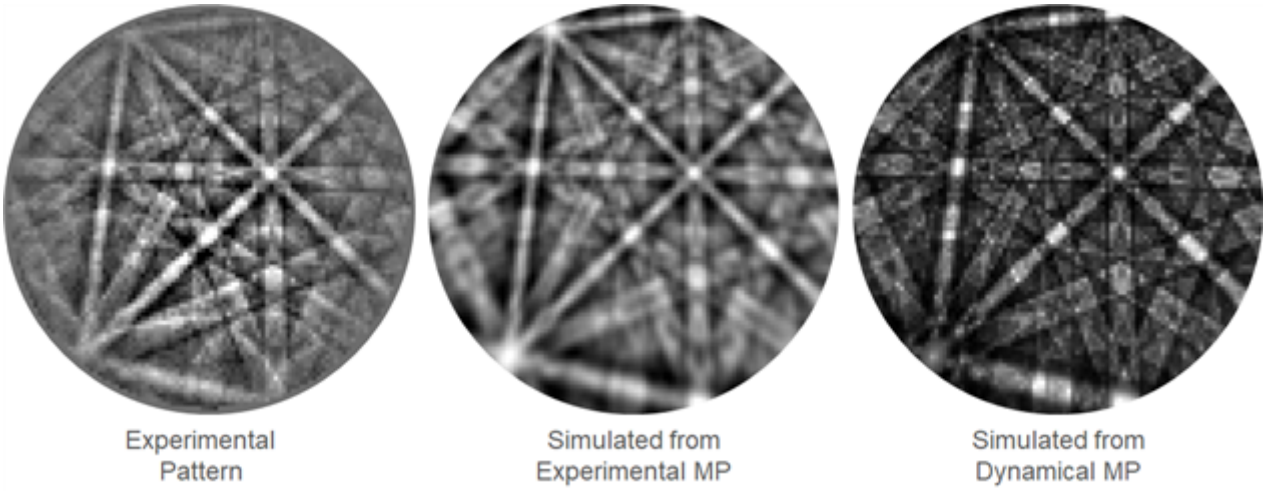

Keywords:

EBSD, Forward-model, spherical-indexing, master-pattern

Reference:

[1] Callahan, P. G., & De Graef, M. (2013). Dynamical electron backscatter diffraction patterns. Part I: Pattern simulations. Microscopy and Microanalysis, 19(5), 1255-1265
[2] Lenthe, W. C., Singh, S., & De Graef, M. (2019). A spherical harmonic transform approach to the indexing of electron back-scattered diffraction patterns. Ultramicroscopy, 207, 112841
[3] Day, A. P. "Spherical EBSD." Journal of microscopy 230.3 (2008): 472-486

740

Revealing the vacancy ordering in Prussian blue analogues through serial electron diffraction

Mr Shihui Feng[1], Dr Hanna Boström[1], Dr Cheuk-Wai Tai[1]
[1]Department of Materials and Environmental Chemistry, Stockholm University, Stockholm, Sweden

Poster Group 2

The irregular arrangements of the vacancies, interstitials or impurities on the lattice sites in a crystal structure can cause diffuse scattering in diffraction patterns, causing deviation from Bragg diffraction spots. Such diffuse scattering features can be utilized and back-calculated to explore the arrangements of defects within the structure. The Prussian blue analogues (PBAs) are composed of two transition metals coordinated with cyanide ligands, resulting in a specific porous structure with diverse applications such as electrochemical catalysis, ion transportation, and gas absorption. Some researcher elucidated the vacancy networks in series of PBAs using single-crystal synchrotron diffraction. However, above mentioned techniques require large single-crystals (>500 um), which is not suitable for some groups of PBAs.
Here, contributed by high spatial-resolution, transmission electron microscope was applied. We focus on the vacancies ordering in Cu[Co(CN)6] PBAs nanoparticles, which is hard to collecting single crystal x-ray or synchrotron data. Additionally, the presence of cyanide ligands and zeolitic water inside structure makes PBAs can be easily damaged by electron beam within seconds, which hindering structural study using 3D electron diffraction. To address these challenges, the serial electron diffraction (serialED) was introduced to capture single-frame exposure electron diffraction for thousands of nanocrystals. Following by clustering and indexing, the diffuse scattering patterns were analysed from serval main zone-axis diffraction patterns. The diffuse scattering features from HK0 slice closely resembled those reported in the literature obtained by synchrotron methods, confirming the consistency and reliability of our method. The delta pair-distribution function also provides insights into the structural ordering in PBAs.

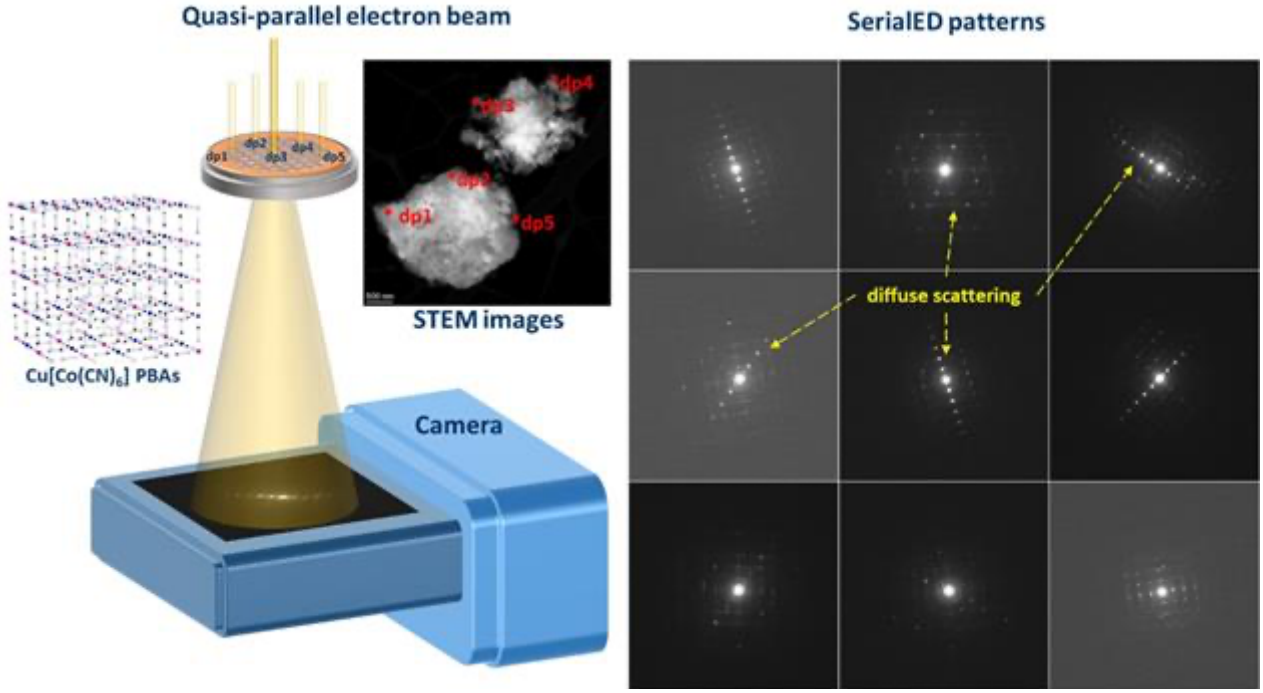

Keywords:

PBAs, electron diffraction, diffuse scattering

Reference:

1. Hidden diversity of vacancy networks in Prussian blue analogues. A Simonov, T De Baerdemaeker, HLB Boström… - Nature, 2020
2.STEM SerialED: achieving high-resolution data for ab initio structure determination of beam-sensitive nanocrystalline materials. P Hogan-Lamarre, Y Luo, R Bücker, RJD Miller, X Zou - IUCrJ, 2024
3.Quantitative three-dimensional local order analysis of nanomaterials through electron diffraction. EM Schmidt, PB Klar, Y Krysiak, P Svora, AL Goodwin… - Nature Communications, 2023

757

EBSD analysis of twin boundaries of prismatic calcite in oyster shells

Dr Katarzyna Berent[1], Prof. Kinga Nalepka[2], Prof. Antonio Checa[3,4]
[1]AGH University of Krakow, Academic Centre for Materials and Nanotechnology, Krakow, Poland, [2]AGH University of Krakow, Department of Strength and Fatigue of Materials and Structures, Krakow, Poland, [3]Universidad de Granada, Departamento de Estratigrafía y Paleontología, Granada, Spain, [4]CSIC-Universidad de Granada, Instituto Andaluz de Ciencias de la Tierra, Armilla, Spain

Poster Group 2

Oyster shells are biocomposites consisting of calcium carbonate crystals with a percentage of organic matrix. The organic fraction in these shells plays a crucial role in stress distribution control, leading to a hierarchical structure with high self-organization and low internal energy. This microstructure, with its unique combination of high strength and fracture toughness, holds significant potential for the development of advanced biomimetic materials.
We studied two specimens from the order Ostreida, Pinna nobilis Linnaeus, 1758 (Mollusca, Ostreida, Pinnidae), which comes from the Mediterranean Sea, and Pteria penguin Röding, 1798 (Mollusca, Ostreida, Pterioidea) collected in Lapu Lapu, Cebu, Philippines. The electron backscatter diffraction (EBSD) technique was used to study the crystallographic relations observed between prisms in a columnar calcite prismatic (CCP) layer. EBSD analysis was performed using a FEI Versa 3D FEG scanning electron microscope (SEM) equipped with an Oxford Instruments Symmetry S2 CMOS-based EBSD detector. EBSD data were collected using Aztec 6.1 software from the polished cross-section. The system was operated in low vacuum (LV-SEM) mode at a pressure of 40 Pa and an accelerating voltage of 15 kV.
The obliquely oriented calcite prismatic grains to the predicted load's direction are observed in P. nobilis. EBSD results show that strictly defined low-energy boundaries, i.e. rotation angles, are preferred. The disorientation described by the 60° rotation about the c-axis is mainly observed. Two symmetrically equivalent orientation relationships correspond to it, and one of them is observed in this case. The twin boundary (0 1 -1 0) is present, positioned perpendicular to the growth line, enabling the prisms to curve. The other preferred disorientations are also generated by twin relationships, with mirror planes characterized by higher indices: (1 -5 4 0) for 38° and (4 7 -11 0) for 18°. These new, previously unknown orientation relationships are common in P. nobilis shells. The shell is ornamented with radial ribs that strengthen it while giving it the flexibility needed to tighten its seal against predators. The growth lines become flatter in the area outside the ribs with the shell thickening, which affects the change in the direction of the c-axis, which becomes more parallel to the normal direction (ND). Such a microstructure improves hardness and compressive strength, which reaches an outstanding value of 700 MPa. In the case of P. penguin, EBSD was combined with theoretical boundary energy analysis using the Gautam-Howe method, which revealed that prisms as basic structural units show good mutual fitting and a sequence of twins arising within them is used to relax internal stresses. Consequently, a low-energy structure with an exceptionally high compressive strength of 600 MPa is achieved.

1. K. Nalepka et al. Ribs of Pinna nobilis shell induce unexpected microstructural changes that provide unique mechanical properties, Materials Science and Engineering: A (2022) 829, 142163

Acknowledgements:
Research project supported by the program „Excellence initiative – research university” for the AGH University of Krakow.

Keywords:

EBSD, twin boundaries, mollusc shells

Reference:

1. K. Nalepka et al. Ribs of Pinna nobilis shell induce unexpected microstructural changes that provide unique mechanical properties, Materials Science and Engineering: A (2022) 829, 142163

789

3D Electron Diffraction Study on the Local Structure of a doped Metal-organic Framework TCNQ@ZIF-4

Dr. Jianbo Song[1], Dr. Zhehao Huang[1]
[1]Department of Materials and Environmental Chemistry, Stockholm University, Stockholm, Sweden

Poster Group 2

Background incl. aims
Zeolitic Imidazolate Frameworks (ZIFs) become a more and more important sub-family of Metal-organic Frameworks (MOFs). ZIF-4 is one of the prototypical structures among ZIFs, which possesses the basic components of $M(im)^2$ (M = Co^{2+}/Zn^{2+} and im = imidazolate). Exclusive investigations have been applied on ZIF-4 such as mechanical properties[1] and thermal behaviors[2], however its conductivity is still missing.
Methods
7,7,8,8-tetracyanoquinododimethane (TCNQ) forms stable radical anions upon reduction, which can serve as an electron acceptor during the charge mobility.[3] Meanwhile, the transition metals, especially Co^{2+} are expected to donate electrons (i.e. to form Co^{3+}). The incorporation of TCNQ in the pores of ZIF-4 is expected to build up the pathway between the electron donor and acceptor to realize the mechanism of hoping transport[4]. A facial solvothermal method[5] was adopted to dope TCNQ@ZIF-4.
Results and Conclusion
Electron diffraction is revealing that the TCNQ has been successfully incorporated in the pores of frameworks. Further fine structures around the pore area urgently need to be resolved.

Keywords:

3D_Electron_Diffraction, Metal-organic Frameworks, local_Structure, Conductivity

Reference:

[1] J. Song, R. Pallach, L. Frentzel-Beyme, P. Kolodzeiski, G. Kieslich, P. Vervoorts, C. L. Hobday, S. Henke, Angew. Chem. Int. Ed. 2022, 61, e202117565.
[2] J. Song, L. Frentzel-Beyme, R. Pallach, P. Kolodzeiski, A. Koutsianos, W.-L. Xue, R. Schmid, S. Henke, J. Am. Chem. Soc. 2023, 145, 9273–9284.
[3] T. J. Kistenmacher, T. E. Phillips, D. O. Cowan, Acta Crystallogr. B 1974, 30, 763–768.
[4] L. S. Xie, G. Skorupskii, M. Dincă, Chem. Rev. 2020, 120, 8536–8580.
[5] A. A. Talin, A. Centrone, A. C. Ford, M. E. Foster, V. Stavila, P. Haney, R. A. Kinney, V. Szalai, F. El Gabaly, H. P. Yoon, F. Léonard, M. D. Allendorf, Science 2014, 343, 66–69.

816

Simultaneous Indexing of Spot and Kikuchi Patterns in Scanning Electron Microscopy (SEM)

PhD Student Yuxuan Zhang[1], Senior Researcher Alice Bastos da Silva Fanta[1], Professor Jakob Schiøtz[2]
[1]DTU Nanolab, Technical University of Denmark, Lyngby, Denmark, [2]DTU Physics, Technical University of Denmark, Lyngby, Denmark

Poster Group 2

Background incl. aims
Introduced in 2011, Transmission Kikuchi Diffraction (TKD) overcame the challenge in characterizing isolated nanoparticles or ultrafine grains in thin film structure, which was a limiting factor in electron backscattered diffraction (EBSD) due to the small interaction volume and insufficient scatterings [1]. Traditionally, TKD relies on indexing the Kikuchi patterns of the forward-scattered electrons from an electron transparent sample, and it can be performed using a standard EBSD detector in either an off-axis or on-axis configuration with a spatial resolution down to a few nm in on-axis configuration [2]. However, the formation of Kikuchi pattern requires sufficient sample thickness, meaning very thin (e.g. 2D materials) or very light (e.g. organic) materials cannot be investigated via the traditional TKD method in SEM. Hence, a different approach has been developed recently to acquire and analyze the spot diffraction pattern in transmission mode in SEM instead, and it has successfully been used to index 2D materials such as graphene at nm resolution across mm range [3]. Since both spot patterns and Kikuchi patterns have been individually indexed in SEM, the natural next-step is to combine the two techniques so that the on-axis TKD configuration can be applied to a wider range of sample thickness. However, when acquiring both spot and Kikuchi patterns, the intense direct beam often drowns out the spot patterns, and the drastic difference in intensity between the spots and Kikuchi patterns (up to 10^3) makes the detection of both patterns with a conventional CCD detector challenging. Here we present our methods for acquiring both patterns without detector saturation and highlight the advantage by simultaneously indexing spot and Kikuchi patterns in a multi-layered Au thin film structure.

Methods
Two methods have been experimented to address the intensity issue: (1) By applying a filter to the CCD detector screen, the intensity near the optical axis can be reduced hence revealing the geometry of the spot patterns. (2) By acquiring diffraction patterns at different exposure time at each scanned location and combining/stacking the patterns via image fusion algorithm, the dynamic range can be greatly increased and both Kikuchi and spot patterns can be revealed.

Results
We will illustrate the simultaneous acquisition spot and Kikuchi patterns using both methodologies and provide a comprehensive analysis of their respective advantages and disadvantages on single and multi-layered thin film with various thicknesses. Finally, we will introduce and evaluate the two approaches for obtaining orientation mapping with both spot and Kikuchi diffraction patterns, as well as discussing their strengths and limitations concerning accuracy, throughput, and computation power requirement.

Conclusion
Both CCD detector filtering and multi-exposure image acquisition are valid strategies to acquire both spot and Kikuchi patterns without detector saturation in on-axis TKD configuration. The simultaneous indexing of both spot and Kikuchi patterns makes up for the thickness limitation of the individual spot/Kikuchi pattern indexing, and expands the range of samples investigated with a single

technique. With this approach, we aim to expand TKD from an exit-surface characterization technique into a volume information extraction technique with the diffraction information of both spot and Kikuchi signals.

Keywords:

TKD, simultaneous indexing, detector saturation.

Reference:

[1]: Transmission EBSD from 10 nm domains in a scanning electron microscope, Journal of Microscopy, 245 (2012), 245–251, R.R. Keller & R.H. Geiss
[2]: Orientation Mapping by Transmission-SEM with an on-axis Detector, Ultramicroscopy, 161 (2016), 17-22, J. J. Fundenberger, E. Bouzy, D. Goran, J. Guyon, H. Yuan, A. Morawiec
[3]: Orientation Mapping of Graphene using 4D STEM-in-SEM, Ultramicroscopy 219 (2020) 113137 Benjamin W. Caplins, Jason D. Holm, Ryan M. White, Robert R. Keller

845

Impact of improved tracking method on structure determination of perovskites from 3D ED data

Dr. Magdalena Cichocka[1]
[1]Technische Universität Darmstadt, Darmstadt, Germany

Poster Group 2

Background incl. aims
Perovskites (ABX_3) and perovskite-related compounds are some of the most chemically diverse crystal structures with many possible substitutions at A and/or B sites, as demonstrated in oxide systems [1,2]. These materials can be produced using facile processing techniques and yield high performance devices, although they are characterized by large compositional and structural heterogeneities at multiple length scales. Even small structural changes can be induced by strain engineering and open a way to enabling new or deliberately modified material properties. XRD structure refinement requires great effort, especially in the case of accurate characterization of small structural distortions, oxygen positions, and octahedral rotations. Additionally, the contribution of several oriented domains makes structure refinement more complex.
Methods
3D electron diffraction (3D ED) technique [3,4], which may or may not be coupled with precession electron diffraction, allows not only to determine an average structural model, but also to refine it with good accuracy. Moreover, tracking methods, which have been developed in our group [5], can significantly improve the diffraction intensities and overall detailed structure description. They also provide support in answering questions about structural details.
Results
In the present work, we perform structure analysis of perovskites to demonstrate its improvement by dedicated data acquisition routines. By implementing dynamic theory in the refinement, 3D analysis of region of interest in the range of tens of nm and accounting for precession motion, it is possible to obtain reliable and accurate refinement of perovskite structures. Taking into account the selective contribution of differently oriented grains allows for a more accurate description of the structure.
Conclusions
Implementing the dedicated data acquisition strategy and improving the diffraction pattern analysis, pave the way for a new routine characterization of structure details in complex perovskite materials. This places 3D electron diffraction even closer to complementary scanning transmission electron microscopy (STEM) and convergent beam electron diffraction (CBED) techniques, which are usually a choice to map octahedral tilts or atomic vacancies at grain boundaries.

Acknowledgment
DFG Fund within FLAIR CRC 1548

Keywords:

3D ED, electron diffraction, perovskites

Reference:

[1] A. S. Bhalla, R. Guo, R. Roy, Mater. Res. Innovations 2000, 4, 3−26.
[2] P. K. Davies, H. Wu, A. Y. Borisevich, I. E. Molodetsky, L. Farber, Annu. Rev. Mater. Res. 2008, 38, 369−401.

[3] M. O. Cichocka, J. Ångström, B. Wang, X. Zou, S. Smeets, J. Appl. Cryst. 2018, 51, 1652-1661.
[4] S. Plana-Ruiz, Y. Krysiak, J. Portillo, E. Alig, S. Estradé, F. Peiró, U. Kolb, Ultramicroscopy 2020, 211, 112951.
[5] M. Santucci, PyFast-ADT: Python-Driven Advancements in Automated Crystal Tracking and 3DED Data Collection, DGK2024 Bayreuth.

855

Achieving High-Resolution Electron Nano-crystallography using HVEM and PED

Master Sang-gil Lee[1], Doctor Seung Jo Yoo[1], Doctor Jin-Gyu Kim[1], Doctor Hyung Joong Yun[1]
[1]Korea Basic Science Institute, Daejeon, South Korea

Poster Group 2

Background
To achieve higher resolution in TEM, a Cs corrector is typically employed as a hardware solution. Alternatively, software processing techniques like Maximum-likelihood (MAL), Exit-wave function reconstruction (EWFR), Iterative wave-function reconstruction (IWFR), and Phase extension offer an affordable solution without requiring expensive hardware. However, these methods necessitate acquiring multiple HREM images (3-20) for processing. HVEMs are beneficial for HREM due to their deeper sample penetration and reduced dynamical effects. PED further minimizes dynamical effects, enabling high-resolution diffraction data even for thicker samples analyzed with lower-voltage TEMs. This study employed a combined approach of HVEM, PED, and phase extension to achieve sub-Ångstrom resolution imaging of Si single crystal samples. Additionally, we conducted a comparative analysis of the results with those obtained using a conventional TEM equipped with a monochromator and a Cs corrector.
Methods
A Si single crystal was prepared using ion thinning and employed as a test specimen for high-resolution electron microscopy (HREM). High-resolution electron microscopy (HREM) imaging of the Si [211] zone axis was performed using a high-voltage electron microscope (HVEM). The high-resolution images used for comparative analysis were obtained using a conventional TEM equipped with a monochromator and a Cs corrector at an accelerating voltage of 200kV. An energy-filtered precession electron diffraction (EF-PED) pattern was obtained using an energy-filtered TEM equipped with a precession unit. The specimen thickness was estimated using the log-ratio method and information from the low-loss spectra. Image processing of the HREM data involved background noise reduction and phase extension using a combination of software programs (Digital Micrograph, CRISP, HREM filters, and VEC).
Results
A high-resolution (HR) image of the Si [211] projection with an atomic resolution of 1.2 Å was obtained using a high-voltage electron microscope (HVEM). Additionally, a precession electron diffraction (PED) pattern satisfying the quasi-kinematical condition was acquired with an enhanced spatial resolution of 0.63 Å using a beam precession system. By applying the phase extension technique to these combined data, Si atomic columns with an atomic spacing of 0.78 Å in the Si [211] projection were successfully resolved.
Conclusion
The HVEM and PED combination method has demonstrated its potential to achieve high resolution even in thick samples by leveraging HVEM's high penetration power and PED's ability to minimize dynamical effects. By employing this technique, the reduction in resolution caused by sample thickness in high-resolution imaging analysis using Cs-corrector can be partially compensated, which is expected to significantly aid in the accurate analysis and understanding of the structure and properties of nano-crystals.

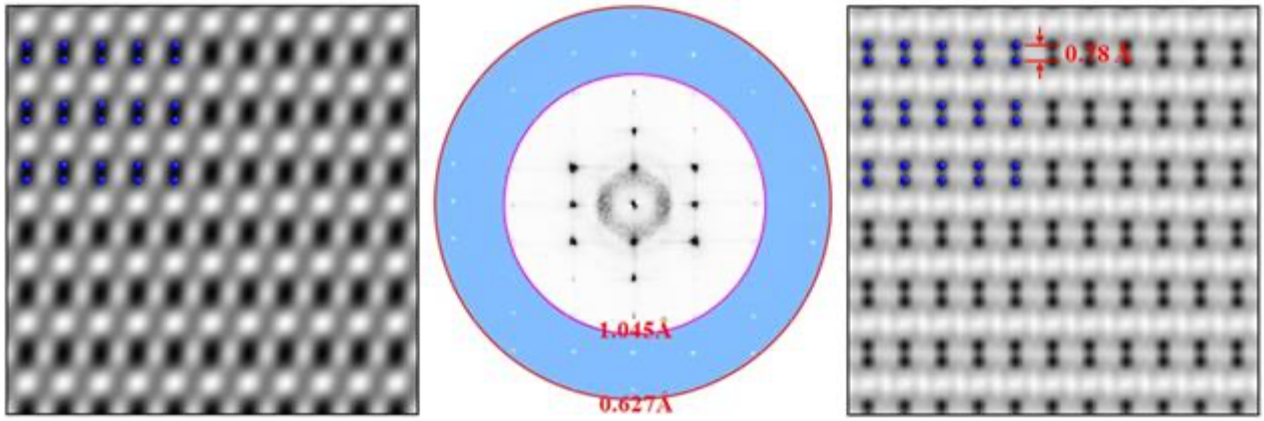

Keywords:

HVEM, PED, Phase extension technigue

Reference:

S. H. Oh, Y. J. Kim, H. S. Kim, Experiment of usefulness of IWFR analysis for HVTEM images with a series of defocus steps obtained from a relatively thick crystal, Korean J. Microscopy, 38(4) 363-374 (2008)

931

Direct observation of charge modulation in nanoprecipitates by 4D STEM

Dr. Juhyun Oh[1], Prof. Young-Woon Kim[1], Prof. Cheol-Woong Yang[2], Prof. Cheol-Hee Ahn[1], Prof Miyoung Kim[1]
[1]Department of Materials Science and Engineering, Seoul National University, Seoul, Korea,
[2]Department of Materials Science and Engineering, Sungkyunkwan University, Suwon, Korea

Poster Group 2

Background incl. aims
Charge modulations induced by structural, compositional and electronic variation in a solid can be investigated using various analytical techniques, including scanning tunnelling microscopy/spectroscopy, Raman spectroscopy, and recently available four-dimensional scanning transmission electron microscopy (4D-STEM), depending on the nature of the modulation. We explore the interplay between charge density modulation and structural distortion in nanoscale moiré structures, $MgZn_2$ nanoprecipitates imbedded in Al matrix using 4D-STEM.
Methods
A series of diffraction patterns by 4D-STEM offers a wide range of information, which includes local electric fields and charge density, in addition to atomic configurations. We integrated intensities at different scattering angles and directions to extract various types of images. Template matching was employed to the real space, depth-sectioned STEM images to locate the accurate atomic positions, which facilitated the mapping of local strain distributions within the imbedded nanostructures. Density functional theory (DFT) calculations are performed to find the origin of the charge modulation and multislice simulations are further employed to compare the experimental results with the theoretical prediction.
Results
We present center of mass (COM) images derived from the in-plane diffraction patterns of the MgZn2/Al heterostructure. Interestingly, the images clearly reveal charge density modulations which are highly dependent on the depth of the probe position in the specimen. Moreover, strain mapping within the Al matrix is intricately linked to charge modulation, suggesting the potential influence of structural distortion on the charge modulation. The periodicity and the location of the modulation are further analyzed to determine the correlation with the moiré supercell structures.
Conclusions
A series of multislice simulations generated numerous COM images, encompassing single atoms to stacks of multi-layers, at different probe depths. We propose that the primary contribution to the modulated charge distribution originates predominantly from the interface area between the $MgZn_2$/Al heterostructure. Furthermore, we demonstrate how manipulation of COM images provides more detailed insights into the structural and compositional variations within materials.

Keywords:

4D-STEM, Charge, Nanoprecipitates

emc2024 COPENHAGEN

972

Characterization of Precipitates in Petroleum Steels by Using Precession Electron Diffraction Technique

Umut Savaci[1], Servet Turan[1]
[1]Department of Materials Science and Engineering, Eskisehir Technical University, Eskisehir, Türkiye

Poster Group 2

Background incl. Aims
Steel has wide variety of grades and properties and not every type of steel applicable for all applications. Due to that reason, correct type of steel needs to be selected for a specific application. For example, for the petroleum and natural gas pipeline applications where pressurized fluid is transported for long distances, American Petroleum Institute (API) X70, X80 or X100 steels are used due to their properties such as high strength, fracture toughness, weldability, corrosion resistance and deformability. API steels are ferritic steels and to obtain the desired properties like high strength, this type of steels is micro alloyed with elements such as Nb, Ti and V with precipitation hardening. Properties of API steels, are modified by the thermo-mechanical rolling by tailoring the microstructure, in addition to the micro alloying. During production and rolling processes several precipitates with different compositions can be formed. Therefore, it is important to determine which precipitate is present in the produced steels, because mechanical properties of material may change with the type of the precipitate. This study aims the characterization of precipitate particle found in the petroleum steel by both conventional and novel precession electron diffraction methods in order to confirm which phase is formed during production.

Methods
In this study, thermomechanically rolled API-X70 steel sample was used. Samples are characterized by conventional TEM and STEM imaging techniques and in addition Precession Electron Diffraction (PED) technique is applied to characterize present phases as well as orientation relationship between the different phases. TEM sample was prepared with conventional mechanical thinning followed by an Ar-ion beam milling. Electron transparent sample is examined by using 200 keV field emission TEM (JEOL-JEM2100F) equipped with STEM high angle annular dark field (HAADF) detector (Fischione-Model 3000) and energy dispersive X-ray (EDX) spectrometer (JEOL-JED2300T). The TEM phase and orientation mapping results are obtained with nano sized probe (at NBD alpha 5 and 0.5 nm spot size) that is scanned in a user specified area over the sample up to 0.7° of precession angle and obtained diffraction patterns are analyzed with ASTAR™ V2 via template matching algorithm.

Results
Microstructure of the samples were investigated by the TEM and STEM imaging methods and these images revealed that steel matrix contains high atomic number element containing precipitate particles according to its contrast with respect to matrix. The sizes of the precipitate particles were ranging from 20 to 80 nm. Chemical composition of the precipitates was tried to be analyzed with EDX, however due to the thickness of the sample, x-ray signals were collected both from precipitate and over or underlaying matrix phase. Because of that reason exact chemical composition cannot be differentiated from the elements present in the matrix. In order to determine the type of the precipitate, phase identification was done by using the precession electron diffraction method by using the crystal structure differences between candidate precipitate phases. For this purpose, phase identification was conducted with calculation and template matching of diffraction patterns of all the possible precipitate phases with experimental diffraction patterns. With this method, phase identification with high reliability was conducted with the additional X-ray spectrum obtained from the precipitate particle.

Conclusions

In this study, precipitate particle present in the API-X70 steel was successfully identified by using different TEM/STEM techniques, which cannot be identified by the EBSD due to the size of the precipitates. For the identification of the both X-ray spectrum as well as phase maps, obtained by the precession electron diffraction method, were used as a complimentary technique to each other in order to eliminate limitations of these methods.

Keywords:

PED, Steel, Precipitate, Phase identification

995

Detection of quasicrystalline symmetries in electron diffraction data

Oskar Ryggetangen[1], Dr. Ruben Bjørge[2], Dr. Sigurd Wenner[2], Prof. Randi Holmestad[1]
[1]Department of Physics, Norwegian University of Science and Technology, Trondheim, Norway,
[2]Department of Materials and Nanotechnology, SINTEF Industry, Trondheim, Norway

Poster Group 2

Introduction

Under certain alloying conditions, quasicrystals have been demonstrated to appear as nano-precipitates in aluminium alloys [1]. In addition to these exotic structures, crystalline approximant phases with similar compositions may appear in the very same systems. The approximants accommodate local icosahedral coordination, giving rise to pseudo-fivefold symmetric diffraction patterns when viewed along given irrational crystal directions [2]. In principle, the distinction between quasicrystalline and approximant diffraction patterns is sharply defined. However, in dealing with experimental data – especially from nano-sized precipitates – the difference is not necessarily obvious. In the following, we utilize scanning precession electron diffraction (SPED) in mapping out fivefold and pseudo-fivefold symmetries in selected material systems and discuss the designation of quasicrystalline precipitates based on diffraction data alone.

Methods

Four model systems were selected for the investigations: A powder of quasicrystalline AlCuFe, a modified 6082 aluminium alloy containing dispersoids of the α-AlFeSi approximant phase, an AlMgCuAg alloy, and a sample of this same alloy which was rapidly solidified though melt-spinning. A JEOL JEM-2100F transmission electron microscope equipped with a NanoMegas precession system and a Quantum detectors Merlin direct electron detector was used in the acquisition of the diffraction data. Data analysis was carried out using the PyXem python library [3].

Results and discussion

The quasicrystalline AlCuFe powder contained particles with large grains with a seeming lack of defects, producing dense fivefold symmetric diffraction patterns. The melt-spun AlMgCuAg was found to contain ~100 nm sized quasicrystalline particles, without any immediately obvious orientation relationships to the Al matrix. Diffraction patterns obtained from these particles were less dense than those from the large-grained AlCuFe sample, although a diffraction tilt-series confirmed their quasicrystallinity. Several different phases were present in the heat treated AlMgCuAg samples, some of which exhibited approximate fivefold rotation symmetries. The particles in question were sparsely distributed in the sample, and ~5 nm in diameter.

Figure 1 (a) shows a precession electron diffraction (PED) pattern obtained through SPED from a particle of interest in the heat treated AlMgCuAg alloy. The diffraction pattern exhibits approximate fivefold rotational symmetry, and sets of reflections fall onto rings with relative spacings which are roughly multiples of the golden mean $\tau=(1+\sqrt{5})/2$. The same diffraction pattern is shown in (b), represented in polar coordinates. Here, the first-order ring is clearly discernible.

Figures 1 (c) and (d) show electron diffraction patterns from particles found in the melt-spun AlMgCuAg sample and quasicrystalline AlCuFe particles, respectively. Both patterns exhibit a striking tenfold rotational symmetry, though it is noted that the patterns obtained from the – comparatively small – particles present in the melt-spun AlMgCuAg are considerably less dense than those acquired from the large-grained quasicrystalline AlCuFe powder.

The classification of presumably quasicrystalline nano-precipitates in aluminium solely by employment of (S)PED is non-trivial. However, we were able to designate these small particles as

quasicrystals up to some tolerance. SPED allows for simultaneously sufficient spatial resolution and field of view to record the sparsely distributed ~5 nm precipitates in the AlCuMgAg sample and show that they are essentially quasicrystalline. Especially, as may be seen in Figure 1 (a), the quasicrystallinity of these particles dominate in the low-resolution domain of the diffraction pattern, hinting at long-range icosahedral ordering.

Complementary diffraction techniques, such as combining SPED with rotation electron diffraction, may help to further improve the accuracy of quasicrystal identification in complex sample systems. As such, it is possible to envision a fast and accurate routine for the mapping of quasicrystalline precipitates over relatively large projected regions – greatly aiding the study of the nucleation and growth of these exotic phases in metallic matrices.

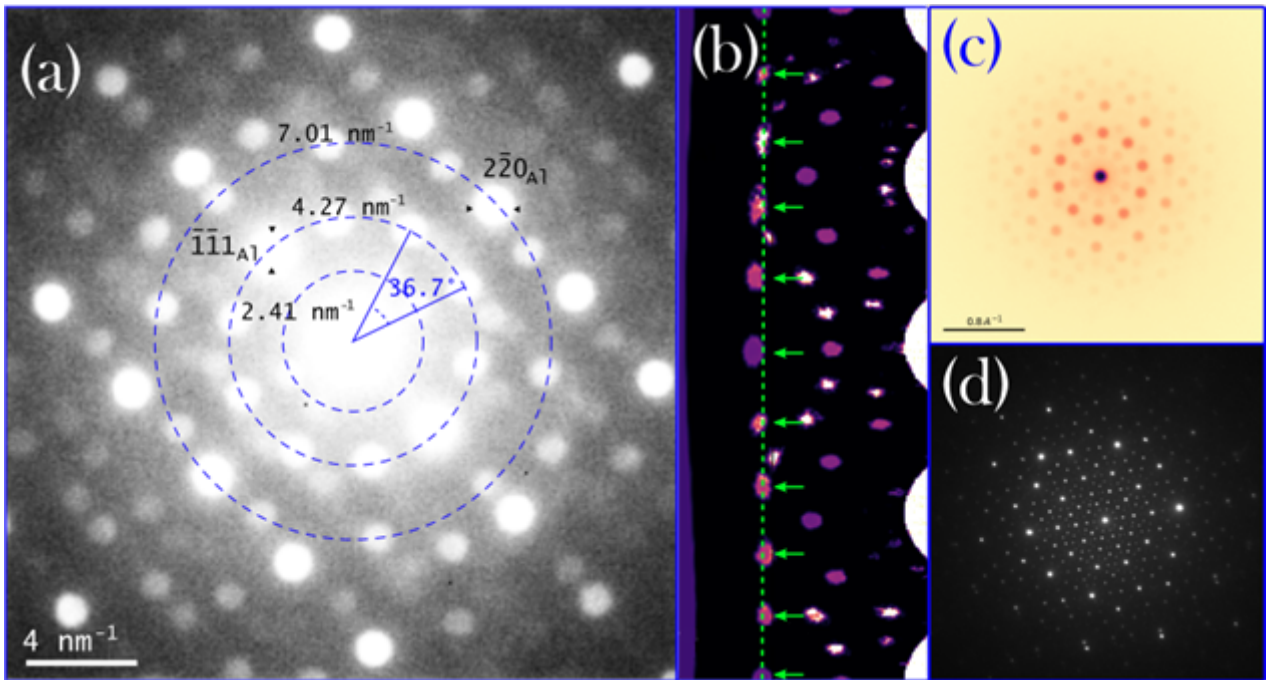

Keywords:

Electron diffraction, quasicrystals, aluminium alloys

Reference:

[1] M. Mihara-Narita et al. (2016) https://doi.org/10.1016/j.msea.2016.01.087
[2] S. Lee et al. (2013) https://doi.org/10.1002/chem.201203758
[3] Pyxem, 10.5281/zenodo.2649351

997

Ultrafast Microbeam Electron Diffraction at 15-keV

Johannes Otto[1,2,3], Leon Brauns[1,2], Rudolf Haindl[1,2], Jan Gerrit Horstmann[1,2], Armin Feist[1,2], Murat Sivis[1,2], Claus Ropers[1,2,3]
[1]Department of Ultrafast Dynamics, Max Planck Institute for Multidisciplinary Sciences, Göttingen, Germany, [2]4th Physical Institute, University of Göttingen, Göttingen, Germany, [3]Max Planck School of Photonics , ,

Poster Group 2

Ultrafast electron diffraction (UED) facilitates the time-resolved investigation of structural dynamics on an ultrafast timescale. In a UED experiment, a pump laser pulse triggers electronic and structural dynamics inside an investigated sample, which is diffractively probed by an ultrashort electron pulse at a variable time delay. Repeating the experiment with different time delays between the laser excitation and electron probing allows for a tracing of the dynamics with femtosecond resolution [1]. The performance of a UED instrument is largely determined by the electron source. Current dedicated setups are predominantly employing planar photocathodes [1]. In this contribution, we present a newly developed ultrafast electron diffraction setup based on a high-coherence electron microscope gun using a nanotip photoemitter [2]. Due to the small emission area of the tip, the electron source generates a low-emittance and high-peak-brightness photoelectron beam for ultrafast microbeam diffraction.
The setup is based on a ZrO/W(100) Schottky-type field emitter, as shown in graphic a). We trigger photoemission from the emitter's front facet by illumination with femtosecond laser pulses (515 nm center wavelength, duration about 200 fs) generated at a maximum 610 kHz repetition rate. The electron pulses are accelerated to a kinetic energy of 15 keV into the sample chamber hosting the sample mounted on a 3-axis manipulator. The diffraction pattern is recorded by a phosphor-screen microchannel-plate assembly and a CMOS camera. For quantitative beam characterization, we use a Faraday cup with fA-resolution and a knife-edge at the sample position to measure the beam current and emittance, respectively. By a measurement of the transient electric field effect, we characterize the temporal overlap at the sample plane and the overall current-dependent time resolution of the instrument [3]. To demonstrate high spatio-temporal UED performance, we carry out ultrafast microdiffraction on a free-standing 1T-tantalum disulfide film (1T-TaS_2).
The emitter operates in the linear photoemission regime with approximately one electron per pulse at the typical laser powers applied in the experiment. Using knife-edge scans, we determine a root-mean-squared (rms) beam size at the sample of 2.54(8) µm and an rms divergence of 0.27(1) mrad, leading to an energy-normalized emittance of 167(7) nm mrad. Measurements of the transient electric field effect yield upper limits to the full-width-at-half-maximum (FWHM) electron pulse duration of 1.02(3) ps and 2.10(3) ps for photoemission fluences of 0.05 mJ/cm² and 0.24 mJ/cm², respectively. The difference in pulse duration follows from increased stochastic and space charge broadening for higher pulse charges.
The small electron beam diameter at the sample position allows us to acquire a scanning electron diffraction dataset of a free-standing 1T-TaS_2 film. Using this 4D-Dataset (x, y, kx, ky), we can map the intensities of a selected diffraction spot in real-space as shown for the (01) spot in graphic b). We attribute the local maxima in the real-space image to a wrinkled structure of the flake. 1T-TaS_2 is subject to a charge-density-wave phase (CDW) accompanied with a periodic lattice distortion. At room temperature, the CDW structure is nearly commensurate (NC) to the underlying lattice (locally commensurate with a nearly regular array of discommensurations). However, upon heating above 353 K, the CDW becomes incommensurate (IC) to the underlying lattice with wave vectors aligned to the host lattice. This structural phase transition can be laser-driven, which was extensively studied in the past, allowing us to use it as a benchmark UED experiment for our setup [4,5]. We observe the

NC-IC phase transition in 1T-TaS_2 with an intensity decrease of the NC diffraction spots and a rise of IC spot intensities after laser pumping, as plotted in graphic c). We measure the reduction in NC peak intensity with a FWHM time resolution of 1.09(7) ps. Combining the emittance, beam current, and pulse length, we can calculate a peak brightness of $3.0(3)\times10^{11}$ A/m²/sr for our electron gun.
We developed an ultrafast electron microdiffraction setup with enhanced spatial and momentum resolution at an energy of 15 keV. The low-emittance source allows us to conduct high-resolution spatial scans of crystalline samples and carry out time-resolved studies of the dynamics in inhomogeneous structures and for small sample dimensions. Furthermore, the setup is ideally suited for in-situ measurements under ultrahigh vacuum and/or cryogenic conditions.

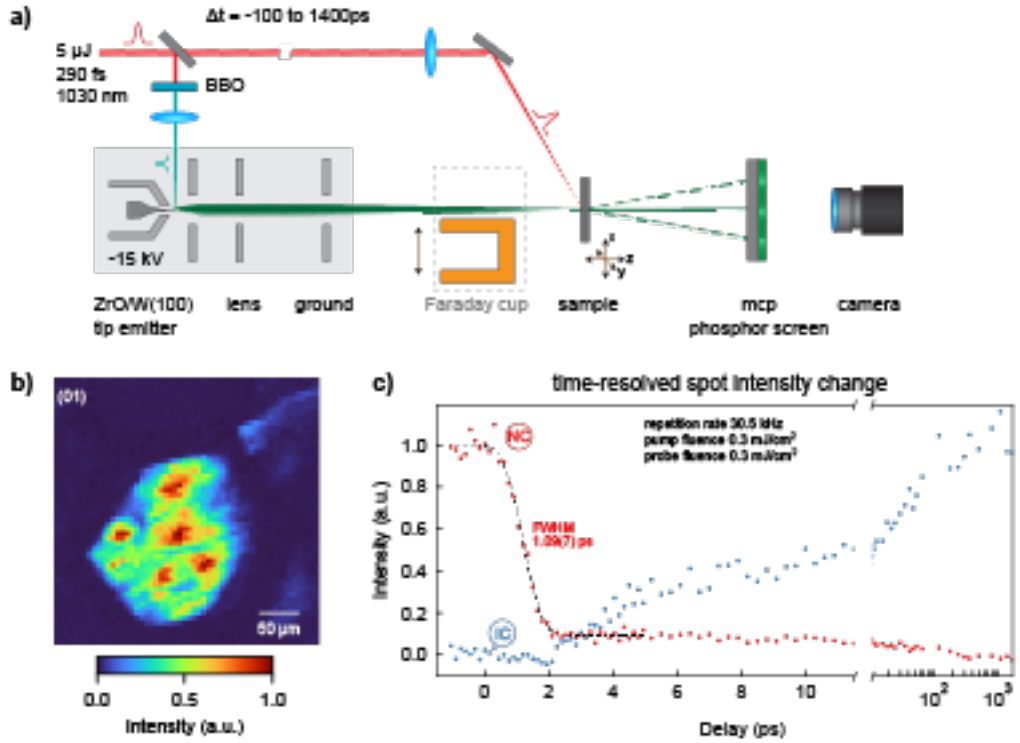

Keywords:

ultrafast, Schottky-emitter, photoemission, 1T-tantalum-disulfide(1T-TaS_2), laser

Reference:

[1] D. Filippetto et al., Rev. Mod. Phys. 94 (2022).
[2] C. Ropers et al., Nano letters 7, 2784 (2007).
[3] S. Schäfer, W. Liang, and A. H. Zewail, Chemical Physics Letters 493, 11 (2010).
[4] M. Eichberger et al., Nature 468, 799 (2010).
[5] T. Domröse et al., Nature materials 22, 1345 (2023).

1026

Differentiation of phases in phase change memory materials using 4D STEM

Xue Bai[1], Dr. Janghyun Jo[1], Prof. Dr. Rafal E. Dunin-Borkowski[1]
[1]Ernst Ruska-Centre for Microscopy and Spectroscopy with Electrons, Forschungszentrum Jülich, Jülich, Germany

Poster Group 2

Background incl. aims
With the rapid development of modern information technology, the novel approaches for storing and processing large volumes of data are being developed, from general concepts such as memory in computing, multi-level storage and neuromorphic computing to specific techniques such as new designs of circuits and storage devices. Different electronic devices are under development, such as magnetoresistive random access memory, resistive random access memory, phase change memory (PCM) and ferroelectric memory. PCMs that are based on chalcogenide materials are promising choices for data storage because phase transitions between amorphous and crystalline phases are quick and efficient. Such phase transitions result in changes between high and low resistance states, which correspond to “0” and “1” logic levels in data storage, respectively. They are also promising for realizing multi-level storage. However, the resistance of the amorphous phase in a PCM cell can drift over time. It is important to determine the underlying mechanism of resistance drift and to develop methods that can be used to differentiate between local crystalline and amorphous phases efficiently. 4-dimensional scanning transmission electron microscopy (4D STEM) enables structural identification at nm resolution. In this project, new analysis methods based on 4D STEM are applied to phase identification in phase change materials.
Methods
With the help of a fast pixelated detector (EMPAD), full 4D STEM datasets of diffraction patterns were collected as the electron beam was scanned across areas of interest. Approaches based on fluctuation electron microscopy (FEM) and radial Fourier analysis (RFA) were applied to analyse the datasets to create radial spectra from the diffraction patterns. Multivariate statistical analysis based on principal component analysis and non-negative matrix factorization was used to distinguish between different phases in the PCM materials, allowing the creation of maps showing the distribution of amorphous and crystalline phases.
Results
The approach was applied to study crystalline nanomaterials on amorphous layers to differentiate between different phases. First, test samples were studied to find optimal experimental parameters. The developed method was then applied to the PCM material Ge2Sb2Te5 (GST). Crystalline clusters in the amorphous GST layer could be distinguished using both FEM and RFA based methods. The two methods were compared with each other. RFA was found to have better robustness to noise.
Conclusions
We have developed a method that can be used to differentiate between amorphous and crystalline phases in PCM materials by combining 4D STEM with FEM and RFA. Both FEM and RFA could distinguish successfully between amorphous and crystalline phases. However, RFA was more robust to noise than FEM. The two methods are complementary and can be used alongside each other to study unknown phase change materials, ultimately during switching.

Keywords:

phase change memory materials, 4D-STEM

1032

Anomalous effects of strain in selected area diffraction patterns due to boron doping in silicon

Miss Kaviyadharshini Dhamotharan[1], Dr Buddhika Mendis[1]
[1]Durham University , Durham, United Kingdom

Poster Group 2

Semiconductors have a significant impact on our lives due to their role in the fabrication of electrical devices. The sensitivity of its conductivity to temperature, illumination, magnetic field, and minute amount of impurity atoms make semiconductors one of the most important materials for electronic applications. It is important to study defects since it can significantly alter the electrical properties of a semiconductor. Microscopic lattice defects such as point defects, dislocations induce local electronic density of state changes and distort the surrounding lattice structure. The effect these interruptions of the crystal lattice have on the scattering of photons or charged particles such as electrons can be used to study the defect.

The effect of static atomic displacements associated with misfitting boron atoms in silicon (B-Si) has previously been studied using high angle annular dark-field (HAADF) imaging by Perovic et al (1). It was found that the HAADF contrast of the boron doped silicon (B-Si) layer is brighter than elemental silicon (Si), despite the decrease in atomic number. This could be due to static atomic displacements arising solely from the displacement of Si atoms from their equilibrium lattice sites adjacent to substitutional boron atoms (2). This type of contrast is called Huang scattering contrast. In addition, high concentrations of boron can also modify the phonon properties of the material (3), which affects the thermal diffuse scattering (TDS). Perovic et al. (1) had attributed the anomalous HAADF contrast to TDS, although the effects of Huang scattering were not considered.

We have used transmission electron microscopy (TEM) to analyse strain around point defects in silicon highly doped with boron, i.e., degenerate doping (B-Si). Fig 1 shows selected area diffraction patterns (SADPs) of elemental Si and B-Si from [100] and [110] zone-axis orientations obtained at room temperature. For [100] Si (Fig 1a) there is streaking arising from (largely acoustic) phonon scattering along [010] and [001] crystallographic directions around the Bragg reflections. The halo ring pattern around the unscattered beam is thought to be due to FIB specimen preparation artefacts. For [100] B-Si (Fig 1b), the streaking is reduced, which could be due to the smaller thickness of this sample. However, diffuse scattering in the form of a cross-shaped pattern between the unscattered and 040 Bragg beams is evident (dashed lines in Fig 2b). The diffuse scattering is not observed for elemental Si, suggesting modification of phonons due to boron doping. This is also consistent with our Raman results, which shows significant peak broadening upon degenerate doping. It should be noted that anomalous low angle scattering due to boron was not observed in other zone-axis orientations, such as [110] (Figs. 1c and 1d).

Radial intensity profiles from Si and B-Si are obtained from the [100] and [110] zone-axis diffraction patterns (Fig 2). The total intensity has been normalised for a direct comparison. For [100] the (t/λ) specimen thickness ratio, measured using electron energy loss spectroscopy, was 0.75 for B-Si and 1.01 for Si. Therefore, at high scattering angles the intensity for Si should be higher than B-Si due to the larger atomic number (Z) and specimen thickness. However, the opposite trend is observed (Fig 2a), which is also consistent with the previous results of Perovic et al. [1]. The anomalous high angle scattering is also observed for [110], although its effects is smaller (Fig 2b; the (t/λ) ratio for the two samples were similar, i.e., 0.71 for B-Si and 0.67 for Si).

The diffraction intensity at high scattering angles is due to localised scattering, and therefore we expect the intensity to be dominated by Huang scattering from the boron point defect atoms. On the other hand, the diffuse scattering in the zero order Laue zone pattern is likely to be dominated by phonons, and here we find evidence of changes in the phonon configuration due to boron doping.

We acquired diffraction data of B-Si under liquid nitrogen cooling, which suppresses TDS but not Huang scattering, to investigate if the diffraction intensity at high scattering angles is solely due to Huang scattering, as boron doping in silicon induces local vibrational modes above the optical mode frequency of 16 THZ (4). Fig 3 illustrates the SADPs alongside a comparison plot detailing the radial intensities of B-Si at room temperature and -173 degrees Celsius. Due to nitrogen cooling, phonon modes above the frequency of 2.07 THz were supressed, which includes the TDS due to local phonon modes from boron doping. The radial intensity of B-Si at higher scattering angles in Fig 3b did not decrease; rather, it slightly increased upon cooling. This suggests that the intensities at high scattering angles were not predominantly contributed by TDS, as most of the phonon modes were suppressed. Hence, the intensity at higher angles is more likely to be contributed by Huang scattering, given that the vibration modes contributing to TDS were supressed.
In summary, the effect of strain due to point defects has been studied in boron doped silicon using SADPs from [100] and [110] zone axes. Anomalous diffuse scattered intensity is observed at both small and large scattering angles. It is concluded that boron gives rise large angle to Huang scattering due to the intrinsic strain in the lattice, as well as altering the phonon configuration, and hence thermal diffuse scattering.

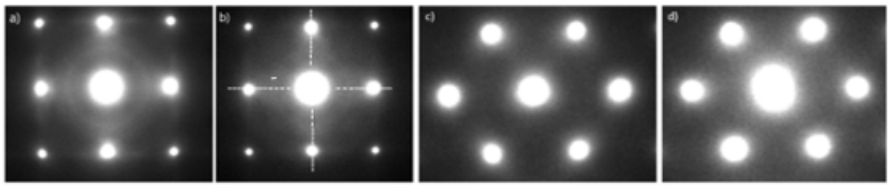

Fig 1: Diffraction patterns (DP) of Si and B-Si for different zone axes. a) Si DP for [100]; b) B-Si DP for [100], dashed lines denote cross shaped pattern due to diffuse scattering; c) Si DP for [110]; d) B-Si DP for [110].

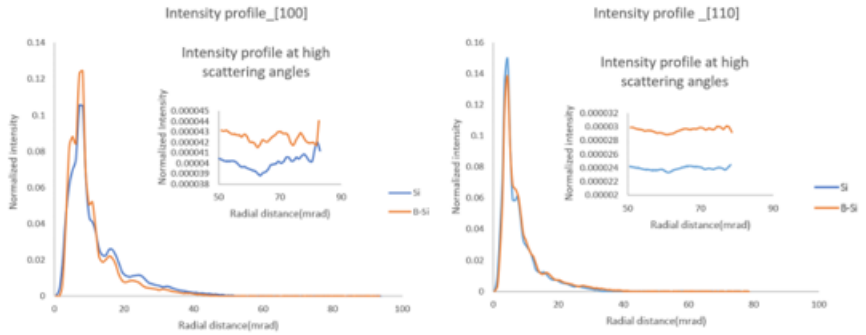

Fig 2: Comparison of radial intensity profiles (IP) of Si and B-Si for different zone axes. a) IP comparison for zone axis [100]; b) IP comparison for zone axis [110].

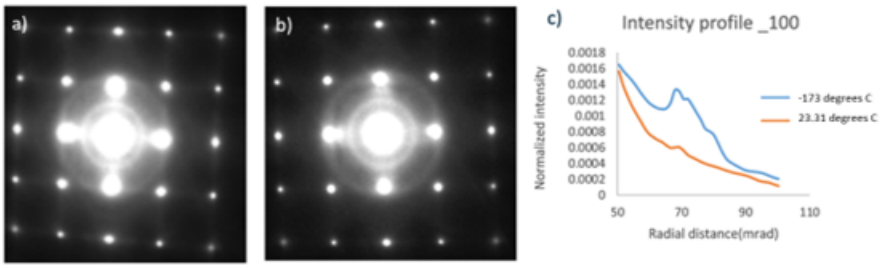

Fig 3: SADPs of B-Si at room temperature and B-Si -173 degrees C for [100]; b) Comparison of radial intensity profiles (IP) of B-Si at room temperature and B-Si at -173.55 degrees C for [100].

Keywords:

High angle scattering, TEM

Reference:

1) D.D. Perovic, C.J. Rossouw, and A. Howie, Imaging elastic strains in high-angle annular dark field scanning transmission electron microscopy. Ultramicroscopy, 52(3):353–359, 1993.

2) Peisl, H. "Defect properties from x-ray scattering experiments." Le Journal de Physique Colloques 37.C7 (1976): C7-47.

3) Bourgeois, E., and X. Blase. "Superconductivity in doped cubic silicon: An ab initio study." Applied physics letters 90.14 (2007): 142511.

4) Nazarewicz, W., Balkanski, M., Morhange, J. F., & Sébenne, C. (1971). Raman scattering from localized vibrational modes of boron impurities in silicon. Solid State Communications, 9(20), 1719-1721.

1045

Electron Diffraction on Biological Samples

Ing. Vendula Hrabalová[1], dr. Jaromír Bačovský[1], Ing. Radka Martínková[1], Helmut Gnaegi[2]
[1]Delong Instruments, Brno, Czech Republic, [2]Diatome Ltd., Port, Switzerland

Poster Group 2

Background incl. aims
Animals have the ability to generate a diverse array of minerals at various locations within or surrounding their cells. An example of this mineralization process is evident in the development of rigid skeletal structures. Especially skeletal hard parts like bones, teeth, shells, and exoskeletons are prime examples of biomineralization [1]. Carbonate apatite crystals constitute a significant portion of various mineralized tissues in vertebrates. In the mentioned structures, like bones and mineralized tendons, these crystals typically manifest as thin, irregularly shaped plates [2].
Electron diffraction experiments provide valuable insights into lattice parameters and symmetries and sometimes help uncover hidden crystals. Directing electron beams at these samples can explain their crystal arrangements, which helps to understand the mechanical properties of the materials, mineral composition, and integrity. A comprehensive understanding of the composition and characteristics of biomineralizations can be invaluable in diagnosing pathological calcifications, which are implicated in several severe diseases. Identifying and analyzing these crystals in tissues can provide crucial insights into underlying mechanisms and progression of such conditions, aiding in early detection, accurate diagnosis, and effective treatment strategies. Electron diffraction proves instrumental in diagnosing conditions such as Alzheimer's disease, which is characterized by abnormal accumulation of metals in the brain [3].On the bone samples, electron diffraction aids in identifying hard tissue calcification, which compromises elasticity, hardens these tissues and disrupts their function.
Electron diffraction offers a significant advantage in its ability to analyze a much smaller area, typically at the nanometre scale [4], compared to X-ray diffraction, making it feasible to detect locally ordered structures (nanocrystals).
This technique is also generally suitable for examining thin layers, such as 2D crystals. Consequently, this method proves particularly valuable for studying membrane proteins that readily form 2D crystals but face challenges in forming 3D structures [5].

Methods
Low Voltage Transmission Electron Microscopy (LVEM) is a valuable technique in life science and materials research. LVEM operates at lower voltages, typically below 25 kV. This lower voltage regime offers distinct advantages, especially enhanced contrast. When assessing micrograph quality, spatial resolution and image contrast are key criteria. Low voltage improves contrast mechanisms, which is particularly beneficial for samples containing light elements, such as biological specimens. Enhanced image contrast helps to identify suspicious crystal structures in tissues. Moreover, low-voltage electron diffraction has a distinct specific advantage yielding from the dimensions of the Ewald sphere, providing more information [6].
The Low Voltage Electron Microscopes (LVEMs) by Delong Instruments integrate TEM and STEM (including dark fields in both regimes) and SEM (BSE) imaging modes. The LVEMs offer Electron Diffraction (ED) and eventually Energy Dispersive X-ray Spectroscopy (EDS), which makes them altogether highly versatile tools for material analysis.
The samples were sectioned with 35° diamond knives at a feed of 20-30nm using ultramicrotomy method.

Results

This study performed electron diffraction on selected biological samples, namely manganese-bound bacteria, bones, shells, and urea, and explored the advantages of analyzing biological samples using low voltage electron diffraction. The experiments were carried out using low-voltage electron microscopes LVEM 25E with an accelerating voltage of 25 kV and LVEM 5 operating at approximately 5 kV.

Conclusion

In summary, electron diffraction proves invaluable for analyzing biological materials, offering insights into crystal structures and tissue properties. Particularly, it aids in studying thin layers and 2D crystals, contributing to understanding membrane proteins and the structural complexity of hard biological materials like bones and shells. Additionally, it shows potential in diagnosing diseases such as Alzheimer's. This study highlights the utility of low-voltage transmission electron microscopy in such analyses, providing enhanced contrast and analytical precision for diverse biological samples.

Keywords:

Electron Diffraction, LVEM, biological samples

Reference:

[1] WEINER, S.; et al., 1983. Electron diffraction of mollusc shell organic matrices and their relationship to the mineral phase. Online. International Journal of Biological Macromolecules. p. 325-328.
[2] MORADIAN-OLDAK, J.; et al., 2009. Electron imaging and diffraction study of individual crystals of bone, mineralized tendon and synthetic carbonate apatite. Online. Connective Tissue Research. p. 219-228.
[3] PLASCENCIA-VILLA, et al., 2016. High-resolution analytical imaging and electron holography of magnetite particles in amyloid cores of Alzheimer’s disease: orientation and arrangement of mineralized collagen fibrils. Online. Scientific Reports. p. 219-228.
[4] EGLI, Martin; et al., 2016. Diffraction Techniques in Structural Biology: orientation and arrangement of mineralized collagen fibrils. Online. Current Protocols in Nucleic Acid Chemistry. p. 219-228.
[5] PUECH, Pascal; et al., 2021. Combining low and high electron energy diffractions as a powerful tool for studying 2D materials: orientation and arrangement of mineralized collagen fibrils. Online. Applied Physics A. p. 219-228.

1149

Impact of In Situ and Ex Situ Annealing on Al-Cu Heterogeneous Nanostructures: A Comparative Study

Lucia Bajtosova[1], Elena Chocholaková[1], Barbora Kihoulou[1], Jan Hanuš[1], Miroslav Cieslar[1]
[1]Faculty of Mathematics and Physics, Charles University, Ke Karlovu 3,12116, Prague, Czech Republic

Poster Group 2

Background incl. aims

Water-based aluminum batteries are a promising alternative to commonly used lithium batteries due to properties such as low production costs, safety in handling, and high theoretical capacity [1]. However, the formation of an oxide layer prevents achieving the desired electrochemical properties. By annealing Al-Cu multilayer heterogeneous nanostructures, the formation of a dendritic Al2Cu structure enveloped by pure aluminum can be achieved by a eutectic transformation [2]. Techniques such as FIB (focused ion beam) [3] for sample preparation and in-situ TEM analyses enable detailed monitoring of phase transformations and structural dynamics of materials at high temperatures. Research in this area is key to the development of new materials with potential applications in energy, especially in the context of improving performance and efficiency of water-based aluminum batteries.

The main objective of this work is to analyze the structural and phase changes of multilayer nanostructures at elevated temperatures through in-situ annealing in TEM. Another goal is to compare the processes occurring in lamellae annealed in-situ with lamellae created from ex-situ annealed material. The results contribute to a deeper understanding of properties of Al-Cu multilayer heterogeneous nanostructures and their potential for applications. Moreover, they validate the experimental in situ methods employed in studying the microstructural processes.

Methods

Al-Cu multilayer heterogeneous nanostructures, consisting of alternating thin layers of Al and Cu nanoparticles, were prepared using magnetron sputtering. The transmission electron microscopy (TEM) and scanning TEM (STEM) with high-angle annular dark field (HAADF) imaging on a Jeol 2200FS was used for the characterization of samples. This was complemented by energy dispersive spectroscopy (EDS), scanning electron microscopy (SEM) analyses and automated orientation and phase mapping (ASTAR). Cross-sectional lamellae were prepared using a focused ion beam (FIB) on a Zeiss Auriga SEM. In situ annealing was conducted within the TEM using a GATAN heating holder.

Results

Films of the Al-Cu heterogeneous nanostructures, with thicknesses of 200 nm and 1 µm, were produced. The thin films were annealed in situ to investigate structural changes. Cross-sectional lamellae made from the 1 µm thick films revealed a gradient structure, showing an increasing amount of Al towards the bottom of the specimen. The impact of film thickness on the resultant structures was examined through comparative analysis of in situ annealed lamellae of two different thicknesses and lamellae prepared from ex situ annealed film. Surface modifications, grain size, and the distribution of Al2Cu within Al were mapped using SEM, EDS, and HAADF detectors together with ASTAR imaging techniques.

Conclusion

This study demonstrates the capabilities of in-situ annealing for exploring the structural and phase transformations in Al-Cu multilayer heterogeneous nanostructures. Through characterization techniques, including TEM, STEM, EDS, and ASTAR, a gradient structure with varying aluminum concentration was observed, particularly in multilayer films. The comparisons between in-situ and ex-situ annealed lamellae, highlight the thermal behavior and potential of these nanostructures for advanced material applications, such as in next-generation battery technologies.

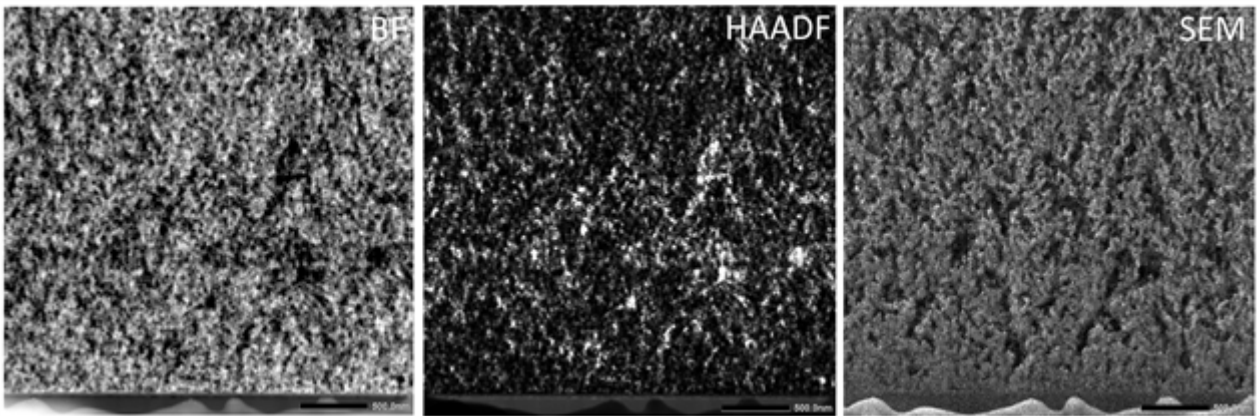

Keywords:

Al-Cu multilayer nanostructures, In-situ TEM

Reference:

[1] Xu, X. et al. (2021) Engineering strategies for low-cost and high-power density aluminum-ion batteries Chem. Eng. J., 418, 129385
[2] Y.Y. Tan, Q.L. Yang, K.S. Sim, Li Tao Sun, Xing Wu, Cu–Al intermetallic compound investigation using ex-situ post annealing and in-situ annealing, Microelectronics Reliability, Volume 55, Issue 11, 2015, Pages 2316-2323, ISSN 0026-2714, https://doi.org/10.1016/j.microrel.2015.06.050.
[3] Langford, R.M. (2006), Focused ion beams techniques for nanomaterials characterization. Microsc. Res. Tech., 69: 538-549. https://doi.org/10.1002/jemt.20324

1248

TEM strain measurement methods on SiGe/Si films for accuracy tests

Dr. Roberto Balboni[1], Prof. Matteo Ferroni[1,2], Dr. Fabiola Liscio[1], Dr. Anacleto Proietti[3], Dr. Chiara Mancini[3]
[1]CNR-IMM, Bologna, Italy, [2]University of Brescia, Brescia, Italy, [3]University of La Sapienza, Roma, Italy

Poster Group 1

Background incl. aims
Transmission electron microscopy (TEM) is still considered a key analysis technique when high spatial resolution is required, even considering the generally lengthy, difficult and sometimes troublesome sample preparation. Such important advantage applies to imaging, structural and diffraction analysis and analytical investigations. The analysis and quantification of strain fields in crystalline materials also takes advantage of the TEM spatial resolution and over the last decades several TEM based techniques were developed [1].
In the framework of the CHALLENGES project financed by the EC (Grant agreement 861857 [2]), several methods have been used to validate the results of Tip Enhanced Raman Spectroscopy (TERS) in the characterisation of semiconductors (Si based) wafers and structures. Strain was one of the physical quantities measured in either thin film or patterned structures and TEM methods were used as standard reference. A series of three Si1-xGex heterostructutres, deposited as thin films onto a Si substrate, at different Ge concentration and thickness (see Table I), were used as 'standard strain' samples in order to compare all the techniques adopted (that includes optical based as well as diffraction based ones, such as TEM and X-ray Diffraction, XRD) onto the same samples. The Ge nominal concentration and SiGe film thickness were #1: 20%/45 nm, #2: 30%/29 nm and #3: 40%/22nm, respectively.
We therefore took this opportunity to test different standard TEM strain analysis methods, namely Convergent Beam Electron Diffraction (CBED), Geometric Phase Analysis (GPA) and standard Selected Area Diffraction (SAD), in such samples using a conventional TEM, with the aim of evaluating the accuracy of the measurements with particular reference to the strain relaxation related to the lamellae thickness.

Methods
Thin cross-sectioned lamellae for TEM analysis have been prepared from the wafes using a Zeiss XBeam 340 FIB, with Ga ions accelerated at 30 KeV, then at 5 and 2 KeV for a final polishing to reduce the amorphous and crystal damaged layers thickness at the thinned surfaces. In each lamella a series of 3 thin regions at different thicknesses were prepared. The local crystal thickness in each region was evaluated by means of two-beams (004) CBED and resulted of about 100 nm, 200 nm and more than 450 nm, from the thinner to the thicker ones in each lamella.
The TEM measurements were performed in a FEI Tecnai F20T equipped with a Schottky emitter and operated at 200 kV accelerating voltage.
The samples film strains have also been measured with high resolution XRD using a Rigaku SmartLab X-ray diffractometer.

Results
CBED strain analysis was performed in STEM mode by obtaining diffraction pattern along several lines proceeding from the substrate to the surface after having oriented the sample along the <230> zone axis [3]. The CBED measurements were performed only in the thicker (>450 nm) regions of the sample. It was possible to obtain good and measurable patterns only up to regions close to the Si/SiGe interface. In the centre of the film the High Order Laue Zones (HOLZ) lines split or blurred out, thus preventing any measurement.

Since strain values were of the order of 10-2 and the film thicknesses were at least 20 nm it was possible to use also conventional SAD that showed comparable results with those obtained with the more sophisticated and instrumental requiring Nano Beam Diffraction (NBD). The SAD measurements showed a split of the (400) reflection family, corresponding to the Si and the SiGe regions, confirming that the crystal deformation was uniaxial in all samples, i.e. along the growth direction, as expected in a tetragonally distorted crystal. The mismatch values obtained vary considerably in the same sample at different thicknesses of the lamella: in Table 1 the mismatch values obtained in the thicker regions are reported.
Finally, good quality HREM images were recorded only in the thinner area of the samples, in both film and substrate, and from these we obtained the corresponding mismatch values from GPA analysis. From this analysis too the distortion showed an uniaxial behaviour but also smaller mismatch values if compared with those obtained by SAD in thicker regions.
All the results obtained are summarised in Table I, together with the measured Ge concentration (as obtained by energy dispersive x-Ray spectroscopy) and High Resolution XRD (HRXRD) measurements. From the results shown in the table it is quite evident that phase analysis gives lower values for the measured mismatches, and it reasonable to assume that a larger strain relaxation occurs here since the sample should be thinned to a lower thickness value to collect HREM images. Moreover, samples #1 and sample #2 show a similar residual strain, while sample #3 keeps a much higher value. This could be due an increased rigidity in sample #3 related to the much smaller film thickness. The small discrepancy between SAD and HRXRD results suggests that small strain relaxation could still occur even in thicker areas.

Conclusion

The application of well established TEM techniques for crystal strain evaluation in simple SiGe/Si heterostructures showed some limitations. Despite the High strain sensitivity, CBED confirmed to be ineffective in samples regions were an high strain gradient or a strong strain relaxation occur. Both GPA and conventional diffraction were able to measure the uniaxial deformation, but best results were obtained in thick lamellae (>450 nm), thus confirming that the relation between strain vs. local sample thickness plays an important role in measurement accuracy.

Table I

	Nominal Ge	EDX Ge %	ε_1 by CBED	ε_1 by SAD	ε_1 by GPA	ε_1 by HRXRD
#1	20%	21.5±2.0	N.A.	$1.2\times10^{-2}\pm0.2$	$0.5\times10^{-2}\pm0.2$	1.3×10^{-2}
#2	30%	34.0±3.0	N.A.	$1.8\times10^{-2}\pm0.2$	$0.6\times10^{-2}\pm0.2$	-
#3	40%	40.5±2.0	N.A.	$2.3\times10^{-2}\pm0.2$	$1.8\times10^{-2}\pm0.2$	2.7×10^{-2}

Keywords:

Transmission Electron Microscopy, Crystal Strain

Reference:

[1] A. Béché, J. L. Rouvière, J.P.Barnes and D.Cooper, Ultramicroscopy 131, (2013) 10-23
[2] https://www.challenges2020.eu/
[3] A. Armigliato, R. Balboni and S. Frabboni, Appl. Phys. Lett. 86, 063508 (2005), https://doi.org/10.1063/1.1565181

1261

Combining 3D-ED and Z-contrast imaging: crystallographic structure solution of Ca2MnO3Cl

Dr Stéphanie Kodjikian[1], Dr Christophe Lepoittevin[1], Dr Fabio Denis Romero[1]
[1]Univ. Grenoble Alpes, CNRS, Grenoble INP, Institut Néel, 38000 Grenoble, France

Poster Group 1

Background incl. aims
Mixed-anion compounds are much less explored than monoanionic materials such as oxides. However, the possibility of forming heteroleptic coordination polyhedra can result in significantly different emergent properties and the different anion properties such as charge, ionic radii, electronegativity, and polarizability add new degrees of freedom to control and tune the electronic and atomic structure of materials. We have recently succeeded in preparing Ca_2MnO_3Cl (powder) which adopts a novel structure type. However, obtaining the structure of this new compound was tricky because of the powder's extreme sensitivity to humidity, and because of the presence of secondary phases, which made indexing the powder X-ray diffraction pattern particularly hard.
Methods
Particularly well-suited to the study of nanomaterials, Transmission Electron Microscopes (TEMs) have recently become indispensable in nanoscale crystallography, thanks to major technological advances such as the invention of spherical aberration correctors, the development of fast, sensitive pixel detectors, cryogenic methods, beam precession, etc... which have led to the advent of 3D Electron Diffraction (3D-ED) methods for solving nanocrystal structures. The microscopist now has reliable diffracted intensities at his disposal, enabling him to calculate a structural model ab initio, then refine it on the basis of dynamic theory, thanks to the development and constant updates of dedicated crystallography programs [1-3], or use X-ray or neutron diffraction. He can also compare the resulting structure with atomic resolution images and maps, recorded in parallel in a state-of-the-art TEM. We performed 3D-ED, Z-contrast imaging and Energy Dispersive X-ray Spectroscopy (EDX) to determine the crystallographic structure of the new mixed anion oxyhalide Ca_2MnO_3Cl. Then the structural model was refined using powder X-ray and neutron diffraction [4].
Results
Ca_2MnO_3Cl crystallizes in a novel structure type stabilized by the small ionic radius of Ca and the strong Jahn-Teller effect of $Mn^{3}+$. The resulting structure (9.752 Å × 6.4946 Å × 6.5763 Å, space group Cmcm) contains 1-dimensional chains of MnO4 square planes, with an angle ~120 ° between neighboring planes. At low temperatures, this material adopts magnetic arrangements with ferromagnetic chains coupled antiferromagnetically. On applying a magnetic field, it experiences a spin flop transition leading to a magnetic unit cell four times larger than the nuclear one.
Conclusion
We will describe the process leading to the structure of the new oxychloride Ca_2MnO_3Cl, emphasizing the importance of the TEM part to solve ab initio its crystal structure, which opened the doors to the comprehension of its magnetic state.
Acknowledgments
The TEM facility JEOL NEOARM at CNRS Institut Néel was co-financed by the European Union under the European Regional Development Fund (ERDF, contract no. RA0023813).

Keywords:

3D-ED, Z-contrast, mixed-anion compound, crystallography

Reference:

[1] L. Palatinus, PETS - Program for analysis of electron diffraction data, Prague: Institute of Physics of the AS CR (2011)
[2] L. Palatinus, P. Brázda, M. Jelínek, J. Hrdá, G. Steciuk, M. Klementová, Acta Crystallogr., Sect. B: Struct. Sci., Cryst. Eng. Mater. 2019, 75 (4), 512– 522
[3] V. Petříček, M. Dusek, L. Palatinus, Z. Kristallogr. 229 (2014), 345-352
[4] F. Denis Romero, C. Lepoittevin, S. Kodjikian, C. V. Colin, M. A. Hayward, JACS 2023, 145 (42), 23346-23351 ⟨10.1021/jacs.3c09088⟩

1277

Evaluating the Efficacy of Laboratory-Based X-ray Diffraction Tomography for Crystallographic Analysis in Pure Iron

Postdoc Fellow pardis Mohammadpour[1,2], PhD student Mehdi Mosayebi[1,2,3], Research scientist Daniel Paquet[3], Research scientist Pierre-Antony Deschênes[3], Research scientist Laurent Tôn-Thât[3], Facilities Manager Brian Langelier[1], Proffesor Nabil Bassim[1,2]
[1]Canadian Center for Electron Microscopy, Hamilton, Canada, [2]Materials Science and Engineering Department, McMaster University, Hamilton, Canada, [3]Hydro-Québec, Institut de recherche d'Hydro-Québec, Varennes, Canada

Poster Group 1

Background
Iron (Fe) alloys are fundamental to various industrial applications due to their diverse mechanical properties and structural versatility. Understanding these alloys' grain structure and crystallographic characteristics is crucial for optimizing their performance. Here, a newly developed laboratory-based Diffraction Contrast Tomography (LabDCT) was used for non-destructive three-dimensional grain mapping and crystallographic analysis of pure iron. LabDCT, within a commercial laboratory X-ray microscope (Zeiss Xradia 630 Versa), uses a synchrotron-style tomography detection system and, combined with conventional absorption tomography, enables analysis of defects, deformation, grain growth, and phase transformation. This study aims to evaluate the efficacy of XRD-CT in characterizing pure iron, comparing the obtained grain and crystallographic data. The aim is to use the data from pure iron as a reference point for the future characterization of more complicated Fe alloys. To validate the results obtained from LabDCT, this study also employs 3D Electron Backscatter Diffraction (EBSD) tomography on the same volume. This comparative analysis seeks to highlight the potential advantages and limitations of LabDCT, advancing its application in material science and industrial contexts.
Experimental Method.
A cylindrical piece of pure iron with a diameter and height of 450 µm and 1800 µm Lab-based Diffraction Contrast Tomography (DCT) scan and X-ray absorption tomography were performed using the Zeiss Xradia 630 Versa Micro X-ray Computed Tomography (Micro-XCT) system. A helical phyllotaxis Lab DCT (HP-DCT) scan was used to cover a larger field of view. The DCT Scan was performed using an accelerated voltage of 100 kV, a power of 14 W, A letterbox aperture of (375 µm × 375 µm), DCT 4X objective detector with 2.5 mm x 2.5 mm detector beam stop to block the transmitted X-rays. The specimen was rotated 360°, over which 181 projections with an exposure time of 60 s per projection were collected. To Satisfy the Bragg condition, the source and detector were positioned within an equal distance from the sample. A helical scan was used to cover a larger field of view. For serial sectioning tomography, a dual-beam TFS Helios G5 Xe PFIB system was employed. The sectioning and EBSD scans were carried out under the following conditions and controlled by the FEI Auto-slice-and-view software. The slice thickness was set to 2 µm, and EBSD was collected every other slice for a final z-resolution of 4 µm. A current of 0.2 µA was used for slicing the block, and a 5° rocking mill was used to prevent curtaining effects. 2D EBSD maps were collected at 20 keV with a current of 13 nA using an Oxford Symmetry detector and the Aztec control software. Each EBSD map covered the entire sample face with indexing at 4 µm step size to provide approximately cubic voxels for the 3D reconstructions. In total, 75 individual slices were collected on a sequence of X-Y planes.
3D Reconstruction
To reconstruct the DCT data and grain mapping, version 3.2.5 of the data reconstruction software, GrainMapper3D by XnovoTech® was utilized. Importing the raw data, thresholding, alignment, and clean-ups, were all carried out using DREAM.3D software to reconstruct the EBSD-FIB Tomography

data. Following the reconstruction, 3D datasets were visualized using Dragonfly Pro and ParaView software.

Results

Fig 1a shows the DCT-reconstructed 3D volume of the pure iron and the three 2D cross sections of the grains in the XY, XZ, and YZ planes. Fig 1 b illustrates a 3D-EBSD reconstruction of the volume corresponding to the top 300 µm of the sample. To match the EBSD and DCT results, a slice-by-slice observation was carried out to reveal the internal microstructure of the material. The 3D variation of the grain morphology and crystallography was precisely tracked through the entire volume of the material using both 3D-EBSD and DCT datasets. After identifying the corresponding 2D slice in the lab-based DCT dataset, comparisons were made between lab-based DCT and EBSD techniques in terms of grain size, shape, and texture. A grain-by-grain comparison of the DCT and EBSD data is shown in Fig 1C. Although the LabDCT effectively determined the center of the mass position and large grains' shape, the EBSD data showed more accuracy in terms of the grain boundaries and grain shapes and detection of smaller grains. Furthermore, the DCT method was able to image larger volumes in a shorter time.

Conclusions

The quality of the 3D grain maps of pure iron obtained with LabDCT and 3D FIB-EBSD was compared in terms of grain size and shape. The centre of the mass position of grains in DCT was found very close to 3D EBSD. The grain size and number of grains in DCT were underestimated compared to the grain size obtained in the EBSD. The grains in the EBSD image are more complex than the DCT grains due to the higher resolution of the EBSD method. Overall, a promising agreement was observed between the DCT and EBSD data.

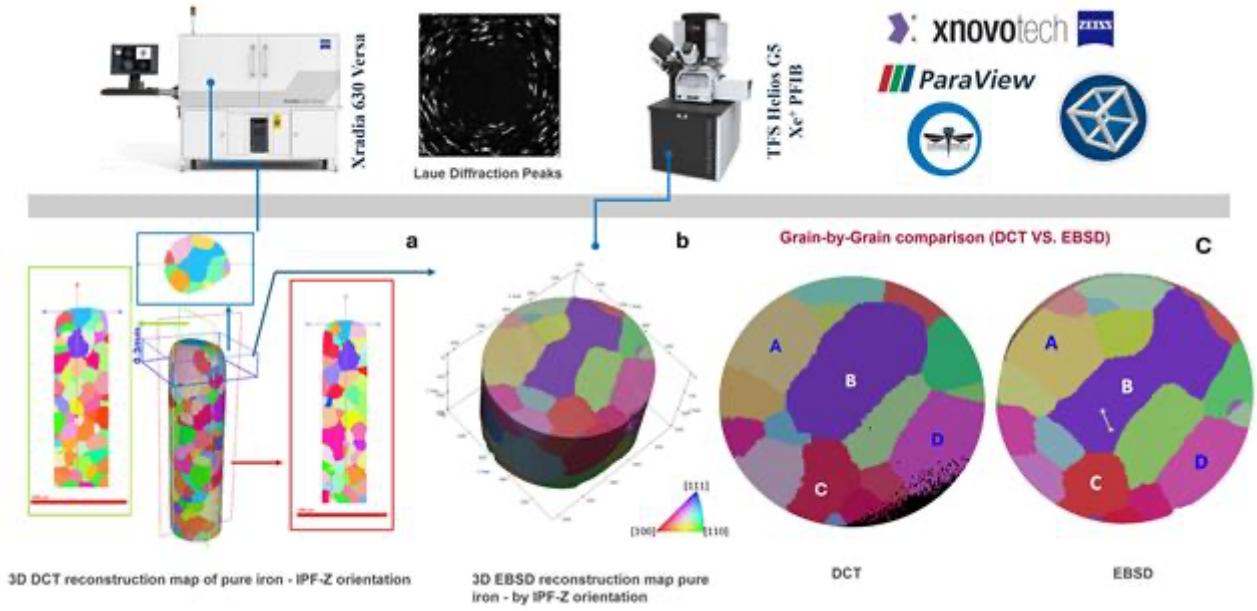

Keywords:

LabDCT, XCT, 3D FIB-EBSD, Grain-mapping

Reference:

[1] Holzner, Christian, et al. "Diffraction contrast tomography in the laboratory–applications and future directions." Microscopy Today 24.4 (2016): 34-43.

[2] Ball, James AD, et al. "Registration between DCT and EBSD datasets for multiphase microstructures." Materials Characterization 204 (2023): 113228.

[3] Burnett, T.L., et al. "Large volume serial section tomography by Xe Plasma FIB dual beam microscopy." Ultramicroscopy 161 (2016): 119-129.

[4] Groeber, Michael A., and Michael A. Jackson. "DREAM. 3D: a digital representation environment for the analysis of microstructure in 3D." Integrating materials and manufacturing innovation 3 (2014): 56-72.